The Bidirectional Link Between Visual Processing and Optomotor Flight Behavior in Drosophila

Dissertation
zur
Erlangung des Doktorgrades (Dr. rer. nat.)
der
Mathematisch-Naturwissenschaftlichen Fakultät
der
Rheinischen Friedrich-Wilhelms-Universität Bonn

von
Philippe Jules Fischer
aus
Luxemburg, Luxemburg

Bonn, 2023

Angefertigt mit Genehmigung der Mathematisch-Naturwissenschaftlichen Fakultät der Rheinischen Friedrich-Wilhelms-Universität Bonn

1. Gutachter:	Prof. Dr. Michael Pankratz
2. Gutachterin:	Prof. Dr. Ilona Grunwald-Kadow
Tag der Promotion:	15.05.2024
Erscheinungsjahr:	2024

Abstract

Animals that explore the world need to reliably move in a preplanned direction. With the optomotor response, flies stabilize a straight path during flight by visual feedback. Unintended deviations from a straight path are perceived as rotation of the scenery around the fly, and smooth syndirectional flight turns minimize the asymmetric optic flow. At the same time, voluntary turns cause optic flow that is indistinguishable from visual input due to involuntary, external causes. Therefore, a motor-command efference copy has been postulated to counteract reafferent sensory perceptions that arise from volitional actions, and to provide context to resolve the ambiguity in perception. In flies, HS (horizontal system) cells are thought to mediate optomotor responses to horizontal motion. During spontaneous flight saccades, HS cells have been shown to receive input that could function as an efference copy to mitigate stabilization reflexes.

Here, I investigated how this putative efference copy suppresses the processing of visual motion in HS cells by recording intracellularly during tethered flight. First, it is shown that looming-elicited avoidance saccades exhibit similar effects as spontaneous saccades. Additionally, the visual experience of the looming stimulus influences the subsequent responses of HS cells. Importantly, an inhibitory efference copy suppresses the processing of excitatory optic flow during both left- and rightward saccadic turns. We found that this effect is limited to a subset of HS cells and does not markedly reduce responses to inhibitory optic flow.

To refine our understanding of this efference copy mechanism and resolve the counter-intuitive findings, I reconstructed the reafferent visual input to each HS subtype during escape saccades. The reafference is biphasic and largely symmetric for left- and rightward saccades, and thus

supports a functional role for reduced excitatory responses in both directions. In contrast, the reafference is not evidently different for HSS, which suggests a functional subdivision between subtypes.

To improve our understanding of the efference copy function and flight control, I investigated the impact of DNp15, a descending neuron postsynaptic to HSN and HSE. Intracellular recordings show that DNp15 prefers rotational to translational optic flow by integrating binocular information and relays graded potentials. The connectome suggests that DNp15 controls head and flight turns during panoramic visual stimuli. Through silencing and activation experiments, it is found that this neuron is essential for slow optomotor turns of both the head and wings, but acts in conjunction with other descending neurons.

This work contributes to our understanding of a feedforward pathway from vision to behavior and how visual processing is internally fine-tuned for behavioral context.

Acknowledgments

First and foremost, I want to thank my supervisor Bettina Schnell. Not only did you teach me a very challenging technique and help me when I did not know how to continue, but especially your never-ending patience and kindness will never be forgotten. Thank you for your insights, inspiration and for showing me how to be a better scientist.

I want to thank my partner, wife and mother of my children, for putting up with all the times I was late, all the times I was distraught, and for pushing me forward in life. Thanks to Cora and Lysio, who constitute the most lovely element of surprise in this endeavor.

My thanks go out to Prof. Michael Pankratz for enabling me to graduate, being part of my thesis committee, as well as to Kevin Briggman for his advice.

To the other members of the NFC group, former and current, for making all this time spent at the institute and outside into a great experience, pandemic or not. To colleagues and friends at Caesar, who made it an inspiring place and provided interesting discussions that broadened my horizon.

Special thanks go out to Aiman Ume as well, who performed the silencing experiments presented in this thesis.

Finally, to my parents who instilled a deep curiosity and brought me up to this path.

Contents

List of Figures

1 Introduction

Among the primordial questions that humans of all cultures have asked is the question about who or what we are. While the question is arguably more philosophical in nature, a physicalist approach to it focuses on our intrinsic nature, and how we interact with the environment. In this tradition, over the past century neuroscience has emerged and made significant progress in describing how nervous systems control certain actions and coordinate the disparate functions of organisms. However, there is still a significant gap in understanding the chain of internal processes that lead from external factors to an interaction with the environment. This thesis aims to contribute to that effort by investigating the neural processing that links visual perception to flight behavior on a cellular level in the fruit fly *Drosophila melanogaster*.

1.1 Flight behavior

Among the arthropods, only insects have evolved the ability to fly, helping them to spread around the globe and populate many ecological niches. Assisted by virtue of being a human commensal, the small *Drosophila melanogaster* in particular has spread around the globe without diverging into multiple species, a feat only possible by dispersing quickly through air travel and reaching rich human-adjacent food sources [83]. Release-and-capture experiments have demonstrated that *D. melanogaster* is able to cover 10 km in a day [31].

1.1.1 Course stabilization and redirection

Optomotor response

Estimates of the metabolic cost of flight indicate that this distance, flown across open desert, is at the upper end of what *Drosophila melanogaster* is able to achieve [41]. In return, it means that flies needed to keep a stable heading for several hours. Keeping a stable heading involves both wanting to fly straight and actually being able to correct for deviations. Flies presumably use all available sensory cues to determine heading, like tracking landmarks [113] or celestial cues [151] and wind direction [34]. Short-term deviations and destabilization are corrected mainly by visual and proprioceptive cues. Because it is amenable to manipulations in the lab, the role of visual feedback for flight control has been studied in detail for many decades in *Drosophila* and related species [63, 73, 105, 136]. Deviations from a straight path cause rotational optic flow that is coherent in a large part of the visual field. In aeronautic terms, these rotations are referred to as yaw, roll or pitch when they occur around the vertical (z), longitudinal (x) or transversal (y) axis respectively. In the optomotor response, flies correct for unintended deviations by turning in the same direction along these three axis [11], minimizing the rotational optic flow [73, 158] (**??**). The yaw optomotor response has been studied in detail to a greater extent than reactions along the roll or pitch axis, because of ease of measurement via torque meters [148], such that the term optomotor response will hereafter refer to the yaw response, unless explicitly stated.

In flies, the optomotor response engages both the head and the body. Interestingly, although the neck motor neurons are coupled to visual output neurons via chemical and electrical synapses, head optomotor movement occurs only while the animal is actively walking or flying [59, 67]. Furthermore, the retina has been shown to be mobile within $\approx\pm 6^{\circ}$ and follow large-scale motion, which was labeled as an optokinetic reflex and interacts with the optomotor response [51].

Under laboratory conditions, the optomotor response has been found to scale with the temporal frequency of a moving contrast rather than the angular velocity of features [11]. Finally, the visual input that evokes the largest optomotor turns has been shown to be dependent on the behavioral state of the fly. Walking flies respond the strongest to visual features moving at a temporal frequency of 1 Hz to 4 Hz, which is shifted to higher velocities in the range of 3 Hz to 12 Hz during flight [45, 64].

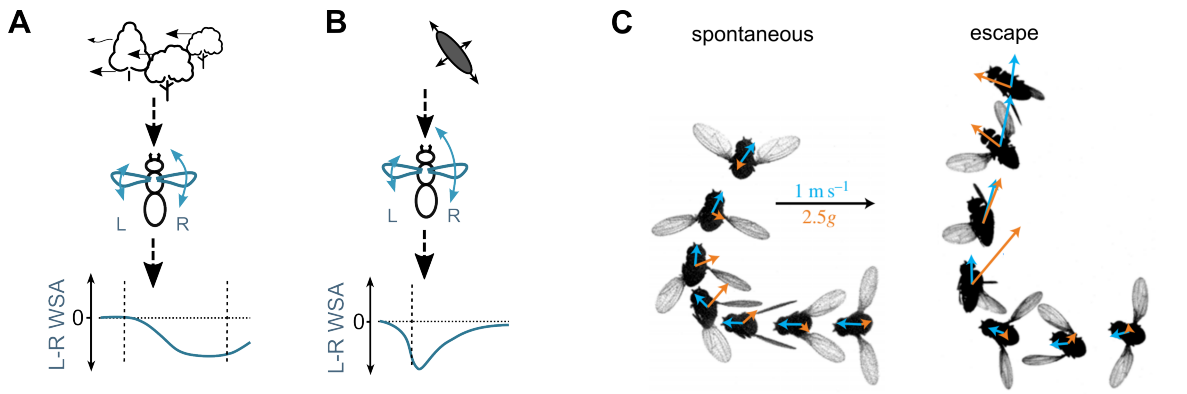

Figure 1: Optomotor and saccadic flight turns
(A) Schematic depiction of optomotor (left) and avoidance/escape (right) responses. Panoramic visual motion to the left evokes syndirection flight turns typically marked by slowly rising left (L) minus right (R) wing stroke amplitude (WSA). **(B)** Laterally expanding objects evoke escape saccades, marked by a sharp transient L-R WSA of large amplitude. **(C)** Example flight trajectories of *Drosophila hydei* during spontaneous (left) and escape (right) saccade show differences in sequence of body orientations. Arrows mark lift and velocity vectors (reproduced from [42]).

Flight turns

In contrast, however, everyday observations of flies in messy kitchens everywhere tell us that flies in general, and *Drosophila* in particular, typically fly in a zigzagging pattern. These intermittent rapid turns are referred to as saccades, in analogy to rapid gaze shifts in vertebrates and are characteristic for insect flight more broadly [12, 13, 89]. During optomotor stimuli, flies typically interrupt the syndirectional smooth turns by rapidly turning in the opposite direction. Due to the circumstances under which they occur, these are referred to as reset saccades [22], or occasionally as nystagmus saccades in analogy to mammalian eye movements [52]. Vision more broadly plays an important role in triggering saccadic turns, not only for reset saccades during optomotor turns, but also by signaling approaching obstacles or predators [142] (**??**). Saccades are not necessarily triggered by external factors, as flies still perform rapid turns in a stationary environment without visual input [73]. Additionally, other sensory modalities like wind mechanoreception feed into the decision as well [19]. Overall, saccades are initiated for a variety of reasons and the processes which prompt the fly to perform them are an open question under active research.

On the aerobatic side, saccades are remarkably fast maneuvers, effectively changing flight direction by up to $\approx 150^\circ$ over the course of only a few wing strokes, lasting <100 ms [108]. Mirroring the multitude of reasons that prompt a fly to perform a saccade, the execution may vary depending on the reason and external circumstances. To an opportunistic observer, these

saccades seem essentially the same at first, but discrepancies in the sequence of motions that compose them have been recorded in free flight using high-speed cameras [42]. So-called spontaneous saccades consist in a controlled redirection of the upward force with near-constant magnitude generated by the wings and involves rotation about mainly two out of three possible body axes, namely roll and yaw. In contrast, escape saccades begin by pitching up, and flies generate larger torques than during spontaneous turns, and reduce travel in the original direction as far as possible. (**??**). Thus escape saccades effectively prioritize speed and redirect away from the looming disc at the expense of stability of the flight and motion blur at the level of the sensory systems [107, 108]. Because of the technical difficulties in reliably measuring the position and orientation along all three axis of a freely moving small *Drosophila* in a sufficiently large volume, our knowledge is limited and it is uncertain how many different saccadic motion patterns could meaningfully be distinguished and what is their incentive. For example, collision avoidance is likely to be executed in a more controlled fashion than predator-escape saccades, where speed is paramount and being unpredictable could be an asset. Given that the internal motivation for individual saccades are unknowable in practice, it is more useful to distinguish between the two known types: escape/avoidance saccades to an approaching visual stimulus and other, course-changing or spontaneous saccades in the absence of a clear incentive.

As in the optomotor response, the head also moves during saccades in a way similar to the generated flight torque, though head movements start later and are executed with higher angular velocity [128]. It is worth noting, that the head yaw movement has been found to precede the saccadic body motion in bumblebees when approaching a specific site [12]. It remains to be seen, however, if this discrepancy is a matter of species, or if the head-body coordination depends on the reason for the maneuver. In tethered flight, where neither collisions nor predators play a role, flies spontaneously perform saccades, albeit at a reduced rate to what is observed in free flight. Whether this discrepancy is due to proprioception, internal state or optic flow is still debated.

1.1.2 Tethered flight

Due to its small size, ease of breeding and excellent accessibility to genetic manipulation, *Drosophila* is a prime model organism to study how a complex behavior like flight is generated and coordinated. Pioneered by Kunze [88] and Von Fermi and Reichardt [148] on bees and larger insects and adapted to *Drosophila* by Götz [62], flies have long been tethered (affixed) to pins to scrutinize their flight behavior in the lab by measuring the torque that they generate.

This has since been largely superseded by systems measuring the wing stroke of both wings separately by analyzing the video stream of IR-sensitive cameras, which allows to concurrently track additional body parts (e.g. in [22, 97, 138]). Such systems allow for other tethering methods, most importantly pyramidally-shaped holders which can be filled with saline and allow to dissect an area of the cuticle and to access the fly brain directly while leaving enough room for the wings to move. This enables targeted electrophysiological recordings and imaging techniques in behaving flies [97, 133, 153].

While visual input can be presented simply by placing flies in the center of e.g. rotating drums, or by means of various electronic displays [79, 120], other sensory modalities are harder to control for. In particular, proprioception is arguably impossible to fully implement, for the simple fact that the fly necessarily needs to stay locked in place, thus limiting the realism of experiments. The lack of proprioceptive feedback (or, alternatively, the unexpected proprioceptive perception) impacts the behavior of flies in certain ways that are not fully explored. Notably, flight maneuvers in rigidly tethered flies last much longer and exhibit larger differences between left and right wing motion than in free flight. To alleviate some concerns about the classical rigid-tether preparation, a magnetic tethering scheme was developed which allows for low-friction yaw movement [8], which demonstrated that proprioceptive feedback is the main reason for these discrepancies during saccades by providing the necessary signal for ending the maneuver. In contrast, visual feedback appears to be largely irrelevant during saccades [7]. Further investigations led to the conclusion that visual and proprioceptive feedback interact during flight control in a way that modulates the gain of visually evoked motor commands [6]. The absence of such feedback can cause artifacts in the behavior of rigidly tethered flies, as was recently shown to be the case for the stripe-fixation paradigm, but the optomotor response is a robust feature of behavior [123].

Overall, while rigid tethering is indispensable to record neural activity, it is important to keep in mind that the time course is different from free flight. Nevertheless, through decades of experimentation, a solid base for tethered flight has been laid down, which provides numerous reference points for what can be considered “normal” behavior in tethered flight, and which can be compared to results in free flight. Additionally, all direct observations of neural and muscular activity during flight are necessarily obtained in rigidly tethered animals, such that it should correlate best to tethered flight. Most relevant to the context of flight in open-loop experiments is the circumstance that flight behavior a) can never be fully observed as 3-dimensional maneuvers and b) are generally of considerably larger amplitude and longer duration.

1.1.3 Flight apparatus

A deeper understanding of the neural underpinnings that govern behavior on a cellular level requires a working knowledge of the motor system that these neurons actuate. In contrast to vertebrates, flying insects – apart from the Odonata family – don't control their wings directly. Instead, large asynchronous, stretch-activated power muscles contract the thorax and the mechanical properties of the exoskeleton translate the contractions into wing motion via the wing hinge and scutellar lever arms. By the stiffness of the scutellum during flight, the two wings of a fly are coupled to oscillate together with the same frequency and phase [37]. Despite this coupling through the cuticle, the indirect power muscles are involved in oscillating only one wing during courtship song [49]. To enact such asymmetries in wing motion, steering and indirect control muscles are necessary to modulate the movement of the highly complex wing hinge in intricate ways. The 13 smaller steering muscles attach to the base of the wing hinge and adjacent sclerites [40]. In this way, they modify how the wing hinge can operate, how the contraction of the thorax is transmitted to the wing, and the trajectory that the wing takes. The so-called indirect control muscles attach to other points of the cuticle. They are considered to mainly modulate the stiffness of the thorax, thus adapting the wing stroke frequency. Exactly how individual muscles change the flight trajectory is largely unknown, although certain muscles have identified functions (e.g. [72, 147, 149]). For instance, the first basalar muscle b1 is known to partially absorb mechanical work and in this way modulate the wing stroke amplitude if it is activated in a different phase, which makes it relevant for steering in e.g. the optomotor response, in conjunction with the b2 muscle. Thus, the renowned aerobatic performance of flies is effected mainly by changing the aerodynamic parameters of the wings, e.g. the angle of attack or stroke amplitude, but with probable contributions from the power muscles.

In *Drosophila* and other flies, the posterior pair of wings has evolved into halteres, small club-shaped appendages which move in phase with the wings and serve as proprioceptors. Although halteres are independently actuated by steering muscles, they move at the same frequency and a constant phase-shift with respect to the wings, mediated by exoskeleton structure [37] and are indispensable to stabilize flight [54]. While tethered flies are able to sustain flight and perform optomotor turns, proprioceptive feedback from halteres is necessary for natural free flight maneuvers [6].

1.1.4 Neural control of flight

In *Drosophila* and most other insect species, flight is mainly powered by the asynchronous muscles which are stretch-activated and need excitatory motor neuron input at a lower fre-

quency only. Steering, however, is mediated by regular synchronous muscles, which means that each muscle contraction is a direct consequence of motor neuron input. The motor neurons that actuate the appendages of a fly reside in the ventral nerve cord (VNC), in distinct areas according to the limb that they control. In that way, the VNC can be divided into ventral neuropils for each leg, an intermediate integrative area and the dorsally located tectulum which is innervated by motor neurons targeting the neck, wing and haltere muscles [30]. The three thoracic neuromeres, labeled pro-, meso- and meta-thoracic neuromere (Pro-, Ms- and MtNm respectively), are fused in *Drosophila* into a consolidated ganglion. Whereas the leg neuropils have discernible boundaries separating the neuropils for each leg, the tectulum is less segmented. This may reflect tight interactions between wings and halteres, or be a consequence of evolutionary development, where wings have evolved as outgrowths on the dorsal side and the tectulum is a duplication of the intermediate area. Each of these neuropils contains motor neurons, sensory afferents and local interneurons of the corresponding limb. Additionally, they are interconnected not only by descending and ascending neurons providing common input, but also by intersegmental interneurons exclusive to the VNC.

The premotor circuits that form these neuropils coordinate the activity of the various motor neurons, and integrate proprioceptive feedback. Steering muscle motor neurons of the fly are precisely timed to fire one spike per wing stroke, like the b1 muscle. Moreover, motor neurons typically fire at a precise phase of the stroke even when they are not active at every stroke [72]. Indeed, phase shifts of the spiking activity in b1 is known to cause changes in wing stroke amplitude, by changing the way that the muscle absorbs mechanical energy (as described in **??**) [147]. While the power muscles are driven by a central pattern generator, the steering muscles depend on proprioceptive feedback [71]. In flight, the halteres (and to a lower extent the wing) provide proprioceptive feedback to the motor system to stabilize flight [160]. The fact that steering motor neuron spikes are phase locked, which is abolished when the afferents are ablated, indicates that wing-synchronized afferents from the halteres control wing steering.

Since flight is guided by visual input, and activity in certain muscles (e.g. b1, b2 and i1) reflects the visual input, visual activity must be integrated with the ongoing flight, which raises questions about timing. Visual perception is transferred to the VNC by descending neurons, but there is no evidence to suggest that these signals arrive in a way that is coherent with the phase of wing strokes. Anatomy shows however that many descending neurons project axons to areas associated with the halteres [91]. Thus, a working hypothesis of how flight is visually controlled revolves around descending input to the halteres to effectively modulate the phase at which the haltere afferents trigger wing steering muscles. This could either mean that descending neurons converges with mechanosensory afferents, or that it acts on muscles

at the base of the halteres to modify the haltere trajectory. The idea that signals from the brain affect flight behavior via the halteres is referred to as the control-loop hypothesis [38, 39]. While that is an intriguing possibility, it is not the only way in which wing motion is modulated. Notably, flies still perform visually-evoked turns when the halteres are ablated or fixed in place (in tethered flight) [110], such that visual input is not exclusively mediated via the halteres.

When deconstructing specific behaviors, like flight turns or courtship song, it is evident that very similar movements of one wing occur under entirely different circumstances. Wings can move in a way that is fully symmetrical for straight flight course or pitching maneuvers, coordinated but with distinct fine-tuning for yaw and roll turns, or be fully disjunct when only a single wing moves during courtship. Dopaminergic interneurons in the VNC are critical to synchronize both wings [125], which exemplifies how a small number of neurons can generate different behaviors by modulating premotor circuits.

1.2 Visual system

1.2.1 Motion detection and the lobula plate

Vision is an essential sense for course stabilization in flight [90]. As a member of the *Diptera*, the complex eye of *Drosophila* is of the neural superposition type, which combines the visual acuity of the apposition eye with a neural architecture that pools the photoreceptor responses from neighboring ommatidia in a way that preserves the spatial resolution. This enhances the light sensitivity and allows them to fly at relatively high speed in low light conditions such as at dusk and inside dim rooms. The columnar structure of photoreceptors in the retina is preserved throughout the optic lobes, passing the visual information through the lamina and medulla neuropils to the lobula and lobula plate (LOP) (for review see [14]). Motion is detected through inter-ommatidial correlations in luminance over time, and fully emerges as the defining characteristic of the neuronal activity of T4 and T5 cells. The visual system distinguishes between luminance increments and decrements (On/Off), feeding into two concurring motion detection pathways in T4 and T5 cells, which accordingly track moving On or Off edges respectively. In the lobula plate, axonal projections from T4 and T5 cells exhibit direction-selective responses, and segregate into distinct layers by the directions that they encode [98] (**??**). Thus, the activity of neurites in each layer reflects visual motion in one of 4 cardinal directions, front-to-back (FtB), back-to-front (BtF), upward or downward. This neuropil harbors the dendrites of some of the most characteristic neurons of the Dipteran

family, the lobula plate tangential cells (LTPCs). Recognizable by their large somata and dendritic trees, several LPTCs have first been characterized in *Calliphora* before *Drosophila* became the preferred model organism in this area of research. Subsequently, homologous LPTCs were discovered in *Drosophila* through their similar response characteristics or anatomy. LPTCs identified in both *Drosophila* and *Calliphora* process optical flow across a large field of view. Notably these include cells of the horizontal system (HS cells) [129], cells of the vertical system (VS cells) [80] and others like the H2 cell [152].

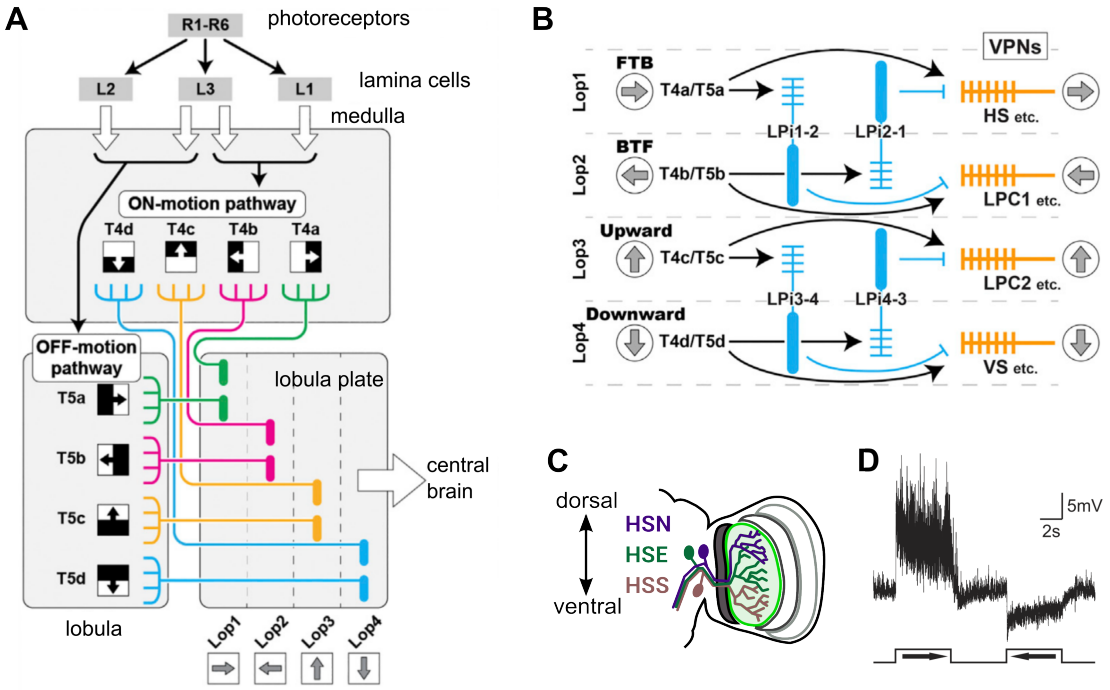

Figure 2: Visual motion is integrated by HS cells via On and Off-sensitive neurons
(A) Visual information is sensed by photoreceptors and split into On and Off pathways in the lamina. Subsequently T4 and T5 cells compute visual motion for On and Off edges respectively via intermediate processing steps, and provide local motion information to separate layers in the lobula plate according to cardinal direction. **(B)** LPTCs extend dendrites into specific layers in the lobula plate, where additional LPi (lobula plate intrinsic) cells provide inhibitory input from layers with opposite direction tuning (A and B reproduced from [134]). **(C)** Three HS cells receive input in the lobula plate with strongly overlapping receptive fields which tile the space from dorsal (HSN) to ventral (HSS). **(D)** HS cells are tuned to rotational stimuli, depalorizing during PD and hyperpolarizing during ND visual motion, but do not fire action potentials (reproduced from [129]).

1.2.2 HS cells

In particular the HS cells have been under scrutiny in *Drosophila*. Their defining characteristic is the sustained depolarization to full-field FtB motion, as well as a sustained hyperpolarization to the opposite, BtF motion [28, 129] (**??**). Three HS cells exist in each hemisphere, tiling the visual field dorso-ventrally, albeit with large overlapping areas, and are accordingly labeled HSN (N=north), HSE (equator) and HSS (south) (**??**). The bulk of HS cell input stems from the lobula plate, where they receive direct excitatory, cholinergic drive from T4/T5 cells in layer 1, which corresponds to the FtB signal [98, 130]. Additionally, LPi (lobula plate intrinsic) cells provide inhibitory, glutamatergic input that causes the hyperpolarized BtF response [100] (**??**).

It is worth noting that, while HS dendrites are located in the ipsilateral lobula plate, their receptive field extends to the contralateral side. This part of the receptive field is attributed to connections with other LPTCs, like H1, H2 and CH cells, which traverse the midline and convey information on contralateral motion vision [134]. Furthermore HS cell physiology is shaped by gap junctions that couple the axons of the three HS cells in each hemisphere. Additionally, they form electrical synapses with contralateral LPTCs, and remarkably also with downstream neurons, especially the descending neuron p15 (DNp15). In general, the abundance of gap junctions especially in insect brains raises intriguing questions about their functional implications for computation. In the case of HS cells, these gap junctions have been shown to play an important role in shaping their receptive field [117] and in stabilizing their membrane potential by shifting the electrical resonance frequency of the cell membrane [2].

On a functional level, HS cells are known to strongly contribute to the optomotor response of the head and the body in both walking and flying animals. Unusually, HS cells are non-spiking cells within a neuronal circuit, meaning that the motion signal is encoded as tonic de- or hyperpolarization of varying amplitude instead of a spike rate. Through optogenetic activation experiments, HS cell activity has been found to be sufficient to evoke slow turning in both flight and walking that resembles optomotor turns [20, 57, 69]. In contrast, bilateral silencing approaches has proven inefficient in suppressing optomotor turns, while head rotation could be largely abolished. Additionally, unilateral hyperpolarization by light-gated channels was shown to equally evoke turns in walking flies, indicating that the hyperpolarization response to Null-direction motion is transmitted downstream and functionally relevant. These findings suggest that optomotor turning is derived from a comparison of ipsi- and contralateral input where HS cells play a strong, but not unique role. What endows robustness to the optomotor

response and how the comparison between the left and right sides is effected are open questions. Parallel visual pathways could provide redundant and multifaceted input to a single comparator, or there could be parallel circuits for comparison and motor control.

While other LPTCs exhibit similar properties — large dendritic tree, contralateral RF components, gap junction coupling to neighboring, input and output neurons — HS cells in particular have been under close study, and surprising response characteristics have been revealed, which are not directly linked to visual input [56, 57].

1.3 Efference copy and the visual system

Every organism able to sense its surroundings shares a common problem: their own action causes a sensory perception that is indistinguishable from a perception caused by an external factor. Therefore, they need the ability to distinguish external (afferent) from self-generated (reafferent) sensory input. This concept applies to essentially all forms of action (efference) and perception, from simple secretion of molecules to the environment by unicellulars to complex sounds and speech in communicating mammals.

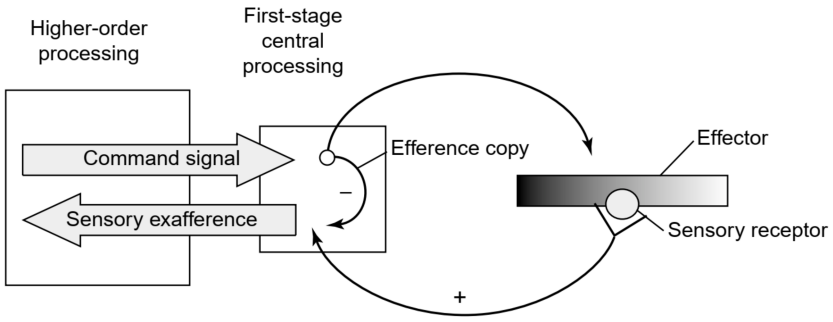

Figure 3: Postulation of an efference copy mechanism
Higher processing areas process sensory exafferent information and provide motor command signals. A motor command that is sent to the effector (muscles) triggers a sensory signal. In a first stage of processing, the reafferent sensation is compared to an efference copy of the motor command with opposing signs, such that the efference copy cancels the reafference (reproduced from [33], simplified from [78]).

Seminal work by Holst and Mittelstaedt [78] suggested that this is achieved via an efference copy (EC), which counteracts the (expected) reafferent input in the context of locomotion and vision in *Drosophila* (**??**). At the same time, an influential study on fish came to convergent conclusions and coined the term corollary discharge [135]. For the purpose of this work,

we will not distinguish between efference copy and corollary discharge, because they refer to the same basic concept. Examples of such mechanisms have been found in a number of organisms and sensory systems, where they serve to stabilize gaze during locomotion [29, 55], to retain a contiguous view of the world during rapid eye saccades [159], to set the gain of reflex-mediating proprioceptors in the muscle spindle in mammals [32] and to filter the self-generated sound in auditory perception in crickets [118] (for review see [32, 33]). Importantly, several known mechanisms for EC indicate that it is finely tuned to the expected reafferent input and does not typically completely silence afferents.

Although EC mechanisms are necessary for virtually all motor action in one way or another and corresponding signals should pervade sensory systems, its neuronal underpinnings have remained largely elusive. As described above, flies fly in a straight path that is interrupted by saccadic turns. The straight paths are stabilized by visual feedback, as flies detect coherent motion of their surrounding, which is referred to as the optomotor response. During intentional saccadic turns, however, the stabilizing optomotor feedback loop needs to be suppressed.

HS cells – described in detail in the previous section – are tuned to the rotational optic flow that is the hallmark of the optomotor response. Based on activation and silencing experiments during walking and flight, they are thought to control yaw optomotor responses that stabilize straight paths. Interestingly, it has been shown that HS cells receive locomotor-related signals. In flying animals, HS cells receive a saccade-related input during spontaneous saccades, which has been posited to function as an EC that suppresses the yaw optomotor reflex [84, 85]. While the sign of this input (de-/hyperpolarizing) is fit to counteract the supposed reafferent input, it has remained unclear how it affects the responses to large-field optic flow in HS cells.

1.4 Descending neurons

In insects and other arthropods, an accentuated dichotomy exists between motor control circuits located in the VNC and the sensory and associated areas in the brain. Motor centers rely on sensory processing and decision-making in the cerebral ganglia. Equally, proprioception that arises throughout the body is first received in the VNC, such that multimodal integration in the head requires information about the body and the state of the locomotion from the VNC. Descending and ascending neurons link these two components of the CNS and form the neck connective. Together, they form an information bottleneck of limited bandwidth, with $\approx$ 1300 DNs and $\approx$ 2400 ANs compared to e.g. $\approx$ 12800 visual projection neurons [43].

Descending neurons (DNs) have their soma and dendrites in the cerebral ganglia and project to the VNC where they connect to motor centers of the wings, halteres, neck, legs and abdomen. Conversely, the soma and dendrites of ascending neurons (ANs) are situated in the VNC with axonal projections towards the cerebral ganglia.

Information bottlenecks are a common occurrence between different areas of nervous systems, and let us investigate fundamental questions about the organizational principles of neural systems. Main axes of inquiry are to determine what kind of information is transmitted and how the bandwidth is optimally utilized with respect to encoding, information compression and later expansion in downstream targets. The pronounced separation between cerebral and ventral ganglia, the limited number of DNs involved and the genetic tools available in *Drosophila* have made this an emerging area of research.

In more practical terms, these aspects are reflected by the open question whether DNs function as command-type neurons, where individual DNs code for complex actions, or if populations of DNs dynamically combine to generate natural behaviors. Indeed, several DNs have been identified that act like command neurons, such as the Moonwalker DN causing flies to walk backwards [9], an anterior DN that is correlated with saccade-like turns [131] and the giant fiber escape pathway [143]. Additionally, activity in certain DNs can elicit complex movement patterns, like repeated head grooming driven by DNg08 activation [21]. However, there is an experimental bias rooted in the difficulty to record the population activity of DNs because of scattered neurites and cell bodies, such that single command-like neurons are easier to detect. Even the observation that a specific DN can elicit a certain behavior does not exclude the possibility that the same behavior is normally coordinated and modulated by additional factors in the wild, like the landing responses elicited by DNp07&p10 [1], or controlled via a different pathway entirely. In studies based on artificial activation assays, certain DNs may appear as command neurons by coactivating interconnected DNs which form a module with coordinated activity under natural conditions. Besides, some DNs elicit certain behaviors when activated, but the nature of the action may depend on the ongoing behavioral state. To our knowledge this has not been definitively established for any particular neuron, but hints to such a mode of operation have been presented by Cande *et al.* [21]. Investigating these questions in DNs may help to elucidate common principles underlying the functional organization of nervous systems.

A new technique for 2-photon imaging in the neck connective during behavior has generated a more comprehensive picture of DN activity in behaving flies [3]. This has allowed to resolve the simultaneous activity of ≈100 DNs. It was concluded that the largest fraction of DNs is active during locomotion (in this case walking), and correlated with turning behavior. The activity

pattern did not strongly reflect the reason for turning, such as an external stimulus or an internal signal. Interestingly, some DNs were found to encode the presence of certain olfactory stimuli rather than a behavioral variable. Notably, a large proportion of DNs is associated with walking activity. On one hand, this may reflect an intricate modulation of many aspects of locomotion apart from simply encoding forward and turning velocity. On the other hand, it might as well indicate that several concurrent pathways are typically active simply to modify the activity of locomotor pattern generators. While some DNs have identified functions during flight or grooming, most efforts to elucidate the role of DNs have been focused on walking. In flight, high throughput screening suffers from difficulties to track the minute details of wing motion in three dimensions using multiple cameras at the higher temporal resolution necessary for flight compared to walking. Additionally, imaging approaches in or close to the VNC don't leave enough space for the wings to move in tethered flight. Therefore, despite general progress in this area, the function of DNs, both individually and as a coordinated population, is still far from conclusively understood, especially during flight.

A notable addition to our knowledge about descending flight control is the discovery of a population of highly similar descending neurons in the gnathal ganglia, namely DNg02, which appear to regulate wing stroke amplitude and are activated by rotatory and translational optic flow, resembling HS cell activity patterns. Additionally their activity is correlated with the contralateral wing amplitude [112]. This is suggestive of a steering command for optomotor turns, but unilateral activation leads to bilaterally increased wing stroke amplitude instead of turning responses [114]. Judging by these results, flight responses may require concerted activity of several DNs, regulating separate aspects of the wing steering process, like specific muscles, firing phase or spike rate. Recent progress has considerably increased our knowledge about the role of DNs and the organization of the motor centers in the VNC [26, 91]. Future work could integrate the findings from DNs with the architecture of the motor centers to build realistic models of flight muscle regulation.

In this study, I aim to contribute to our understanding how specific behaviors are executed through modulation of a network that generates motor commands. By investigating a DN putatively mediating the control of optomotor responses, a base for future work on the flight motor circuit is laid down.

1.5 Genetic toolkit

1.5.1 The Gal4 expression system

First and foremost, *Drosophila* has been a genetic model organism for more than a century. Throughout the past three decades, many genetic tools have been developed, which also serve to manipulate neural function and behavior. Most relevant for neurophysiologists are the possibility to target a population of cells down to the level of single neurons, which can be combined with an effector protein of choice. This is the Gal4 transcription factor adapted from yeast, which binds to the UAS promoter and leads to the transcription of any effector gene. Since the advent of enhancer-trap lines which placed the *Gal4* element in semi-random locations in the genome [15], the Gal4/UAS expression system has undergone several improvements. To mitigate the frequent side effects of inserting the *Gal4* gene into an existing regulatory sequence, copies of regulatory sequences that are likely active in the brain have been linked to *Gal4* and inserted into "neutral" landing sites [116]. Genomic insertions can be reliably targeted to these sites by the PhiC31 integrase and cause no or only little disruptive effects on the phenotype [115]. Additionally, this approach is flexible in terms of the gene that the inserted enhancer elements regulate, so it allows replacing the *Gal4* gene by any other gene of interest like *LexA* or *Gal80*.

A significant improvement to making lines more specific consisted in splitting the Gal4 transcription factor into two smaller factors: the promoter-binding domain and the RNA polymerase-recruiting domains. Each of these can be linked to different regulatory elements. Since both of these are required for transcription of the *UAS-effector* construct, it enables to refine the expression pattern by an intersectional strategy [96]. In this way, large libraries of split-Gal4 lines have been generated and screened, which ideally allow control down to the level of a single neuron per hemisphere. To further exclude effects of endogenous "leaky" expression mediated by unidentified enhancer elements in the vicinity, a so-called empty split-Gal4 line has been generated in the same genetic background to be used as negative control in experiments. Far from being exhausted, this strategy is actively used to generate new collections to target specific neurons like (pre-)motor neurons, descending, ascending and mushroom body output neurons [46, 124, 145], assisted by a refined knowledge of the activation pattern of enhancer elements [24, 102].

1.5.2 Effectors for neuronal silencing

The second component of binary expression systems like Gal4/UAS are the effector genes under transcriptional control of the *UAS* regulatory element. In the context of neurophysiology,

precisely targeted expression allows manipulating the neuronal activity to gain insights into function. Apart from reporter genes like GFP and all its variants, a number of tools are available to suppress or alter neural function. For example, targeted expression of apoptosis-inducing genes permit to ablate specific neurons in a circuit [157]. An important caveat of genetically determined ablation include the fact that expression may start at an earlier point during development. When active in a neuroblast before final differentiation, other cells are ablated alongside the target. Even when only the target is ablated, other cells might partially adapt to fill the gap during development.

For less invasive methods to interfere with neural function, it is possible to impede synaptic transmission. Harnessing the mode of action of Tetanus toxin, expression of only the light chain of the toxin (TeTx) suppresses the fusion of synaptic vesicles by cleaving synaptobrevin [140]. While constitutive presence of very low levels of TeTx in the presynapse should conceptually block all release of neurotransmitter, its efficiency varies strongly by cell type [144]. Combining targeted expression with temporal control, the temperature-sensitive dynamin mutant shibire^{ts} blocks endocytosis and thus leads to a depletion of synaptic vesicles at an elevated temperature around 30 °C [86]. However, flies typically refrain from flying at higher temperatures which limits the usefulness in behavioral assays. Additionally, previous studies reported nefarious effects on microtubules and reduced vesicle counts at lower temperatures as well [61].

Another approach consists in altering the signal transduction in neurons. Notably, neurons can be silenced by ectopically expressing additional potassium inward rectifying channels like the human Kir2.1 [4, 77]. These additional K-conductances have been described to hyperpolarize and shunt neurons in *Drosophila*. Nevertheless, the precise effect depends on the concentrations of ions and other conductances in the cell, which are usually unknown. In general, a variety of tools for silencing neurons exists in *Drosophila*, but each comes with caveats and their respective efficacies differ strongly from case to case [121, 144]. Prudently, more than one method should be applied with appropriate controls.

1.5.3 Optogenetic control of activity

In recent years, genetically encoded light-gated ion channels have risen to become the standard tool for manipulating neural activity. A diverse class of light-sensitive transmembrane proteins called Channelrhodopsins is ubiquitous in unicellular algae, where they serve as light sensors to find areas with suitable light conditions. By ectopically expressing these genes in neurons, the voltage potential can be manipulated simply by illuminating the area without necessarily

worrying about spatial precision. This allows for precisely timed manipulation at the single-cell resolution offered by *Drosophila* genetics.

Since the adoption of the cation-conducting channel ChR2 from *Chlamydomonas reinhardtii* that is most sensitive to blue light, a vivid area of research strives to improve existing and discover new channels to improve their usability for specific application (for an overview see e.g [35, 101]). The main concerns have long been to generate sufficiently large photocurrents at lower light intensity, to reduce desensitization and to increase opening times. Once significant progress had been made, it rapidly became popular for *in vivo* experiments. In the case of *Drosophila* in particular, a major leap consisted in the engineering of red-shifted variants, such that the activating light is markedly less visible to the flies themselves due to their lack of red-sensitive photoreceptors. A variety of red-shifted cation channels exist in the wild, out of which CsChrimson is used most commonly [87] and will be applied in the work presented here. It is worth noting that light-sensing proteins typically rely on a light sensitive cofactor.

Channelrhodopsins rely on retinal as their light-sensitive chromophore that is embedded into the protein, much like vertebrate rhodopsins. The opsins of Dipteran photoreceptors however require 3-hydroxyretinal [70], such that non-hydroxylated retinal is not present at sufficient concentrations in the organism. Therefore, retinal is typically provided in the form of light-sensitive all-trans-retinal (ATR) through the food, such that flies need to be reared in the dark for one or several days prior to experiments [137]. While this allows for easy negative control by not feeding retinal, concerns have been raised that a high concentration of ATR in the food might impact health and that light-deprivation leads to defects [5]. Although supplying flies with high concentrations of β-carotene increases the availability of ATR to the level required for optogenetics [93, 150], currently the standard practice still relies on ATR-supplemented food and adequate controls.

Optogenetic methods have reached wide-spread usage, yet the search for new variants continues in order to enable efficient hyperpolarization *in vivo*. Through engineering of the cation-conducting pore domains, channels selective for anions like Cl^- have been created [155]. However, anion-conducting channels that were discovered in *Guillardia theta* (GtACR1 and GtACR2) dominate current practice in *Drosophila* experiments [103]. Contrary to CsChrimson, GtACR1/2 are tuned to blue light, which is a behaviorally relevant stimulus in itself. Building on the knowledge built over the past two decades, the engineering approach has since provided red-shifted anion-selective channelrhodopsins that function *in vivo* in *Drosophila* [154]. Since the genetic pool of algae is probably not exhausted yet, and that the knowledge of channelrhodopsin function facilitates engineering these, further improvements can be expected in the years to come.

1.6 Goals and thesis outline

Neuroscience is typically focused on internal processes that transform sensory information. However, the relevant variable in terms of evolution is the interaction with the environment, i.e. behavior. Not only does the brain transform sensory information into behavior, but behavior also influences sensory perception. The main motivation of this work was to elaborate on the bidirectional link between flight and the visual system via an efference copy mechanism that suppresses the optomotor stabilization response. As laid out in the previous sections, an EC signal has been reported to act on HS cells during spontaneous saccades. The aim of my thesis is to establish how the reported EC affects the optomotor response, which is controlled by HS cells.

First, by recording intracellularly from HS cells *in vivo* in flying *Drosophila*, I aim to resolve the effect that a saccade-related EC has on the processing of optic flow in HS cells. To facilitate this, saccades are elicited by looming stimuli followed by optomotor stimuli, enabling me to time the saccade onset and to dissect the effect of the EC on both preferred- and null-direction motion. It is shown that the EC is specific to HS subtypes, and that it suppresses processing of preferred-direction optic flow in HSN cells.

Second, to determine the context in which the EC occurs, I reconstruct the reafferent visual input to HS cells during saccades. By leveraging an existing dataset of flight trajectories in three dimensions including body orientation, it is found that saccades elicit optic flow in both preferred- and null-direction. These results offer an explanation for unexpected findings *in vivo*, where preferred-direction responses were markedly suppressed during ipsiversive saccades that were expected to cause null-direction optic flow.

An EC does not only need to be tuned to the reafferent input, but it should also target the appropriate pathway. Thus, to corroborate the role that this EC plays in behavior, I investigated the circuit downstream of HS cells. HS cells are thought to control optomotor responses, yet our understanding of this behavior is incomplete. In the third project, I analyzed the behavioral role of one descending neuron which relays the activity from HSN cells to the VNC through intracellular recordings along with silencing and activation assays in tethered flight. Indeed, this DN is critically involved in the optomotor response under certain stimulus conditions, but unable to evoke turns by itself. Additionally, it reflects the suppressed visual processing observed in HS cells after presentation of a looming stimulus.

2 Saccadic Flight and Reafferent Visual Motion

2.1 Multiple mechansims suppress motion vision in HS cells in flying Drosophila

This section encompasses work that has been published in a peer-reviewed journal under the title "Multiple mechanisms mediate the suppression of motion vision during escape maneuvers in flying Drosophila" by Philippe Fischer (this author) and Bettina Schnell, published in *iScience* vol. 25(10) in 2022, DOI 10.1016/j.isci.2022.105143 .

Here, I present a summary of those findings. The original publication is included as **??**, in accordance with the doctoral regulations of the faculty of Natural Sciences and Mathematics of 2022. The data collection as well as the manuscript writing have been done jointly by Bettina Schnell and this author. Formal analysis, software development and data visualization was conducted by this author exclusively.

An efference copy (EC), by definition, causes a hyper- resp. depolarization which opposes the expected reafferent sensory input of the action. To study the effect of an EC on the optomotor pathway, we performed intracellular recordings of HS cells during tethered flight in head-fixed flies, while monitoring the turning behavior as the difference of L-R WSA. We recorded from HS cells in the right hemisphere only, which depolarize upon clockwise rotation of the visual scene and hyperpolarize when exposed to counter-clockwise motion, without selecting for a specific subtype.

Investigating the hypothesized effect of an EC on visual processing in HS cells required observing flight saccades in conjunction with optomotor stimuli. To elicit turns, we presented a looming stimulus from either the left (contralateral of recording site) or the right side (ipsilateral), mimicking an object approaching at a constant velocity of $1.5\,\mathrm{m\,s^{-1}}$. This stimulus reliably elicited large changes in L-R WSA away from the side of the looming disc, which likely correspond to escape saccades in free flight. Henceforth, these flight responses will be referred to as saccades, despite the fact that the flies could not actually turn away in tethered flight. Leveraging the behavioral variability in this experimental paradigm, trials could be algorithmically sorted into two sets depending on whether the fly executed an escape saccade or not.

For looming stimuli presented on the right side, which elicited turns to the left, we did not find a qualitative difference between trials with and without a saccade. As it has previously been reported that spontaneous saccades to the left are associated with hyperpolarization in HS cells [85], we detected saccades during the periods where no visual motion was shown on the screen. Consequently, we confirmed that on average, HS cells hyperpolarize during leftward spontaneous saccades. However, there exists a large variability between individual cells that could not be explained by the amplitude of saccades as peak L-R WSA.

Applying the activity during spontaneous saccades as criterion to split the recorded cells into a hyper- and a non-polarizing subset, we found that only the spontaneously hyperpolarizing subset also hyperpolarizes during escape saccades with a similar amplitude. Thus, the equivalence of spontaneous and escape saccades for HS cell activity was demonstrated.

Similarly, the activity of HS cells to looming from the left side was compared between trials with or without saccades. Splitting the cells into subsets by the mean activity level during saccades, we obtained a hyperpolarizing and a non-polarizing subset. The subsets obtained by independent criteria applied to looming from the left and right were largely the same, hinting at a functional subdivision among HS cells. Interestingly, the hyperpolarizing subset exhibited a biphasic activity during spontaneous saccades, in which an initial depolarization is followed by a larger hyperpolarization, whereas the average of all cells was depolarized.

Furthermore, motivated by the existence of functional groups and, between these, different responses to the looming stimulus itself, we hypothesized that the subsets we identified correspond to HS cell subtypes. By recourse to a previously recorded dataset of identified HS cells obtained by Bettina Schnell in a different context in the lab of Michael H. Dickinson, we were able to prove that the three HS subtypes exhibit significantly different activity during spontaneous saccades. Indeed, this confirms the existence of a hyperpolarizing subtype,

namely HSN, in contrast to the depolarizing HSS subtype. Thus, HS subtypes were shown to be functionally specialized, and that an EC mechanism acts on the level of single cells. HSN activity in this dataset strongly resembled the corresponding signal of the hyperpolarizing set recorded in leftward spontaneous and escape saccades.

Finally, the effect of this inhibitory input to HS cells due to saccades could be addressed by coupling the looming to optomotor stimuli. First and foremost, the processing of excitatory visual motion was clearly suppressed during escape saccades towards the right and the left in the hyperpolarizing subset only. Thus we have identified evidence for a true EC, suppressing excitatory reafferent optic flow. Additionally, for looming stimuli on the right side (ipsilateral to the recording site), motion vision was partially suppressed by the visual experience alone in both subsets, but saccades caused stronger and longer-lasting inhibition in the hyperpolarizing subset only. Therefore, careful experiment design and interpretation is necessary to disambiguate between efference copies and other effects in the visual system. Surprisingly however, inhibitory optic flow processing was not suppressed during rightward saccades, for which the reafferent optic flow is conceptually inhibitory.

In conclusion, we provided evidence for a true efference copy acting on HS cells, tuned to block reafferent optic flow as a consequence of behavior. While the hyperpolarizing saccade-dependent input to HSN cells has been described before [85] and that it is correlated to the cell's response to yaw stimuli [84], this work demonstrated that it is effectively blocking the typical response to yaw motion as previously postulated.

Shortly before this project was completed, another study found evidence for an EC acting on HS cells during escape saccades evoked by ipsilateral looming stimuli [52]. Some of the observed discrepancies may be attributed to the different categorization of saccades as "small saccades", whereas we considered those as "no-saccade" trials. However, while their approach delivered more pronounced EC potentials by presenting PD motion to depolarize HS cells *before* the looming stimulus, it does not directly show how the EC affects the processing of visual motion that is the consequence of the saccade. Additionally, we present results from both left- and rightward saccades and analyze the effect on both PD motion vision. This leads to a more complete picture and unexpected findings with respect to ipsiversive saccades as well as ND motion vision.

It was previously unsuspected that the hyperpolarizing signal does not generalize to all HS cells. Even though all three subtypes share highly similar response characteristics to optic flow, and thus presumably require a similar EC [84], the hyperpolarizing signal is instead limited to the HSN subtype, and putatively influences HSE via gap junctions. Moreover, the EC

signal that was recorded here exhibited a biphasic time-course for putative HSN cells during rightward, and for putative HSS cells during leftward saccades. It is possible that the different HS cell subtypes receive different visual input because of their diverging receptive fields, and therefore require an efference copy fine-tuned to act only on specific subtypes. Alternatively, different HS subtypes might serve different functions during flight control. A saccade in free flight is a complex maneuver consisting of rotations and counter-rotations along all three body axis as well as translatory movement. This makes it difficult to judge, what the changes in L-R WSA correspond to, exacerbated by the fact that changes in L-R WSA have been shown to be much smaller in free than in tethered flight.

2.2 Fly perspective model

In **??**, we found that HS subtypes are differentially targeted by efference copy signals, especially when comparing HSN to HSS. Strikingly, HSN cells receive a hyperpolarizing input during saccades, which strongly reduces the response to excitatory, but not inhibitory optic flow in our experiments. When reasoning about yaw turns in a plane, turns to the right for instance elicit optic flow towards the left, which is inhibitory to HS cells in the right hemisphere. The fact that hyperpolarization is not obviously reduced in this situation casts doubt on the interpretation that the signal we observed acts to suppress reafferent visual input. However, flies perform banked turns to escape looming objects by first rolling around the longitudinal body axis and pitching upwards before the body starts to yaw significantly. Thus saccades involve rotation in more than 2 dimensions and the fly body does not perform a yaw turn in a plane, but along a more complex trajectory [42, 108].

I therefore modeled the visual experience of a fly in terms of optic flow during a saccade by retracing the visual input during escape turns measured in free flight. As depicted in **??**, from a dataset of escape saccade trajectories in free flight [109] I selected traces where the looming stimulus approaches from a direction comparable to the looming stimulus in our own experiments in **??**. By integrating the rotational velocities, the angle along each body axis was reconstructed (**??**). These saccade trajectories, onsets and reconstructed body angles were used to reconstruct the first-person-view of a fly during saccades in a naturalistic setting. The resulting local optic flow was averaged over the area of the visual field that is perceived by each ommatidium. The movies in **??** and **??** in **??** show the scene from a fly's perspective and the corresponding optic flow for an exemplary saccade.

As a result, a full representation of optic flow on the level of the fly retina is obtained for all traces (**??**). Inspection of the image sequences reveals that important shifts from a straight translational optic flow pattern become apparent early on in the trajectory. The onset of a saccade is defined via a threshold of the body acceleration in the horizontal plane (not rotational acceleration), following the original publication. Because flies initiate rapid turns by banking their body – i.e. rolling and pitching first – changes in body orientation and the accompanying reafferent optic flow precede the defined saccade onset. Nevertheless, the magnitude of optic flow experienced by the fly before a deviation in yaw heading becomes apparent is considerable.

Interestingly, the translational optic flow caused by objects that are in the closer vicinity is strongly reduced during the maneuver. Rather than objects drifting out of the field of view in

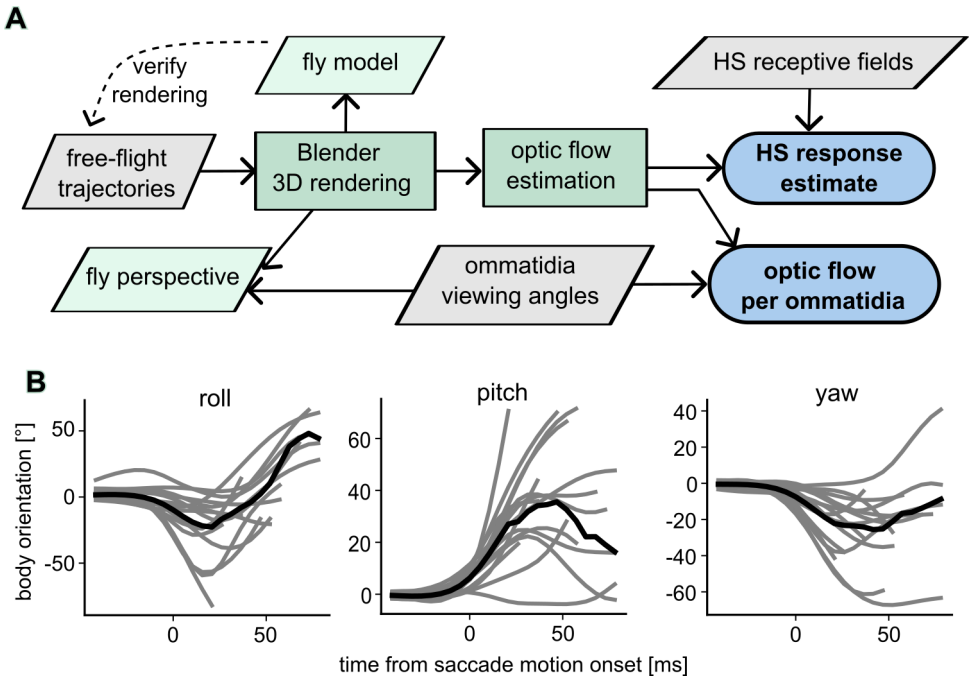

Figure 4: Fly perspective modeling approach
(A) Schematic workflow representing external input as white diamonds, output as green rhombus, processing steps as green rectangles and end results as blue ovals. **(B)** Angles around the three body axes in the traces selected for simulation and homologated to represent turns to the left for plotting (reproduced akin to [109]) by inverting roll and yaw (not pitch) angles with individual traces indicated in gray and average in black.

our Blender scenery, the shift in linear velocity from forward- to up- and sideward-pointing causes the optic flow of objects in the proximity to become negligible. As a consequence, the estimation of rotational visual motion becomes simpler in the absence of potentially confounding inhomogeneity in optic flow caused by varying distances to objects.

To gain a better understanding of the optic flow that is relevant to HS cells, the receptive field of HS cells in the right hemisphere was applied to the flow map, which has been measured previously in a sufficiently large portion of the visual field [129]. The result corresponds to a qualitative prediction of the membrane potential in arbitrary units during free flight escape saccades. Remarkably, the predicted response in **??** is bi-phasic, with an inversion of the sign shortly after the fly starts to effectively yaw. More surprisingly, the initial response, which largely takes place before the change in azimuthal (yaw) heading becomes apparent, corresponds to the response expected if saccades were executed in the horizontal plane alone. That is to say, when flies perform saccades towards the right, causing the visual field to rotate leftward in a 2D perspective, HS cells in the right hemisphere would hyperpolarize, which

is what is predicted in the first phase. However, this hyperpolarizing Null-direction motion in free flight is first induced by the roll-and-pitch part of the maneuver, and amplified as the change in yaw picks up speed. Analogously, during saccades to the left (**??**), putatively causing preferred-direction optic flow, the depolarization is limited to the first phase before switching to hyperpolarizing input. In saccades to the left, the time course is less stereotyped, which is presumably an artifact of an inconsistent onset detection due to a low threshold. For clarity and because leftward saccades are apparently symmetrical to rightward saccades, I will focus on the rightward saccades in the subsequent analyses.

In our findings on HS subtype-dependent saccade-related potentials, we hypothesized that the subtypes receive different visual input, therefore requiring different efference copy signals. When separately considering the horizontal and vertical components of the predicted HS cell response in **??**, HS subtypes exhibit different response amplitudes. In HSN and HSE cells, the vertical component is negative during the first phase of the leftward saccades (lighter color segments), showing that optic flow is significantly deviating from the cell's preferred vertical orientation. Furthermore, HSN cells typically show markedly larger amplitudes of the vertical component in particular. Nevertheless, the horizontal component is generally an order of magnitude larger for most of the trajectory, so it dictates the response of the cell throughout the trace.

These trace plots are oriented along a diagonal, meaning that the X- and Y-components are correlated. However, the slopes of imagined regression lines through the traces are ostensibly different between subtypes. This has prompted me to further inspect the direction of optic flow vectors with respect to their vertical position in the ommatidial field. As the horizontal component is shown to dominate HS cell responses, I focused on the change of horizontal direction at $\pm 90^\circ$, where an angle $\alpha \in [-90, +90]$ is excitatory for HS cells in the right optic lobe (**??**). For a rightward saccade experienced by an HS cell in the left hemisphere ($\lambda < 0$ e.g. -10°), the angles of optic flow vectors were pointing leftward (inhibitory) regardless of elevation except near the top, outside of the receptive field of HS cells. In contrast, there was a change of horizontal direction at a certain elevation in the right hemisphere. That point, where the vectors bifurcate into left- and rightward pointing, shifts downward across the frontal visual field going left to right. Interestingly, flow vectors rapidly change horizontal direction at $\approx 30^\circ$ over a large portion of the right visual field ($\lambda \gtrapprox 15^\circ$).

More importantly, optic flow over time is generally directed mostly left- and upward (angle $\alpha \in [+90, +180]$) during earlier stages of the maneuver and subsequently shifts to a predominantly rightward direction ($\alpha \in [0, +90]$, violet line) at azimuth positions near the center of HS receptive fields (**??**). As HS cells respond predominantly to horizontal optic flow, this change

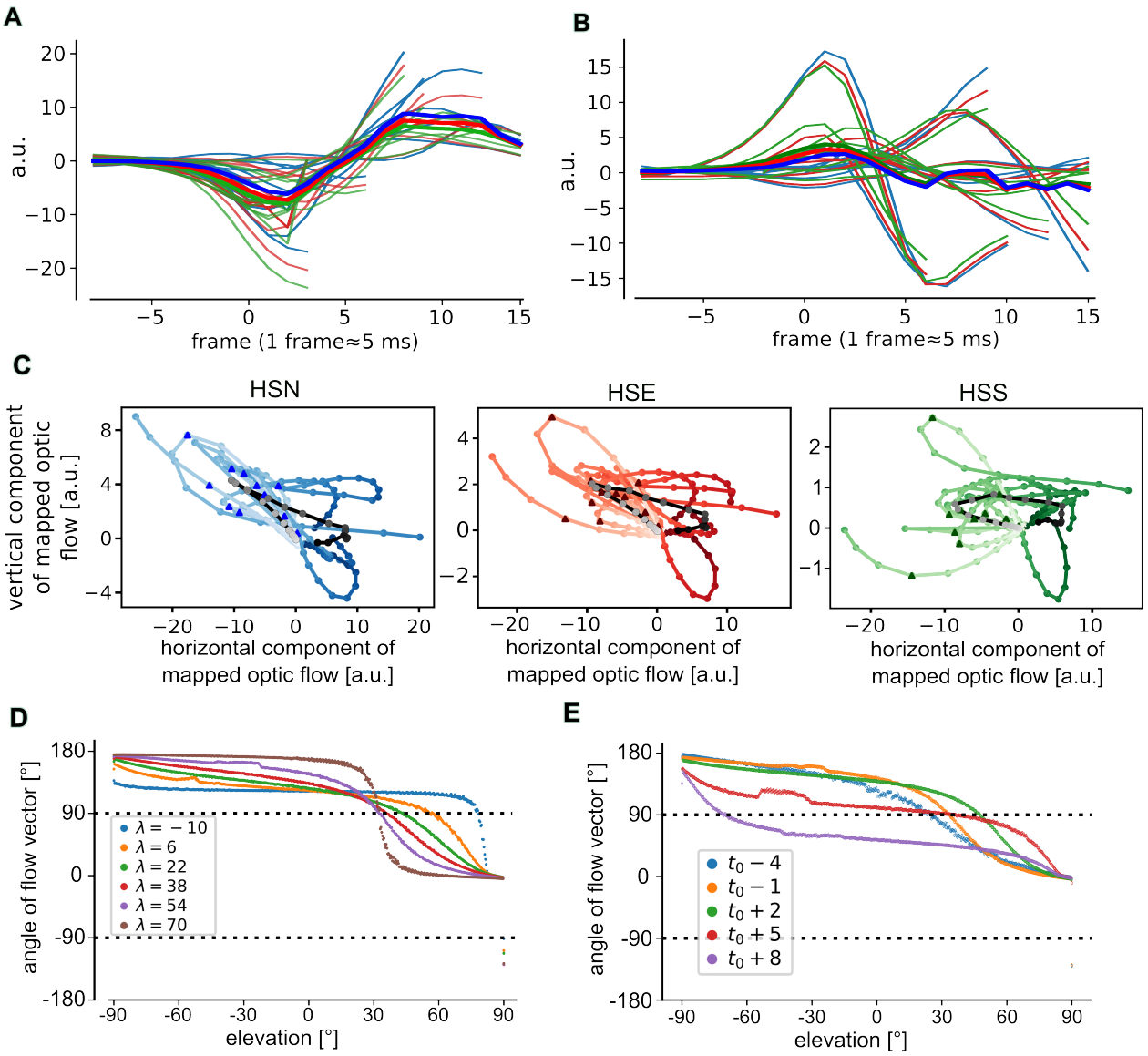

Figure 5: Predicted HS responses during saccades
(A) Reconstructed voltage response of HS cells to reafferent visual motion during saccades to the right in arbitrary linear units, color-coded by subtype with individual trajectories (thin lines) and average (thick lines) of HSN (blue), HSE (red) and HSS (green). **(B)** Same for saccades to the left. **(C)** Reafferent visual motion in rightward saccades divided into horizontal and vertical components weighted by HS subtype sensitivity. Individual trajectories are shown as colored lines progressing from early (light color) to late phases (dark color) and body yaw onset is marked by triangle, with the average in grey for HSN (left), HSE (middle) and HSS (right). **(D)** Angle of flow vector (0°≡right/east and 90°≡up/north) depending on the vertical location in the field of view for a range of lateral positions λ representative for an exemplary trajectory. **(E)** Analogous representation of optic flow vector angle for a range of points in time, with t_0 denoting the onset of yaw acceleration.

marks the transition from hyper- to depolarized, and mirrors the preceding representations. Remarkably, the elevation of ≈30° sits close to the central elevation of the HSN RF, such that little deviations can have a large effect on predicted HSN responses. For instance, inaccuracies of the receptive field measurements could have larger effects here. Reported receptive field maps of HS cells diverge regarding the elevation coordinate by up to ≈20° depending on setup and tethering procedure, which is typically not quantified [117, 129]. The trajectories used here do not include the orientation of the head with respect to the body, although other reports suggest that the head is kept at a tilt of ≈30° in straight flight. Considering the way that receptive fields are mapped in tethered flies, the head appears to be tilted by a similar angle.

If the bifurcation point is moved up- or downward, it implies that the hyperpolarized initial phase may be reduced or increased in HS**N** if such deviations occur in a given saccade, but the surprising depolarization in the second phase is not affected by this. Indeed, in the short timespan of 3 frames (≈60 ms) the bifurcation point migrates from the elevation at ≈30° to ≈−70°, which fully engulfs the receptive fields of all three HS cells in preferred-direction optic flow. This end point is significantly further down than the RF of HSS to the extent that it has been mapped thus far. Only under extreme assumptions could HSS be exposed to very little depolarizing optic flow and remain hyperpolarized. In conclusion, both HSN and HSS responses are likely biphasic and with a depolarized late phase. Accommodating very large experimental uncertainties may either reduce the early hyperpolarization in HSN or the late depolarization in HSS for down- or upward errors respectively. The proportions of de- and hyperpolarization in reality however are likely to differ from the model.

Previous studies suggest that the head undergoes an active counter-roll rotation during saccades in free flight [22, 75]. Head counter-roll is of low latency and high velocity. The head rolls during saccades in rigidly tethered flies in a feed-forward compensatory manner in the absence of feedback from the halteres. To assess how that affects the visual experience during saccades, I repeated the same simulation but with the roll angle set to 0 throughout the maneuver. Under the assumption that the head completely balances the roll, predicted HS cell responses are of lower amplitude than under non-attenuated roll angles, presented for rightward saccades in **??** in **??**. Separate consideration of vertical and horizontal components show that the horizontal driving component is attenuated more than the vertical, but still dominates the response (**??**). However, the shape of the curve is not qualitatively modified, and still exhibits the same biphasic property. Counter-pitch rotation of the head has not been separately described during saccades, and is supposedly included in the counter-roll motion. Given that the pitch range of the head is small compared to the roll range (20° against 90°), and that it is also smaller

than the pitch angle of the body during saccades, feed-forward counter-pitch is probably not a significant factor.

Taken together, these simulations show how the combined action of rotational and translational motion in three dimensions affects the visual input to a model fly in ways that are not necessarily intuitive. In particular, the reafferent optic flow caused by performing escape maneuvers is biphasic. Saccades to the left are roughly symmetrical to saccades to the right. Counter-intuitively, the second phase is marked by optic flow that is syndirectional with the change in yaw, i.e HS cells receive excitatory (rightward-moving) optic flow during rightward saccades. While the initial phase exhibits the hyperpolarization that could be expected for this case, it occurs before the yaw heading is perceivably altered, and is initially due to the combined roll and pitch rotations. However, the voltage response caused by reafferent optic flow did not differ significantly by HS subtype. Nevertheless, there exists a critical point where optic flow switches from inhibitory to excitatory close to the center of HSN receptive field. Thus, small imprecisions or deviations may notably change the amplitude of the initial phase of the reafference to HSN, but predictions for HSS and HSE would remain qualitatively the same. In conclusion, I have shown here that the reafferent input to HS cells is more complex than expected in free flight, and that the yaw motion elicits HS responses opposite of what is to be expected from turns in a horizontal plane. Therefore, suppressing excitatory input is indeed a functionally valid mechanism for an efference copy signal in HSN cells.

2.3 Discussion

By measuring intracellular HS cell activity during saccades we uncovered a subtype-specific inhibitory input which is able to suppress the processing of visual motion. Related publications have posited this signal to function as an efference copy, blocking the reafferent input [85]. Our data indicated that the supposed efference copy mainly suppresses excitatory input. While we can not exclude the suppression of inhibitory input at an earlier phase, inhibitory drive following saccades is less affected, although a saccade can arguably cause reafferent input of either polarity, depending on yaw direction. So far these ideas were implicitly based on rotations in the horizontal yaw plane only. In this mindset, a leftward rotation necessarily causes rightward reafferent motion. In contrast, taking into account all three real axes of rotation could yield additional insights.

A reafference matching efference copy

In an attempt to reconcile the apparent contradiction of this supposed efference copy acting on the wrong input as well as its biphasic nature, the visual experience of a fly was reconstructed during escape saccades along 3-dimensional trajectories including body orientation. Through this model, it was discovered that the reafferent input to HS cells follows a biphasic pattern. For example, during a rightward saccade an initial hyperpolarizing optic flow is followed by depolarizing visual motion. Remarkably, this transforms the supposed inhibitory reafference into an excitatory one during the later stage of the saccade for HS cells in the right hemisphere. Thus, the 3D model resolves the apparent contradiction in our measured response after rightward saccades and attributes a physiological role to the suppressed excitation. Moreover, the measured activity of HSN cells during spontaneous saccades is biphasic, with a sign that opposes the biphasic reafference demonstrated by the model.

However, not all aspects of our data are easily explained by this simulation. While the modeled reafference matches the putative efference copy during rightward (ipsiversive) saccades, a discrepancy appears during leftward (contraversive) saccades. HSN cells receive a purely hyperpolarizing input, whereas the model predicted an early excitatory reafference, followed by inhibition. This could imply that the EC is tuned to the initial phase of the reafferent for contraversive turns, and that silencing the inhibitory reafference of the later phase is functionally not important. By suppressing depolarization, downstream motor action could be suppressed as well. It has been shown that unilateral hyperpolarization induces corrective

turns in walking flies [20], implying that HS cell activity is compared across both hemispheres to determine motor action. During flight, only unilateral depolarization has been performed thus far [69]. Assuming that flight is analogous to walking, this puts boundaries on the mismatch between left and right HS membrane potential, but does not preclude the possibility that the EC functions by pulling both HSN cells down to a hyperpolarized state. Alternatively, the EC signal that we and others recorded in both ipsi- and contraversive saccades [85] could have different ethological implications in these two situations.

A caveat in comparing the modeled reafference to the measured voltage lies in the fact that flight maneuvers like saccades exhibit a markedly prolonged time course in rigidly-tethered flight [7, 73, 142]. Proprioceptive feedback is relevant during saccades, and it is difficult to judge what the L-R WSA metric precisely corresponds to in terms of aeronautics. During free flight saccades, changes in L-R WSA seem to have more impact on roll than on yaw torque, suggesting that the changes in L-R WSA we measure during tethered flight could correspond to the roll maneuver [42]. Either way, given that saccade-related potentials are recorded in fixed flies suggests that this is a predominantly feed-forward mechanism, such that we can reasonably expect the signal to qualitatively follow the same course as in free flight, differences in timing aside.

During flight saccades, flies were shown to roll their head to counteract the roll of the body [22, 84, 128]. While this reduces the reafferent optic flow, we have shown that the reafference remains qualitatively the same because of the remaining pitch rotation. Based on this, I reason that the rapid head yaw during spontaneous saccades alters the time-course and amplitude, but not the qualitative, biphasic nature. HS cells are an important component of the optomotor pathway, feeding into both body and head optomotor turns [67, 69], and an EC acting on HS cells may act on head motion or wing steering. An EC has been implied to play a role during saccades for both the head [84] and flight control [78]. The interpretation of the saccade-related signals we measured is complicated by the fact that a saccade during free flight is a complex maneuver, wherein a final yaw turn is necessary to realign the body with the new heading [107, 108, 127]. Furthermore, the pathway and computations downstream of HS cells by which the visual perception of large-field rotation is translated into the optomotor response are not known.

HS subtypes receive similar reafference

A major motivation for the modeling approach was to explain the different saccade-related potentials between HS subtypes. I explored the hypothesis that the different vertical positions

of the receptive fields of HS subtypes could explain the need for diverging efference copies. However, the predicted drive to HS cells did not show consistent differences between subtypes, let alone input of opposite polarity. Nevertheless, differences exist when considering the vertical and horizontal components separately, while the linear sums of these components are essentially equal for all subtypes. This could allow for additional aspects of the receptive field to come into play, which are not necessarily included in the vector-field representation of a receptive field —for example velocity tuning, adaptation or dendritic interactions. It should also be noted, that the receptive fields of HS cells are not fully mapped along the vertical axis. Especially the RF of HSS presumably spreads further down than currently known, which could reduce the discrepancy to HSN because of additional input. Notwithstanding such details, the overall similarity of the x-y components across HS subtypes suggests that the overall result would remain qualitatively comparable.

Furthermore, there is considerable uncertainty in the model as to the exact orientation of the head and the precise position of the HS receptive fields [117, 129]. Although the direction of optic flow switches direction within the range of the HSN RF, thus replacing inhibition with excitation, the overall response of HSN was estimated to differ in amplitude only, not in polarity. Only under very large errors of the estimated head angle ($\approx 50^\circ$) would we expect to see clear differences between HSN and HSS responses.

Based on these arguments, the precise reafferent inputs to HS subtypes may well vary with respect to amplitude, but I argue that they remain qualitatively similar to one another. Therefore, the diverging saccade-related potentials that we measured experimentally hint at different functional implications of the HSN and HSS subtypes. This would be in line with earlier findings that HSS cell activity is less correlated with head turning than HSN or HSE [68]. Future thorough exploration of the parameter space for various scenarios could provide further evidence for whether the observed saccade-related potentials are related to expected visual input or to different functions in behavior.

Outlook

Here, 3D modelling of visual experience during flight helped to elucidate the role of experimental findings and resolve conflicting ideas. In this way, it may bridge the gap between tethered preparations that allow experimental access, and real life behavior. Nevertheless, limitations of this approach lie in the availability of precise free-flight data which includes the rotation along all three body axis. In future work, the framework established here could be

refined to explore a more complete parameter space and project the visual experience onto the response in other cells, possibly even reverse-fitting the physiological role of a given neuron from electrophysiological recordings. For the question of ECs acting on various levels of visual processing, as new findings uncover the mechanisms behind saccadic flight generation and optomotor turning, this model may be used and extended to test the implications of reafferent input and aid in the interpretation of new data.

3 A descending neuron integrating optomotor stimuli

In our experiments so far, we have found that HSN cells in particular receive specific inhibitory input during saccades that are capable to suppress visual processing. As detailed in **??**, HS cells have long been hypothesized to underlie the optomotor response. On the one hand, optogenetically de- or hyperpolarizing them evokes locomotor and head turns that correspond to their PD or ND direction respectively. On the other hand, silencing HS cells by ectopically expressing Kir2.1 (causing constitutive hyperpolarization) reduces yaw optomotor responses of the head, but body turns are notably less affected [84]. Therefore, it is still debated how the information is relayed and transformed downstream of HS cells to cause optomotor turns in both directions. Indeed, HS cells are known to connect directly to anterior neck MNs, whereas there is no direct link to flight motor centers. It seems likely that descending neurons (DNs) receive visual information not only from HS cells to reliably initiate flight responses. Since we and others have found an EC mechanism at the level of individual HS cells, this raises the question how it could be relayed reliably and what the consequence is on motor patterns. Here, we aim to identify DNs that transmit the information distilled by HS cells to the flight motor center. A survey of the connectome provided by the Hemibrain project [126] points to the postsynaptic partners of HS cells. In particular, DNp15 receives strong input from HSN and HSE, but no or much less input from HSS. Since our previous results indicate a differential role for HSN and HSS with respect to visual motion processing, we chose to investigate the physiology of this neuron in detail.

3.1 DNp15 response characteristics

In an attempt to elucidate the functional characteristics of DNp15, I performed intracellular recordings *in vivo* while confronting the fly with moving stimuli mimicking yaw rotation or translation. The exemplary raw data traces in **??** give an impression of the response characteristics dominated by a sustained de- or hyperpolarization respectively. There is no clear evidence for spikes, which leads us to conclude that this is a non-spiking descending neuron. While short transients follow each motion step, a closer look reveals that every motion step is followed by precisely one such transient, which enhance the de- or hyperpolarization respectively (**??**). Considering the time-course and the absence of additional spikes in between these transients, these are probably artifacts of discrete frame shifts of the stimulus and do not represent action potentials. In a free-flight situation, visual motion is smooth, such that frame shift artifacts are not relevant.

Rotations cause depolarizing preferred-direction and hyperpolarizing null-direction responses which are sustained throughout the stimulus duration (**??**). These have a striking resemblance with HS cell responses to the same type of stimuli. Importantly, the DNp15 in the right hemisphere depolarizes during clockwise rotation, whereas the one in the left hemisphere depolarizes to counter-clockwise rotation. In other terms, rotations including ipsilateral front-to-back (FtB) visual motion are excitatory, while the inverse rotations are inhibitory. In comparison, responses to bilateral FtB or BtF motion, emulating forward or backward translation, are significantly lower and degrade over the course of time (**??**).

Since rotational and translational stimuli evoke different responses although the optic flow ipsilateral to the recording site is the same for e.g. full-field PD and FtB stimuli, DNp15 integrates input from both hemispheres. To disentangle the bilateral contributions, we presented FtB and BtF motion to each side separately (**????**). Ipsilateral motion elicited both excitatory and inhibitory responses similar to full-field rotations, but the tonic component is not sustained to the same degree and of slightly lower amplitude. Contralateral motion on the other hand drives only a depolarization during BtF stimuli, while FtB does not induce significant membrane potential deflections. Taken together, the full-field motion responses reflect the combined inputs from ipsi- and contralateral visual motion. The visual motion response of DNp15 is mainly driven by input from the ipsilateral side and complemented by contralateral BtF input, which enhances full-field PD rotation selectivity and reduces full BtF translation sensitivity.

As the visual scenery of natural environment consists of a distribution of spatial frequencies, we measured the tuning of DNp15 to a range of frequencies by presenting moving sinusoidal

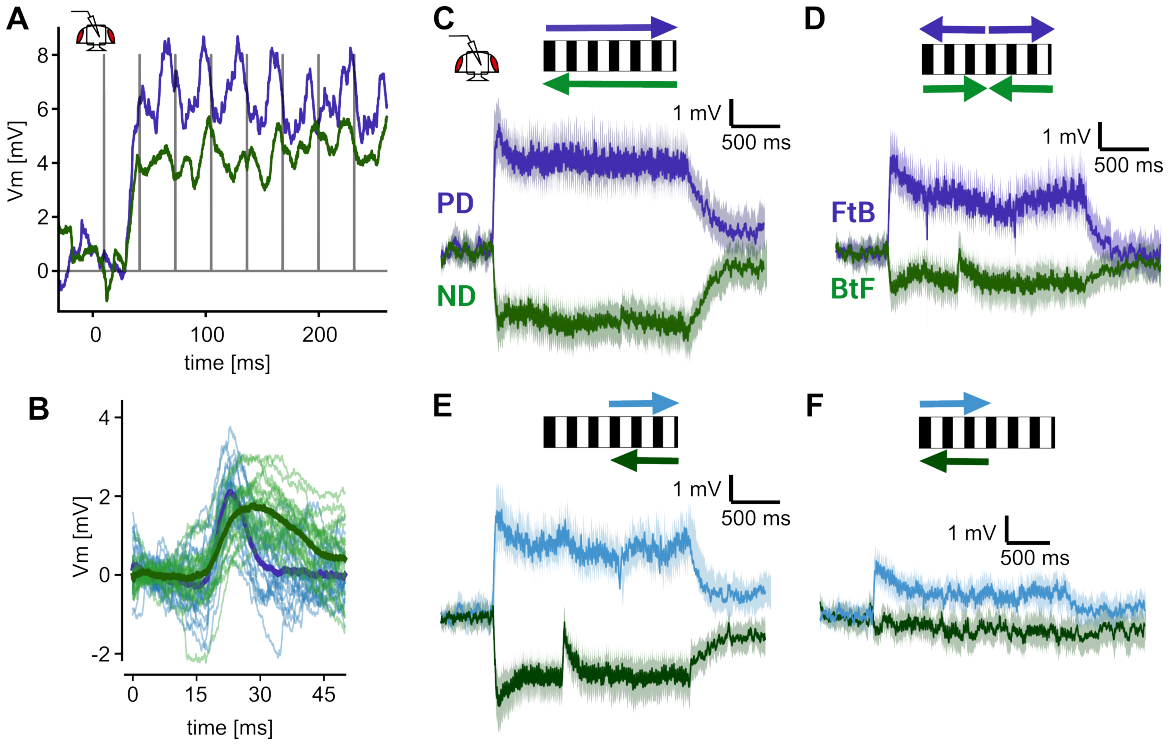

Figure 6: Direction selectivity of DNp15
(A) Exemplary intracellular recordings of DNp15 responses during PD (blue) and ND (green, inverted sign) motion of a sine grating (36° width), grey trace indicates frame shifts of the stimulus. **(B)** Overlay of the voltage response following individual frame shifts of the same trace shown in **(A)** for the preferred (blue) and Null (green) direction (inverted), thick lines showing averages. **(C)** Average ±s.e.m.intracellular voltage response to full-field rotation and **(D)** full-field rectilinear translation in opposing directions from N=7 flies. **(E,F)** Average response to PD (blue) and ND motion (green) on the side **(E)** ipsilateral and **(F)** contralateral to the recording electrode, averaged per fly with s.e.m.

stripes of two different spatial wavelengths at a range of velocities. DNp15 shows a broad tuning curve with a maximum in the lower range of frequencies around 0.5 Hz to 1 Hz (**??**). Responses were largest at the lowest tested frequency of 0.5 Hz, so it is conceivable that responses to even lower frequencies would be larger still. Nevertheless, at 6 Hz the amplitude is still above half the maximum. Additionally, wider stripes consistently evoke larger responses with statistical significance ($p = 0.0002$, paired t-test on the joint normalized PD-ND responses shown in the plot). It is worth noting, that response amplitudes correlate better with the temporal frequency of moving contrast features than with the absolute speed.

After demonstrating in the previous experiments that DNp15 receives both de- and hyperpolarizing drive from the ipsilateral visual system and that its response strongly resembles those of HS cells, next I investigated whether the suppression of PD motion vision in HS

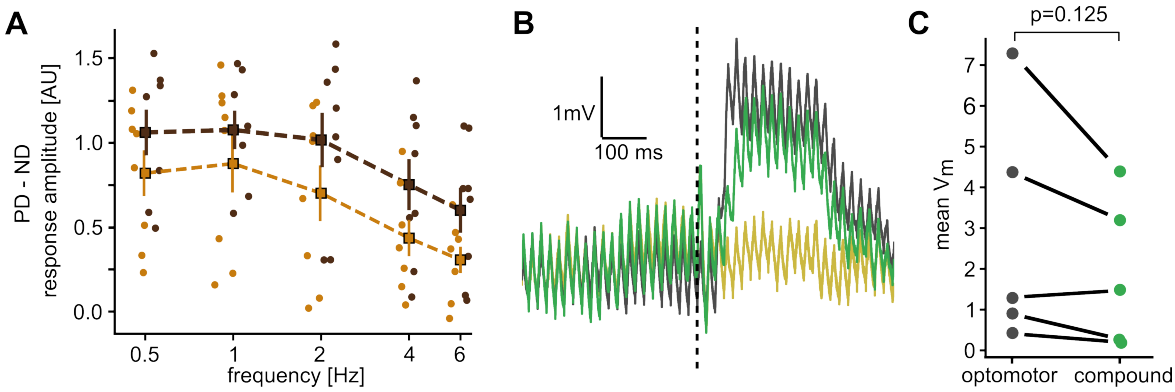

Figure 7: Frequency tuning and looming responses of DNp15
(A) Frequency tuning curve of DNp15 for sinusoidal gratings of 18° (light brown) 36° (dark brown) spatial period, individual dots mark the average response of individual flies (N=8), PD and ND average responses being normalized to largest trial before subtraction, squares mark total average ±s.e.m. **(B)** Average membrane potential during ipsilateral looming followed by PD rotation (N=5 flies). **(C)** Mean membrane potentials during early phase of PD rotation response itself ("optomotor", gray) or following ipsilateral looming (compound, green) for each individual fly (N=5), quantified by averaging in a timewindow 80 ± 16 ms after maximal looming expansion, in the same way as in **??**, p-value obtained by Wilcoxon rank-sum test.

cells that was established in **??** is relayed to the VNC via this neuron. Indeed DNp15 cells exhibit a decreased response to optomotor PD input for a short period after an ipsilateral looming stimulus when compared to the optomotor rotation itself (**??**). This was reproducible across individuals, although we have not obtained a sufficient number of recordings to reach a significance level of 5% (**??**). In accordance with the preceding experiments, this strongly resembles the situation in HS cells (in quiescent flies). Thus, DNp15 can serve as a relay for the reduced visual motion processing, supporting the hypothesis that it is an important component of the neural circuitry mediating optomotor yaw turns.

3.2 DNp15 connectivity

For a better understanding of the response properties and the possible ethological implications of DNp15, the anatomical properties are considered first. The DNp15 was annotated as such by Namiki *et al.* and imputed to be identical to the neuron previously called as DNHS1 [138]. Through the effort of the Hemibrain project [126], the DNp15 neuron was also identified in an EM volume of the central brain, along with most of its synaptic partners in the cerebral ganglia.

As may be expected of a descending neuron, p15 forms close to no presynapses in the central brain, with only 21 traced presynapses compared to 2310 postsynapses. Therefore, it almost exclusively receives input in the head capsule without notable feedback loops. While the optic lobes are not included in this EM volume, light microscopy of a split-Gal4 line specific for DNp15 (R11E07 x R77F05 [111]) indicate no processes in the optic lobes either. For the specific reconstructed instance in the EM data, 193 upstream neurons provide input synapses, which belong to 57 neuron types and a number of traced but unidentified neurons. When only considering neurons which provide >1% of the total number of input synapses, 23 neurons of 13 different types remain, which supposedly define the functional role of this neuron. Reflecting the characteristic responses to visual motion presented in **??**, H2, HSN and HSE account for a substantial part of the input connections. Interestingly, strong input from other neurons in the saddle (SAD), as well as from interneurons linking to the wedge (PS234), suggest that information from the antennal mechanosensory and motor center merges with visually related information at this level.

Additionally, another descending neuron, DNb03 contributes more connections than individual HS cells. DNb03 in turn shares a considerable fraction of upstream partners with DNp15, most notably H2, PS235 and PS055, the latter of which also conveys indirect VS input. However, by far the largest fraction of input neurons are currently unidentified. This issue extends to the second-degree connectivity, because most of the input of the identified upstream partners is unknown as well. In short, DNp15 receives bilateral visual input along with many projections from areas often associated with mechanosensation. It receives additional strong connections from DNb03, with which it shares a substantial part of the common input.

With respect to the ethological role, the connectivity in the VNC is a valuable indicator. Light microscopy suggests that DNp15 axons project into the dorsal regions of both the pro- and meta-neuromere of the VNC. Analogously to the central brain, the recently released reconstruction of an EM volume of the male VNC [26, 99, 141] allows for a detailed analysis of the connectivity, where DNp15 forms ≈6 times more output than input synapses. The postsynaptic partners of both left and right DNp15 were grouped by cell type and only groups exceeding >1% of the total output synapse count were considered in **??**. The axonal projections are predominantly targeted at the neck (light blue) and haltere tectulum (dark blue) and to a lesser extent the posterior pair of legs. The definitions of the neuropil regions can overlap to a certain degree, such that connections attributed to the leg neuropils may in fact belong to neurons in the tectulum. Yet, a large number of synapses can be attributed with certainty to the posterior leg neuropils. For instance, the most prominent leg neuropil neuron IN08B087 in turn projects to neurons in the same as well as other leg neuropils. Strikingly, very strong projections target the

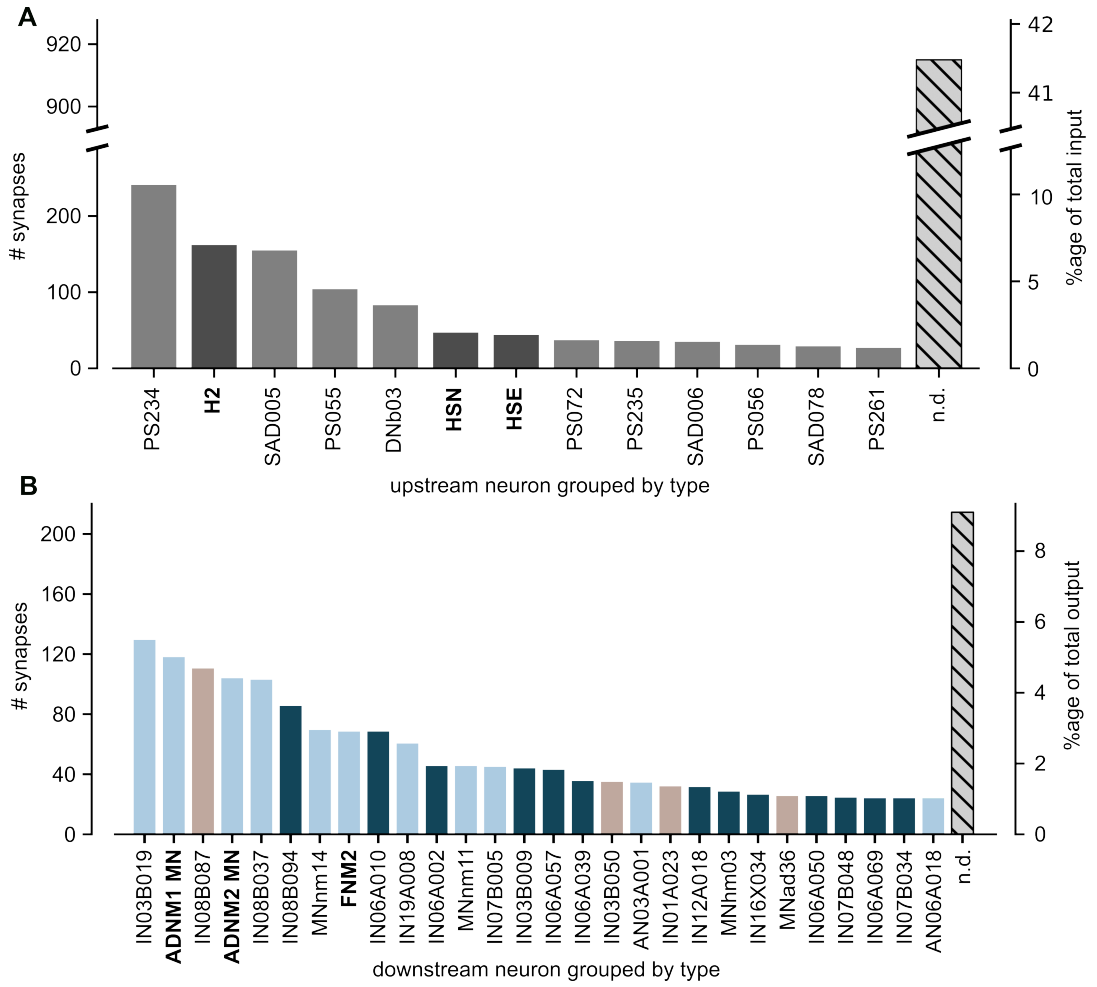

Figure 8: Connectivity of DNp15 in central brain and VNC
(A) Upstream connectivity obtained from the Hemibrain reconstruction, synapse counts summed per neuron type, limited here to those accounting for >1% of input synapses, n.d. are traced neurons of unknown type. The labeled neurons shown represent 13/57 known neuron types and 23/193 total presynaptic neurons. **(B)** Downstream connectivity in the VNC as obtained from the MANC reconstruction [26, 99], synapse counts summed per neuron type, limited to types accounting for >1% of input synapses, n.d. are traced neurons of unknown type. The labeled neurons shown represent 28/202 known neuron types and 110/524 total neurons postsynaptic to DNp15. Colors indicate the primary neuropils where these neurons connect, with the neck tectulum in light blue, haltere tectulum in dark blue, and posterior leg neuropil in brown.

neck motor neurons directly, especially the ADNM1/2 and FNM2 motor neurons. The direct contact to motor neurons is not limited to the neck tectulum, but also encompasses haltere motor neurons, although in the haltere tectulum synapses with interneurons dominate. Taken together, the downstream connectivity suggests that DNp15 plays a role in controlling neck rotation with possibly direct control of motor neurons, and may impact both walking and flight steering. Although there are no notable output synapses in the wing neuropil directly, wing motion may be altered via feedback control of the halteres in line with the control-loop hypothesis.

Furthermore, to facilitate reasoning about the potential role of DNp15 on downstream circuits, I aimed to establish the neurotransmitter that it uses. Expression of a reporter for ChAT transcription colocalizes with the split-Gal4 expression of our DNp15 driver line (**??**), which was not observed for other neurotransmitter markers (VGAT, VGlut, DAT, not shown). Therefore DNp15 is cholinergic and probably excitatory to its postsynaptic partners.

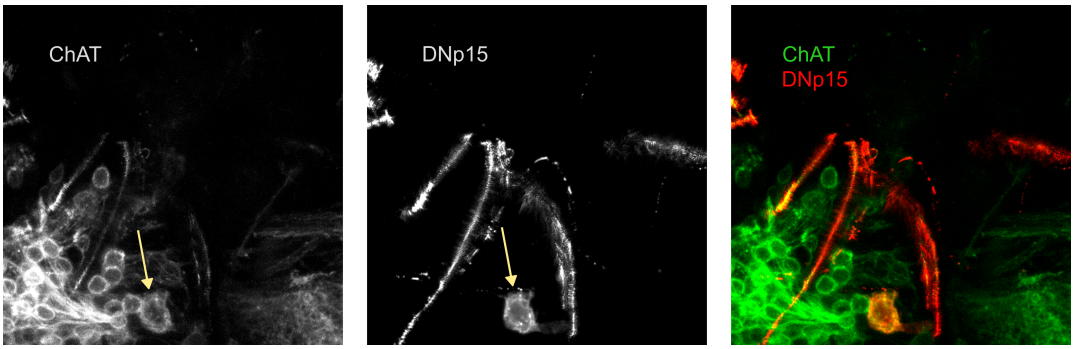

Figure 9: Colocalization of driver line with a marker for acetylcholine
Coexpression of fluorescent reporters under the control of the cholinergic marker ChAT-T2A-lexA (left) and the DNp15 split-Gal4 (middle) line exhibit costaining (right). Maximum projections of a substack encompassing ≈5 µm to reduce ChAT background from neuropil.

3.3 Role of DNp15 for flight behavior

Having established the motion processing properties of DNp15, it is necessary to evaluate its role in flight behavior. Because its response is tuned to rotational optic flow and integrates binocular inputs, I hypothesize that it is crucially involved in optomotor turns. HS cells, a major input to DNp15, have long been posited as an important factor in the optomotor response. For instance, optogenetic HS cell activation leads to smooth flight turns [69]. Under the assumption that HS depolarization and inhibition are translated into optomotor turns via

DNp15, the binocular integration at the DN level could explain why silencing HS cells does not abolish flight turns. At the same time, since hyperpolarization is conveyed to DNp15, a comparison between the left and right neuron of this pair could hypothetically translate unilateral HS hyperpolarization into turning behavior [20].

The optomotor response is often narrowed down to yaw turns during walking or flying, but a fly's eyes can follow motion by turning the body, rotating the head at the neck or by shifting the retina under the cornea. In light of the strong projections of DNp15 onto neck and haltere motor areas, I hypothesize that this neuron is strongly involved in syndirectional smooth tracking of visual motion by recruiting both the neck and wings as effectors.

3.3.1 Role of DNp15 in the optomotor response

A head-free tethering assay

To test this hypothesis, a head-free tethering preparation was developed to fit the same setup as for the electrophysiological characterization (**??**), essentially adapting the conventional rigid-body tethering paradigm to our needs. This preparation positions the fly in the same position and allows measuring the head motion as yaw angle along with the left and right wing stroke amplitudes (WSA). While the head and wings are free to move, the fly's body is fixed in place and does not rotate. Experiments on the head-free tether were conducted by Aiman Ume, a master's student in the lab supervised by me. Conceptualization of experiments, setup, preliminary tests and data analysis were done by the author.

When confronted with wide-field yaw rotation on the LED arena, flies typically exhibited responses that were marked by smooth turns which followed the rotation interrupted by quick saccades in the opposite direction which engaged both the head and wings (**??**). These saccades are reminiscent of the gaze-resetting saccades during the optokinetic nystagmus in vertebrates, and henceforth referred to as "(gaze-)reset saccade" for the purpose of this work. Head and flight turns seem to be largely linked, but differences exist: wing motion is less smooth and saccades less stereotyped. As seen in the CCK example (**??**, light brown), the L-R WSA indicates that smooth turning of the body follows the pattern rotation more closely, while the head exhibited smooth antidirectional turning as well. More importantly, following the saccades, both head and wings perform smooth rotations opposite to the saccade direction (i.e. syndirectional to the stimulus). However, this type of stimulus provoked variable responses, as

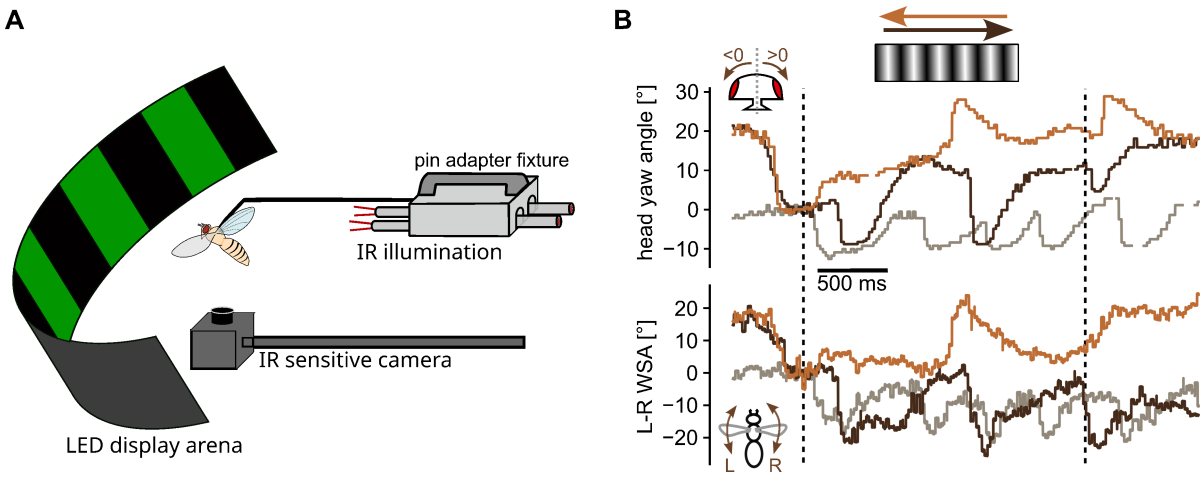

Figure 10: Pin-tethering paradigm for head-free flight behavior
(A) Schematic drawing of the head-free preparation and setup, consisting in tethering a fly to a pin bent to a defined angle, which is attached to the microscope stage by a custom-made adapter. The fly is positioned in the center of the arena and focus of an IR sensitive camera and illuminated from the rear by a pair 850 nm sources via light guides. The camera stream is analyzed in real time to extract head yaw angle and wing stroke amplitudes (WSA). **(B)** Example raw head yaw angle and flight turning behavior recorded in this setup from an empty-split>TeTx control fly upon presentation of an optomotor stimulus moving clockwise (CLW, dark brown) or counter-clockwise (CCK, light brown and grey) shows general pattern of responses with syndirectional smooth motion and nystagmus-like saccades of both the head and wings.

seen in the second CCK example (gray line) where the fly performed syn-directional saccades and anti-directional smooth turns, and which represents a common occurrence.

In this new experimental setup, the same sine-wave gratings were presented to the fly as rotation in clockwise (CLW) or counter-clockwise (CCK) direction, and evoked optomotor turns with very similar, albeit not identical absolute amplitudes (**??**). Linear regression indicates that turning is more pronounced in CCK direction (slope $= -0.69$), but the residual distribution is not significantly skewed from the normal distribution (skew test $p = 0.71$) (**??**) under the assumption that CLW $= -$CCK (i.e. the distribution of CLW+CCK). Thus, control flies are not significantly biased towards one side due to artifacts of tethering, positioning in the arena or innate preferences. As an additional precaution, we calculate the response as the difference of CLW-CCK responses.

Presenting flies to optomotor stimuli of a range of spatial and temporal frequencies, it becomes evident that the smaller stripes of 18° period evoke only small turning responses. In contrast, the same temporal frequency (resp. rotational velocity) of the wider (36°) pattern leads to

prominent optomotor turns. Responses were coherent between wide and thin stripes with linear dependence, such that the thin stripes can be considered to elicit weaker responses with lower signal-to-noise ratio (**??**). Presumably, wider features act as more salient features with respect to the self-orientation implied in the optomotor response. For the sake of clarity, further analysis was focused on the wider stripes.

Suppression of optomotor turns

Next, I investigated whether DNp15 is a relevant part of the optomotor response circuitry. In a first step, the pair of DNp15 was silenced bilaterally using the potassium inward-rectifier Kir2.1 and tetanus toxin light chain (TeTx) respectively. Flight responses to patterns moving at 6 Hz demonstrated that optomotor turns are not completely abolished, but there are clear differences between genotypes (**??**). Flies expressing Kir show a lower response amplitude to wide stripes than TeTx and empty split-Gal4 control flies. Silencing appears to affect thin and wide stripes proportionally, but the control for Kir shows unexpectedly small responses to thin stripes, further prompting us to focus on the wider stripes.

To compare behavioral responses across genotypes and stimulus frequencies, response amplitudes were quantified for each individual fly as the difference between mean L-R WSA for CLW and CCK stimuli, i.e. $\overline{\Delta\mathrm{WSA}}_{CLW} - \overline{\Delta\mathrm{WSA}}_{CCK}$. Prominently, turning behavior was largely abolished at temporal frequencies up to 2 Hz in flies expressing Kir, and reduced at higher frequencies. In contrast, TeTx does not appear to have a significant effect above 1 Hz. Accordingly, flies expressing DNp15>Kir respond significantly less to the stimulus at 1 Hz and 2 Hz than empty-split>Kir flies (2-tailed Mann-Whitney-U, $p = 0.022$ and 0.023 resp.). Empty-split controls for Kir typically show lower responses than controls for TeTx, which hints at an unfavorable genetic background, but ANOVA analysis (one-way, preceded by Levene tests) revealed no significant differences between both empty-split controls and DNp15>TeTx.

As described at the beginning of this section (**??**), in our pin-tethered paradigm, flies were able to move their head to follow the optomotor stimulus. However, after averaging, the head yaw angle does not follow a similar time course as the L-R WSA to the same stimulus. Instead of slowly tracking the rotating pattern, the head appears to on average move in the direction opposite of the rotation (**??**), while the fly attempted to perform flight turns syndirectional to the pattern. This is the case for all genotypes and does not apparently correlate with the difference seen in wing flight turns. The example traces in **??** provide an intuition that this may be due to ongoing activity and significant variability in responses. Additionally, the neck

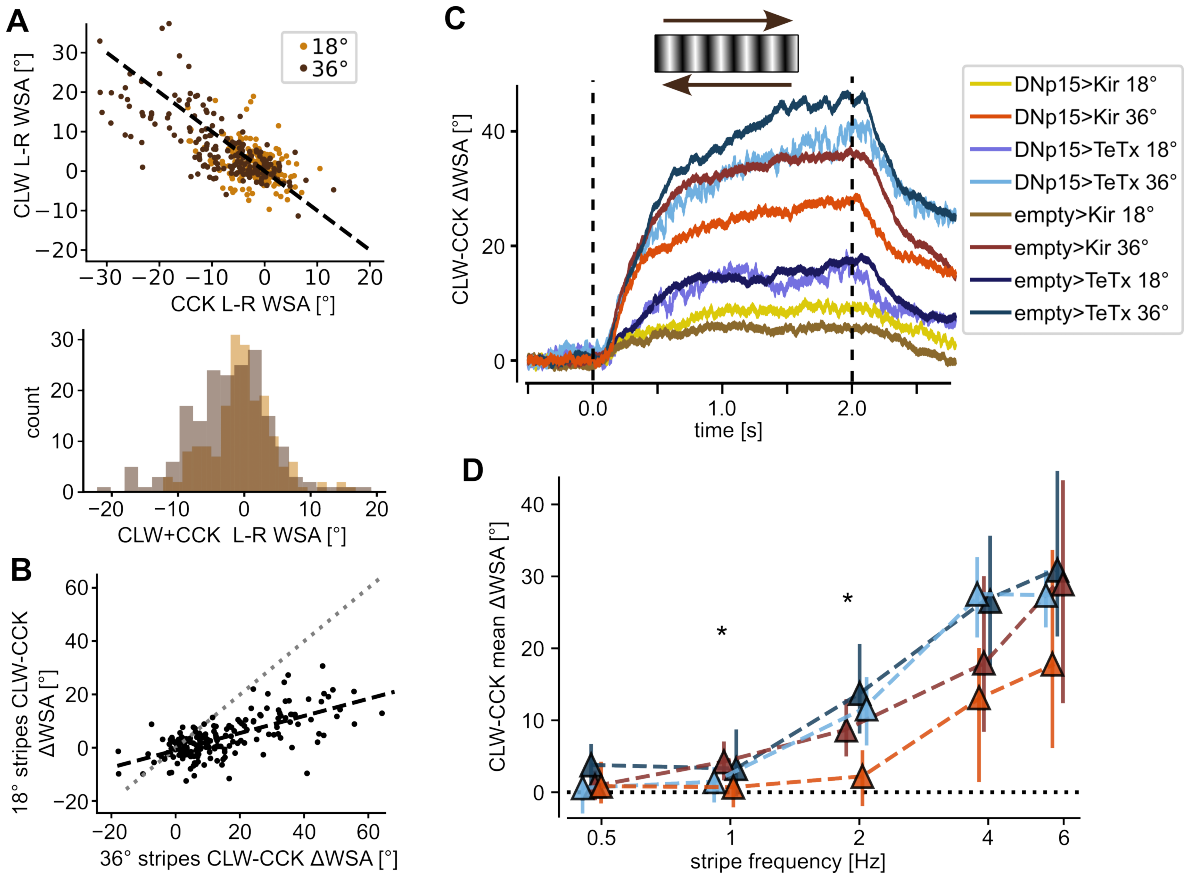

Figure 11: Impact of silencing DNp15 on optomotor flight turns
(A) (*top*) Mean amplitude of optomotor turning response to clockwise (CLW) against counter-clockwise (CCK) sinusoidal stripe rotations for thinner stripes (18° wavelength, light brown, $n = 90$) and wider stripes (36° wavelength, dark brown, $n = 90$), the dashed line indicating the symmetrical case where $y = -x$. Data from 18 empty-split>Kir and 18 empty-split>TeTx ($N = 36$) flies with 5 stimulus conditions (individual dots) for thin and wide stripes each. (*bottom*) Histogram of the residuals of CLW+CCK turning response amplitudes for thin and wide stripes respectively. **(B)** Comparison of mean optomotor turning responses to stripes of the two spatial wavelengths, thinner 18° against wider 36° stripes, where dots represent the average response amplitude for each fly and stimulus condition ($N = 36$ control flies with total $n = 180$ conditions), dotted line marks the unity $y = x$ and the dashed line is the linear regression (slope $= 0.32$, intercept $= -0.90°$). **(C)** Population average turning response to optomotor stimuli as the difference between CLW (typically L-R WSA>0) and CCK (typically L-R WSA<0) for inhibited and control flies (indicated by hue), for both thin and wide stripes (marked by color saturation), for a rotation speed corresponding to 6 Hz frequency of stripes passing a specific point in visual space (N=15/17/19/18 flies for DNp15>Kir / empty>Kir / DNp15>TeTx / empty>TeTx respectively). **(D)** Optomotor turning amplitude by genotype and temporal frequency of the stimulus, quantified as difference between the mean L-R WSA amplitude of CLW and CCK moving wide (36° period) stripes. Shown are the median values and quartile ranges of individual fly-wise average responses, color-coded by genotype with DNp15>Kir (orange, N=15 flies), empty-split>Kir (red, N=18), DNp15>TeTx (light blue, N=17) and empty-split>TeTx (dark blue, N=18). Stars mark significant differences between DNp15>Kir and empty-split>Kir ($p = 0.022$ at 1 Hz and $p = 0.023$ at 2 Hz, Mann-Whitney-U test).

joint has a limited mobility range in the yaw plane (≈±15°) and head saccades have been reported to be triggered by mechanosensory feedback before it reaches its limits at ≈±9° [22]. In contrast, the L-R WSA may exceed 15° for a certain time to continue turning before the fly decides to execute a reset saccade. Thus, average head turning responses presumably appear to be antidirectional due to more frequent saccades and a lower amplitude. Alternatively, this might reflect a behavior that voluntarily disregards or avoids the motion stimulus.

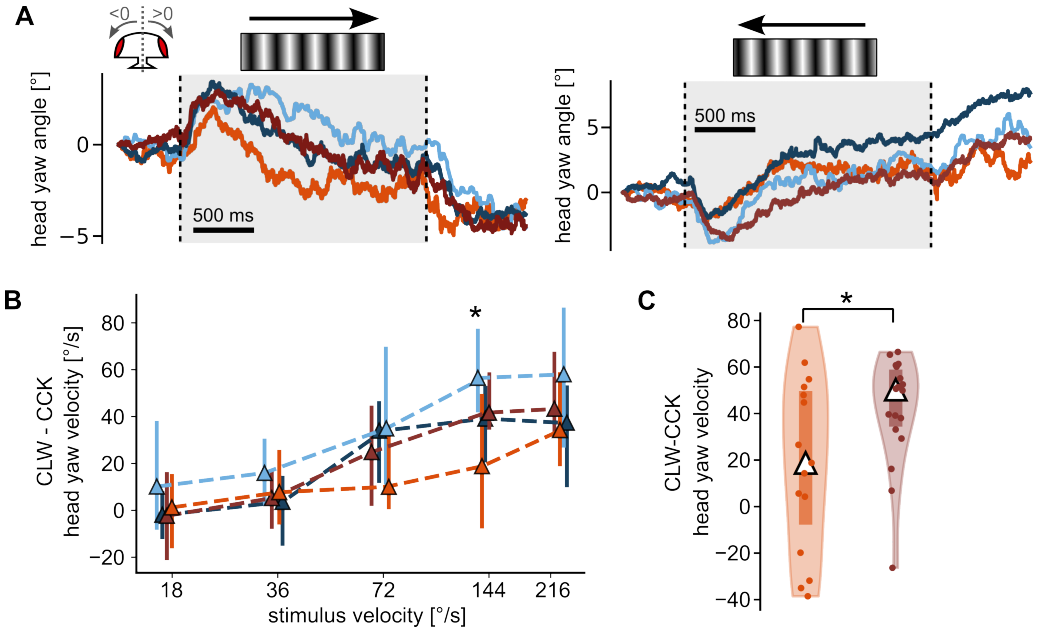

Figure 12: Effect of silencing DNp15 on head yaw optomotor turning
(A) Average head turning responses to horizontally rotating sinusoidal stripes of 36 wavelength with angles >0° representing rightward deflections. Traces are color-coded according to genotype, with DNp15>Kir (orange, N=15 flies), empty-split>Kir (red, N=18), DNp15>TeTx (light blue, N=17) and empty-split>TeTx (dark blue, N=18). **(B)** Head yaw velocity as difference of CLW - CCK stimuli, plotted as median and interquartile range against the rotation velocity of the pattern for silenced and control flies, color-coded as in (A). Bonferroni-corrected ANOVA indicates significant differences across genotypes for 144 $^\circ\,s^{-1}$ ($p = 0.025$). **(C)** Distribution with median and interquartile range of CLW-CCK head velocity for DNp15>Kir (left) and empty-split>Kir (right) with post-hoc t-test ($p = 0.042$, unpaired 2-tailed).

Nevertheless, the initial phase of the response immediately following stimulus onset were on average syndirectional, and allowed us to evaluate the optomotor response of the head. The initial head yaw velocity was calculated by linear regression in a time window of 75 ms, skipping the period before the onset of head turning. The head yaw velocity increased with the pattern velocity up to a maximum velocity which may be due to anatomical limits. The estimated velocity, based on the average head position in individual flies, is notably lower than the pattern velocity in all cases. Comparing DNp15-silenced to empty split-Gal4 control flies,

the median head yaw velocities (given as CLW-CCK) indicate that the pair of DNp15 neurons is relevant for head rotation during optomotor stimuli in a similar stimulus range as for wing steering (**??**). ANOVA analysis pointed at a significant difference only at the stimulus velocity of $144\,^\circ\,\mathrm{s}^{-1}$ (corresponding to 4 Hz) where Kir expression causes a significant reduction of response amplitudes (**??**). TeTx expression did not cause significant differences despite the overall appearance.

At low pattern velocities, the estimated head turning velocity is generally low such that it is difficult to evaluate the effect of silencing neurons. Given that flies often perform saccades to reset the gaze direction before following the pattern rotation, I detected these nystagmus saccades and determined the tracking velocity immediately following them by linear regression (**??**) during clockwise stimuli. In this way, there is a defined starting point for the velocity estimate, which is less affected by ongoing activity and the anatomical limits of the neck. Indeed, the resulting estimates match the pattern velocity more closely before reaching a plateau (**??**). Corroborating the phenotype that is seen for the responses at stimulus onset, flies expressing Kir exhibit a reduced velocity of the head, which is less dependent on the stimulus speed. In the intermediate range of velocities in particular, Kir causes a significantly reduced head speed ($p = 3.6 \times 10^{-5}$). A post-hoc analysis showed that the responses of DNp15>Kir flies are significantly different from those of empty-split>Kir flies (**??**). In contrast, TeTx expression did not affect responses in a systematic way (**??**). Although not all stimulus speeds statistical significance was reached after a Bonferroni correction for the fitting parameters used here, the overall trend leads to the conclusion that silencing DNp15 by constitutive hyperpolarization and shunting impairs the optomotor response of the head, but does not abolish it.

This is in line with the visual impression of the flies' behavior, reflects the observations in the early phase of the optomotor head response, and is similar to what was found for the flight turns.

3.3.2 Optogenetic activation phenotype

The previous experiments have shown that the inhibition of DNp15 can effectively reduce the optomotor response to certain visual stimuli. The next logical step was to test if activation of DNp15 alone can induce optomotor turns.

The optogenetic cation-conducting channel CsChrimson was expressed stochastically using the heat-shock-mediated excision of a stop cassette upstream of the gene. An additional fluorescent reporter fused to the channel permitted to distinguish the expression pattern, which

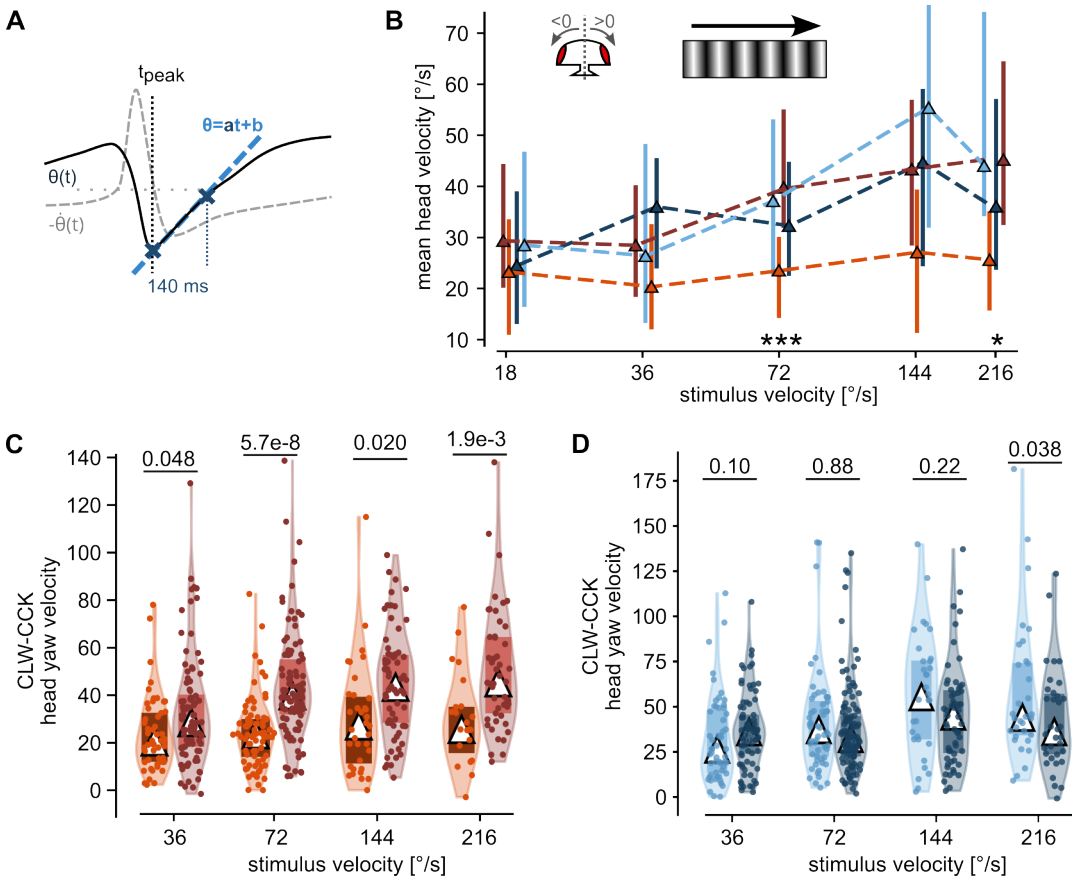

Figure 13: Head velocity following gaze-reset saccades
(A) Schematic of the saccade detection and subsequent estimation of head velocity by linear regression. Saccades were detected as peaks in the derivative with inverted sign and velocity was estimated over 140 ms starting at the peak. **(B)** Head yaw velocity following antidirectional saccades during CLW optomotor stimuli pooled across flies, plotted as median with interquartile range for silenced (light colors) and control flies (dark colors) with DNp15>Kir (orange, $n = [28, 52, 76, 35, 23]$ saccades per stimulus), empty-split>Kir (red, $n = [78, 92, 102, 68, 49]$ saccades), DNp15>TeTx (light blue, $n = [44, 55, 56, 32, 32]$ saccades) and empty-split>TeTx (dark blue, $n = [69, 81, 114, 58, 34]$ saccades). ANOVA analysis with Bonferroni correction indicates a significant divergence starting from $72\,^\circ\,\mathrm{s}^{-1}$ ($p = \{3.6 \times 10^{-5}, 0.17, 0.016\}$ in ascending stimulus order). **(C)** Distribution of head velocities following gaze-reset saccades during CLW stimuli for DNp15>Kir (orange) and empty-split>Kir (red), with median (white triangle), interquartile range (thick bar) and p-values of t-tests (two-tailed, not corrected for multiple testing). **(D)** Same for DNp15>TeTx (light blue) and empty-split>TeTx (dark blue).

could be verified directly by epifluorescence microscopy. In uncertain cases due to suspected (auto)fluorescence, additional staining and subsequent confocal microscopy showed no expression. This suggests that there was either no expression or sufficiently strong expression of CsChrimson, although it is unknown how consistent the expression level was in labeled cells. Consequently, the turning responses were averaged within expression patterns (**??**). The light activation caused a bias for low-amplitude turns toward the left in the absence of noticeable reporter expression. More importantly, expression on the right side neither caused a strong bias to the right (L-R WSA >0), nor did expression on the left enhance the leftward bias. To gain a clearer picture of any low-amplitude effect leading to turns, L-R WSA responses from flies with expression on the left were inverted to match the hypothetical effect of right-sided expression, and pooled together with those (**??**). Concurring with the general impression, activation did not lead to a consistent turning response $>2\,^{\circ}\,s^{-1}$.

Indeed, at the level of individual flies, light pulses reliably evoke low-amplitude leftward turns whereas there is little support for unilateral expression biasing turns to either the ipsi- or the contralateral side (**??**).

Conceivably, a bright light pulse could constitute an aversive stimulus and override an otherwise syndirectional behavioral response. In light of this hypothesis, the same experiment was conducted with a lower light intensity (**??**), which found the aversive light bias to be reduced in flies without expression (p=0.039, paired t-test, blue dots below unity line), but fails to shift the response distribution of unilaterally-expressing flies consistently.

Recently, a group of DNs has been discovered that respond to rotational optic flow but whose unilateral activation elicits bilaterally increased wing stroke amplitudes, expressed as ΣWSA, instead of turns [112, 114]. In the case of DNp15, a transient drop in the total wing stroke amplitude is apparent regardless of expression pattern after light onset, which quickly returns to baseline **??**. An increased ΣWSA is apparent only for unilateral expression on the left, where N_{flies} is the lowest. Conceptually, unilateral expression on either the left or the right is expected to show the same effect on ΣWSA. Taken together, there is no systematic difference between mean ΣWSA at the pre-stimulus baseline and during the light pulse (**??**).

Furthermore, I considered the possibility that DNp15 activity enhances optomotor turning responses in combination with other pathways. Presenting rotational stimuli at 2 Hz with and without simultaneous continuous light pulses should allow us to distinguish the added effect of optogenetic activation. However, scrutiny of the difference between the combined and the purely rotational stimuli showed that pure clockwise rotations elicit larger turns regardless of CsChrimson expression (**??**). Similarly, flies with unilateral expression did not

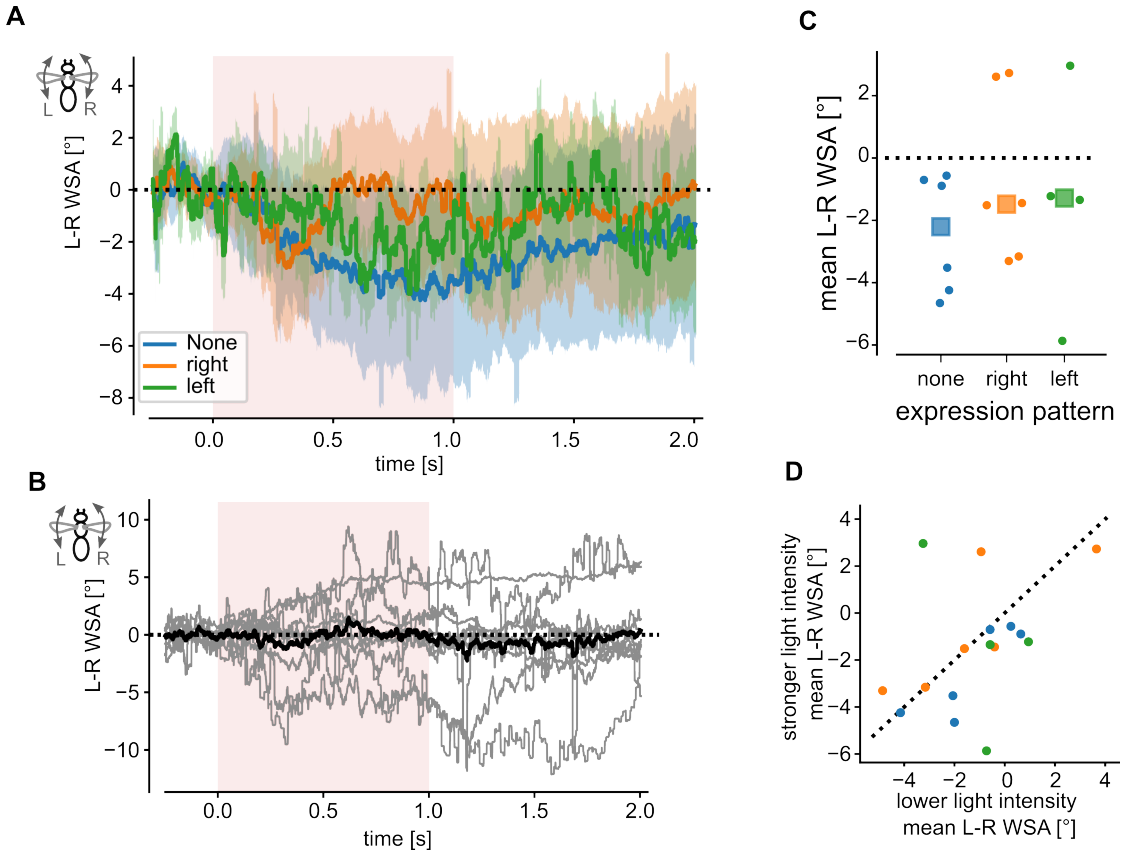

Figure 14: Unilateral activation of DNp15
(A) Turning response as L-R WSA during continuous light pulses as population average for each phenotype of stochastic CsChrimson expression, with unilateral expression on the right in orange (N=6 flies, n=94 trials), on the left in green (N=4 flies, n=60 trials) and no expression in blue (N=6 flies, n=105 trials). **(B)** Pooled turning responses during continuous light pulses, combining flies with unilateral expression on the right with the inverted responses of left-expressing flies, individuals shown in grey, population average in black. **(C)** Distribution of individual flies' mean turning responses during activation, separated by expression pattern. **(D)** Average turning responses of individual flies to pulses of lower against stronger activating light (stronger by a factor of 4).

exhibit distinctive changes in turning behavior due to light pulses which exceeded the effect on negative Control flies (no expression) (**??**).

Finally, one anecdotal recording of DNp15 cell using the same driver and UAS construct without the Stop-cassette indicates that our approach is generally able to sufficiently activate the cell (**??** in **??**) and that the cell did not adapt to the light stimulus over the course of the experiment (**??**). Despite referring to a different effector line, these recordings indicated that the activation reliably depolarizes the cell and is able to balance or override inhibitory stimuli, although full-field excitatory stimuli led to stronger depolarization than the optogenetic

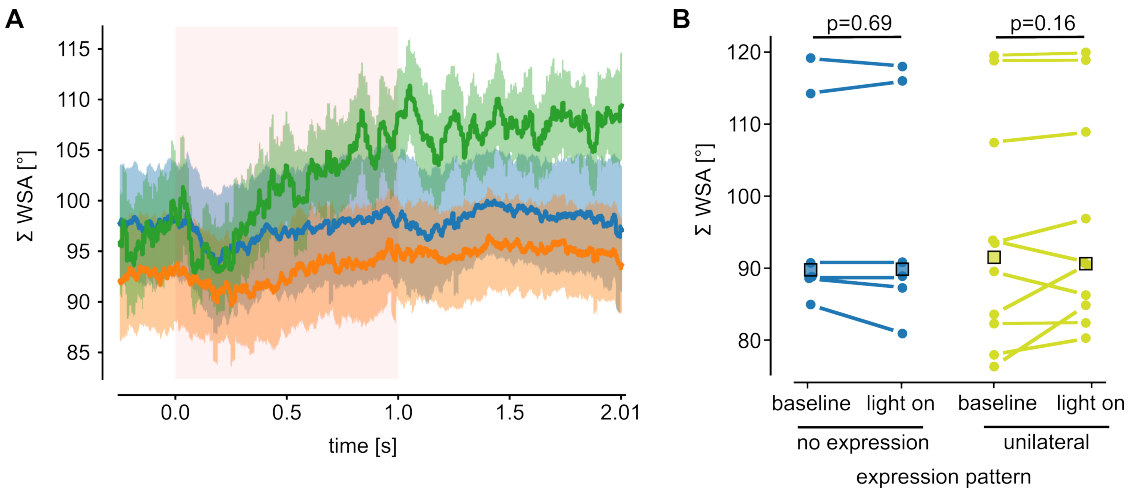

Figure 15: Total wing stroke amplitude in unilateral activation
(A) Sum of left and right wing stroke amplitude color-coded for expression pattern with unilateral expression on the right in orange, unilateral left in green and no expression in blue. **(B)** Responses for each fly quantified as mean sum of WSA before (baseline) and during the light pulse, where flies with unilateral expression (both right and left) shown in yellow and without expression in blue. Indicated p-values tested the pre-stimulus baseline to the response to the light pulse by Wilcoxon signed-rank test, same number of flies as for L-R WSA.

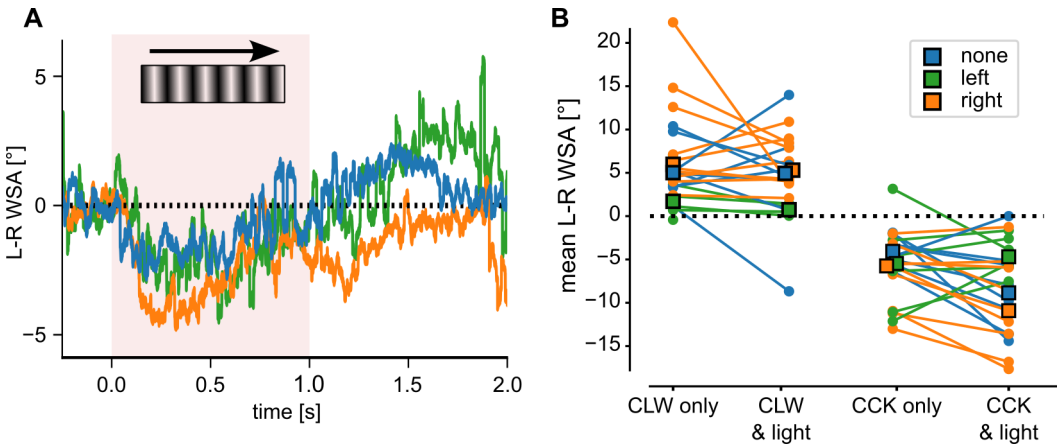

Figure 16: Interaction of optomotor stimulus with optogenetic activation
(A) Differences of turning response to purely rotational clockwise (CLW) motion and CLW motion in conjunction with a light pulse, population average by expression pattern, unilateral expression on the right (orange, N=5 flies) and left (green, N=3 flies) and no expression (blue, N=4 flies). **(B)** Distribution of turning responses for each fly (pooled light conditions), paired for purely rotational motion in CLW or CCK direction, paired with continuous light pulses, with each line joining the response of the same fly and condition, and medians per expression pattern marked by squares.

activation.

3.4 Discussion

3.4.1 DNp15 electrophysiology

The pathway and neural functions linking visual perception to optomotor behavior are still open questions. Because this hinders the interpretation of central findings of the function of the visual system, we aimed to elucidate how HS cell activity is transmitted to the flight motor center and the role that this pathway plays in the optomotor response. Indeed, HS cells have long been posited to be an essential part of the optomotor response pathway, but silencing and activation experiments implied that this picture was incomplete [69, 84]. Additionally, in **??**, we have discussed our findings of a putative EC acting on HS cells along with a reconstruction of HS responses during saccades, but not all of our findings could be easily explained in this framework. Therefore, elucidating the downstream implications of HS activity on behavior should help to interpret our own and others' findings.

Leveraging the connectome reconstructed by the Hemibrain project [126], the descending neuron p15 (DNp15) was determined as a promising candidate because of its strong connections to HSN in particular. A significant proportion of HS output synapses project to descending neurons, out of which DNp15 is the most significant partner. Based on observations in *Calliphora* and EM reconstruction in *Drosophila*, HSN/E cells appear to have a particularly direct effect on head rotations by projecting to ipsilateral motor neurons of the VCN nerve linking to muscles from the neck's anterior side, whereas DNp15 projects to motor neurons of the ADN nerve which links to neck muscles from the posterior side [82, 136]. In this way, HS and DNp15 could jointly be responsible for the head optomotor response by activating the necessary neck muscles on both the head and thoracic side of the neck. From the perspective of DNp15, ipsilateral HS cells are among the most important input partners. Notably, HSN cells are the dominant HS subtype, followed by HSE. The connection of DNp15 to HSN is supplemented by gap junctions, combining chemical with electrical synapses between the same neurons [117]. Additional visual input is provided by contralateral H2, which is a cholinergic neuron selective for back-to-front (BtF) visual motion [152]. This is corroborated by an independent reconstruction of DNp15 in the FAFB EM volume, which reported an even larger proportion of input from HS and H2 cells (28% of total inputs), along with significant GABAergic inputs related to HS and H2 (10% of total) [47].

I have probed its response to visual motion patterns, and found DNp15 to be selective to rotation of the visual field. Consistent with the predicted connectivity, DNp15 receives strong

excitatory drive by ipsilateral front-to-back (FtB) and contralateral BtF motion, in line with the response properties of ipsilateral HS and contralateral H2 cells [129, 152]. At the same time, full-field rotation evokes larger responses than stimuli emulating translational movements. Thus, binocular information is integrated by enhanced activity to preferred direction stimuli. Recent work has reported Ca-imaging results from DNp15 during a similar set of stimuli in walking flies [48]. Similar to my results, they demonstrate that DNp15 is excited by ipsilateral FtB and contralateral BtF visual motion. Interestingly, the enhanced sensitivity to binocular rotation is more pronounced in Ca-imaging data, while the contralateral FtB responses appear smaller than in our recordings, in which ipsi- and contralateral responses sum approximately linearly. This might be due to the non-linear relationship of Ca-concentration and fluorescent reporter activity, or alternatively to the different location of the recording site, dendrite compared to soma. While this discrepancy is not uncommon between Ca-imaging and electrophysiological recordings, given that DNp15 was found to be a non-spiking neuron, the concentration of Ca^{2+}-ions acting as a second messenger might transmit neural information rather than voltage. In contrast, recording intracellularly permit us to accurately determine the hyperpolarization exhibited during null-direction rotations and BtF translation.

When identifying genetic driver lines specific for DNs, Namiki *et al.* [111] established the name DNp15. They suggested that it is the same neuron as DNHS1 described previously in *Drosophila* [138]. The preference for yaw rotational stimuli along with the anatomical layout leave very little doubt that this is the case. In that study, DNHS1 was reported to produce spikes during both flight and quiescence. The data presented in this thesis offers little evidence for action potentials. Nevertheless, voltage transients are present in the trace which could be due to active conductances that enhance signal propagation, similar to what has been described for HS cells [65]. From previously described DNs [1, 106, 146], it appears that active transmission via action potentials is the typical mode of operation in these cells, which seems reasonable because the signal travels a comparatively long distance from the brain to the VNC. Nevertheless, Suver *et al.* [138] found DNOVS1 to be a non-spiking neuron. Moreover, in *Calliphora*, an animal that is noticeably larger than *Drosophila* and hence exhibits longer paths for signals to travel, DNOVS1 relays the output of VS cells in the lobula plate to motor centers without action potentials [66]. Complementary to the previous study by Suver *et al.*, this work focused on unilateral and hyperpolarizing input, and combines these findings with genetic manipulations in behavioral assays.

Strikingly, DNp15 is strongly hyperpolarized when confronted to null-direction motion, with an amplitude of inhibition comparable to the excitatory amplitude for the corresponding preferred-direction stimulus. Additionally, its responses to rotation are highly reminiscent of

HS cell responses because of their sustained profile, slow return to baseline after the stimulus ended, and the near symmetry of PD/ND responses. Other studies have found gap junctions to exist between HSN and DNp15, possibly relying on an unidentified isoform of inx8 to form the hemichannel [117, 138]. Motivated by the similarity to typical HS cell responses, we hypothesized that gap-junctions supersede the chemical synapses from those, transmitting hyperpolarization as well as the slow return to baseline. In preliminary experiments not shown here, RNAi mediated knock-down of *shakB* (inx8) targeting all isoforms [2], the tonic character of PD and ND responses was not abolished despite subtle changes in other aspects. Given that knockdown of innexins is known to often be insufficient, depending on the timing of Gal4 expression, turnover rates of proteins and mRNAs and other factors, more extensive experiments are required before drawing conclusions. Additionally, other unknown innexins or inx8 isoforms may be involved in the formation of the hemichannels between HS and DNp15 cells.

Alternatively, the hyperpolarizing input could be mediated by another upstream neuron. Indeed, HS and H2 cells account for ≈5% of input synapses only, leaving room for currently unidentified visual input. The work from Erginkaya *et al.* [48] adds the newly described inhibitory bIPS to this list. However, the model that was put forward does not explain the hyperpolarization during ipsilateral BtF rotation, because bIPS is mainly driven by contralateral FtB motion. A third possibility lies in a hypothetical baseline drive from HS synapses, which could be silenced by ND motion, thus revealing a hyperpolarized resting membrane potential. Resolving between these possibilities in the future could lead to new insights about how small brains condense information transfer into a reduced number of neurons through gap junctions or constitutively active synapses.

Because it has been demonstrated that behavioral responses can be evoked by hyperpolarizing HS cells which causes turns in the opposite direction than HS depolarization [20], the marked hyperpolarization exhibited by DNp15 as the major downstream partner of HS cells hints at a role in behavior, as it would permit to faithfully relay HS hyperpolarization. In this context, it is worth noting that the amplitude of the DNp15 hyperpolarization during BtF translation was lower than for ND rotation, analogous to FtB and PD depolarization. This could indicate ethological implications of the hyperpolarized membrane potential, supposedly by a downstream indirect comparison of activity levels from the left and right DNp15. While the artificial stimuli shown here would lead to perfectly symmetrical activity in the left and right instance of this and other DNs, in real-life situations the visual landscape is always asymmetrical to various degrees, such that it becomes important to enhance the contrast in cell activity between the left and right side. This enhancement would be possible by reducing

the overall responses to translational optic flow. Indeed, the recent preprint by Erginkaya *et al.* [48] proposes a model that acts to enhance rotational over translational movement in a small network that refines HS and H2 input to DNp15 to suppress translational optic flow via inhibitory synapses. Based on Ca-imaging, this model aligns well with our findings. Nevertheless, some aspects of the hyperpolarized responses are not easily explained. For instance, full-field ND rotation leads to a stronger hyperpolarization than ipsilateral BtF motion alone. However, contralateral FtB motion, predicted to largely provide bIPS inhibitory input, does not in itself elicit hyperpolarization. If this were due to the reversal potential being close to the resting membrane potential, full ND rotation could not lead to a hyperpolarization. In my opinion, this suggests that bIPS requires stronger drive, achievable by binocular input, to reliably become active. Alternatively, feedback loops known to exist e.g. via CH cells [134] could modify the time-course of the responses in ways that need further investigation.

The temporal frequency tuning of DNp15 activity, like the motion response, is strongly reminiscent of the HS and H2 frequency tuning [152], with a peak in the range of 0.5 Hz to 1 Hz in quiescent flies. Like the visual neurons whose tuning it inherits, responses of DNp15 depend on the frequency of contrast changes, a product of velocity and spatial wavelength, rather than the absolute velocity. Ethologically, the velocity is more relevant for course control than the frequency, though the importance of this distinction is mitigated by the broad peak of the tuning in DNp15. Additionally, animals do not necessarily need to match the rotational velocity in a closed-loop real life scenario, because excessive steering immediately causes optic flow in the opposite direction. Instead, it is sufficient to keep the optic flow oscillating close to zero in the way of a differential-feedback control system to achieve a constant heading.

Here, I recorded intracellularly from DNp15 to capture the downstream implications of efference copy mechanisms acting on HS cells. A full interpretation of the significance of the saccade-related potentials in HS cells requires a more thorough understanding of the ethological role of HS cells, and how their activity is relayed downstream. Despite recording from quiescent flies only, the diminished response to a PD rotation following a looming stimulus is observed in DNp15, just like it was described in the previous chapter for HS cells. While this is an effect of the expanding ipsilateral looming disc and not directly linked to saccades, it reveals that the same suppression seen in the HSN subtype prominently features in DNp15 responses as well. Therefore, it is reasonable to assume that the other effects acting on HSN, especially the efference copy during escape saccades, equally inhibits DNp15. Notably, excitatory drive from contralateral H2 cells does not balance the reduced HS input, either because it is not sufficient, or because H2 receives an equivalent saccade-related signal as well. This confirms DNp15 as an interesting target for studying the HS pathway and its postulated role in the optomotor response and how the observed efference copy affects the behavioral output.

3.4.2 Silencing reduces optomotor turns

DNp15 response characteristics, together with aspects of connectivity, suggest that it plays an important role in performing optomotor turns. To assess this hypothesis, we tested whether flies still executed optomotor turns in response to moving sine gratings in a range of velocities when DNp15 was silenced. Indeed, under the influence of Kir (constitutive hyperpolarization), optomotor flight as well as head turns were significantly diminished in both clockwise and counter-clockwise direction under certain stimulus conditions.

Kir expression reduced optomotor responses in a specific window of parameters only. Surprisingly, the largest discrepancy between DNp15>Kir and empty split-Gal4>Kir controls in flight is seen at 2 Hz, despite the intracellular tuning curve indicating a preference for lower frequencies. While statistical tests indicate differences at 1 Hz, the effect size is small due to the overall low response amplitudes, such that it is difficult to estimate the relevance of DNp15 at lower frequencies. Similar proportions were seen for sine gratings with smaller spatial wavelength, but given the reduced response amplitudes, those were difficult to assess.

Silencing DNp15 by Kir did not only reduce flight responses, but also optomotor turns of the head. However, head movements were far from completely abolished, and it was not trivial to distinguish the effect in our data. One reason for this is the pervading spontaneous activity, including both smooth and saccadic movements in either direction. Nevertheless, Two features permitted to analyze optomotor turning: a relatively consistent initial head motion at the onset of the stimulus and smooth motion following the pervasive occurrence of gaze-reset head saccades in every condition. In both cases, the head starts from a position that allows following the stimulus without immediately triggering a saccade when the head reaches an extreme position [22], in the former case starting on average from the midline. Together, analysis of these two features paints a picture that is largely in line with flight responses. While the exact results diverged depending on whether the stimulus onset phase or post-saccade movements were considered, the common trend leads me to conclude that DNp15 is crucial for optomotor turning in the lower range of stimulus frequencies. At higher velocities, the effect of Kir is clearly reduced, mirroring my findings on flight turns.

Owing to the overall noise in the data, additional metrics like saccade frequency, wing-head coupling and more could not be established. One reason for this is that the ideal conditions for recording wing stroke amplitude are somewhat contrary to the ideal conditions for head tracking in terms of lighting and sampling rate, reminiscent of the difficulties experienced by Cellini *et al.* [22] (who optimized for head tracking). Nonetheless, this data may be a relevant

addition to the general knowledge because head motion is rarely reported, even though it could be measured in many studies on tethered-flight.

Why does silencing not affect optomotor behavior at higher frequencies? The tuning curve from intracellular recordings in **??** (without Kir expression) shows decreasing sensitivity of DNp15 to higher frequencies in quiescence. However, the behavioral findings might indicate that the tuning is dependent on locomotor state, and that stimuli with higher frequency could overcome the suppression by Kir. Indeed, previous studies have seen that VS cell responses are tuned to higher temporal frequencies in flight compared to quiescent flies, caused by octopaminergic modulation from the central brain [97, 139]. Related effects of octopamine have been found in LPTCs in blowflies [81, 95] including the H2 cell [94]. In *Drosophila* HS cells, a shift in resting membrane potential and response properties has been shown during flight [132], and, more specifically, the response gain is shifted towards higher temporal frequencies during walking [28]. Consequently, DNs receiving strong visual input may be reasonably expected to exhibit a shift in frequency tuning as well. Alternatively, additional DNs could relay rotational optic flow to the motor system. In that case, a population of DNs controls optomotor behavior by functionally specializing to a range of stimuli.

What might explain the apparent lack of suppression in TeTx-expressing flies? First, there is no direct evidence for the actual presence of TeTx in the axon terminals, leaving room for speculation about expression levels in this split-Gal4 line. In contrast to available TeTx constructs, the Kir2.1 effector is fused to a GFP reporter, enabling us to confirm its expression, which proved to be effective in our experiments. Moreover, multiple studies have demonstrated the variable efficiency of silencing neurons using an array of effectors [121, 144], which point at the difficulty to predict the efficacy of any one effector. TeTx efficacy, in particular, has been reported to differ between cell types.

Alternatively, the discrepancy between flies expressing these two effectors could hint at the distinctive role of electrical synapses which are known to exist in this circuit in parallel to chemical synapses [117, 138]. Indeed TeTx only affects chemical synapses, whereas the constitutive shunting via Kir2.1 conceptually blocks the transmission of signals via electrical synapses as well. Gap junctions are not yet mapped thoroughly in the fly's nervous system apart from specific instances mostly in the visual system, which includes the connection from HS cells to DNp15 in *Drosophila*. In blowflies, a network of gap-junctions couples LPTCs with descending neurons and neck motor neurons of the VCN and FNMN [67, 82, 84], the latter of which are in turn coupled to haltere neurons.

Hypothetically, gap junction coupling to a permanently hyperpolarized cell might even reduce the excitability of connected neurons. How much constitutive hyperpolarization may affect

electrically coupled cells depends on the strength of the connection, which is generally unknown. Nevertheless, it seems unlikely that the effect of Kir2.1 is able to spread to electrically coupled neurons and silence them as well, because expression in HS cells, which are coupled to DNp15 and VNC motor neurons, does not cause a comparable effect, and neither are neck movements abolished in general in DNp15>Kir flies.

Although these silencing experiments have shown DNp15 to be linked to the optomotor response, activation via light-gated cation channels did not cause flight turns. Common confounding factors in optogenetic activation studies include the excitation protocol and expression of the optogenetic channel. In preliminary experiments, different optogenetic effector lines were tested for their expression facilitated by their fluorescent reporter tags. Qualitatively, a line carrying CsChrimson::mVenus inserted into the attP2 site on the 3rd chromosome exhibited weak fluorescence only. The same went for EGFP reporter lines (without CsChrimson), underlining the relevance of considering expression levels for any given combination of driver and effector. Before each experiment, the cuticle was opened so fluorescence could be evaluated *in situ*, without amplification by antibody staining, thus asserting a minimum level of expression.The activating light stimulus was designed to reflect the long-lasting optomotor stimuli presented during intracellular recordings. We established that DNp15 is tonically depolarized during optomotor stimuli and that optomotor responses build up slowly over time, such that a continuous pulse lasting for 1 s was chosen. The lack of effect is surprising insofar as activation of DNp15 has been reported in another study to cause turning in walking flies [47], though this result is not directly comparable. Those experiments achieved unilateral activation by applying a pulse of ATP on cells ectopically expressing the mammalian P2X2 purinergic cation channel [92] in walking flies. The resulting rotational velocity was $\approx 100\,^{\circ}\,\mathrm{s}^{-1}$ and lasted for more than 10 s. Beyond that, EM reconstructions of the VNC show DNp15 axonal projections onto the third and to a lesser extent the first (ipsilateral) leg neuropil, where they synapse onto interneurons and several motor neurons. The number of output synapses to the leg neuropil is comparable to that onto the haltere neuropil. In contrast, downstream partners in the haltere neuropil do not include motor neurons. Arguably, direct connections to motor neurons make it much more likely to observe behavioral effects following activation. Furthermore, optogenetic activation of DNp15 has been attempted to no avail in another study, testing for general changes in WSA without directly evaluating L-R WSA, and corroborates the present findings [112]. In conclusion, there is no evidence that DNp15 activity is directly causing optomotor flight turns.

Intriguingly, our findings for DNp15 are the opposite of activating and silencing its main visual input neurons HS and H2. For both of these, optogenetic activation causes turns in walking

and flying flies, whereas silencing does not abolish optomotor turns [20, 69, 84, 152]. While the lack of a silencing phenotype can be explained by the binocular integration in this DN, the activation phenotype strongly suggests that there are parallel descending pathways. In EM reconstructions, DNp15 stands out as the major downstream partner of HS, other DNs, namely DNa04 and DNp18 are reported as well, notwithstanding potential indirect connections and undefined neurons. Although HS cells are the most prominent, they are not the only yaw sensitive LPTCs, which adds additional avenues for optomotor-related signals.

For instance, recent studies found another population of DNs, labeled DNg02, which are tuned to rotational optic flow [112], but with uncharted connectivity. Surprisingly reminiscent of our findings, silencing largely abolished optomotor flight behavior, whereas unilateral activation did not cause turns [114]. This points a paradigm where flight control requires coordinated activity of a number of DNs. While this seemingly argues against the concept of DNs as labeled lines for motor commands, it does not strictly preclude it as an upstream command signal may be involved under natural conditions.

Indeed, a very recent study presented evidence for populations of DNs forming modules that can be coactivated by a common upstream DN, which is referred to as a command-like DN [16]. In our case, DNp15 receives strong input from DNb03 in the brain, and the latter is recurrent on itself, which could be interpreted in the sense of a command-like neuron. Note however, that this does not necessarily imply that the DNg02 are part of the same hypothetical module. Instead, two facets of flight control may encode independent aspects that occur in optomotor behavior, and allow for flexibility.

3.4.3 Summary

Here, I investigated the visual response characteristics and functional role of a descending neuron to explore its hypothetical role in the optomotor response. The DNp15 is preferentially tuned to large-field rotational over translational optic flow by integrating visual input from both eyes in line with its predicted connectivity. Surprisingly, it is a non-spiking neuron and thus offers an avenue for relaying hyperpolarizing ND optic flow from HS cells to motor centers in the VNC with an amplitude that is similar to PD stimuli. Hypothetically, the hyperpolarization is mediated by the electrical synapses known to exist in parallel with chemical synapses with HS cells, which would demonstrate a functional role for this double mode of communication that is not uncommon in the fly brain. Constitutive hyperpolarization by expressing Kir in DNp15 on both sides strongly suppressed smooth optomotor flight turns as well as reducing

the efficacy with which the head follows optomotor stimuli. With numerous output synapses to the neck and haltere neuropils including neck muscle motor neurons, this behavioral phenotype aligns with the connectivity that is presented in the EM volume reconstruction of the VNC. Additionally, this effect on both the head and wing motion fits to the observation that head and flight turns are strongly correlated. Surprisingly, unilateral activation did not show a discernible effect during flight in head-fixed flies, contrary to what has been reported during walking [47] but corroborating a previous study during flight [112]. Possibly, this discrepancy indicates that different organizational principles underlie steering in flight and walking, where flight turns require simultaneous activity from multiple sources, based on the rationale that the wing joint is a complex structure compared to the mostly linear leg joints and that errors in flight control can lead to crashes. Supporting this idea, another group of DNs has recently been reported to be tuned to rotational optic flow. Similar to DNp15, silencing suppresses optomotor flight turns but unilateral activation does not elicit turns [114]. How the activity of these different DNs is coordinated, and the impact of DN-to-DN connections is an interesting avenue for future investigations. Finally, hyperpolarization and the reduced processing of rotational optic flow that we demonstrated in HS cells during saccades is transmitted to DNp15. Given that DNp15 inhibition reduces flight turns, it is likely that an efference copy acting on HS cells acts via DNp15 to affect flight and neck turns.

4 Broader perspective and concluding remarks

The visual system prominently provides cues that are needed to stabilize intended movements, like straight flight towards a goal, and thus exerts feed-forward control over the motor system. However, during saccades this feed-forward control needs to be interrupted to allow turning. This thesis set out to elucidate the bidirectional link between visual perception and motor control. Progress has been achieved by elaborating on the signal that HS cells receive during saccades. Importantly, it was established that this signal, previously postulated to represent an EC [85], is in fact able to suppress the processing of the expected reafferent visual motion. We further showed that this EC is specific to HS subtypes, and the inhibitory signal to HSN was investigated in detail. A model of the visual reafferent input during escape saccades resolved apparent contradictions in the interpretation of these findings. However, the origin of this EC is still unknown. Future research might attempt to locate its source. The time-course of the EC signal, lasting for more than 100 ms, could hint at a neuromodulatory action, but the time-course could also be prolonged as an artifact of tethered flight like it is the case for the saccade maneuver itself.

Certain aspects of visually guided flight control, like the optomotor stabilization response investigated here, arguably need to be silenced during saccades, while the visual information might still be required for other aspects, like orientation and navigation. Determining whether the input localizes to the dendrite or is due to axonal contacts is an interesting future direction in that regard, because restricting the inhibition to axonal segments allows for dendro-dendritic synapses to relay visual information nonetheless. However, HSE cells show an EC signal resembling either HSN or HSS, which hints at a certain, limited spread of EC via electrical synapses known to exist between HS subtypes [117, 129]. Studies in walking *Drosophila* have

discovered motor-related signals that modulate HS cell activity in a way that is syndirectional with the expected small-scale visual motion [56]. These signals, phase-locked to the step cycle, partially depend on ascending neuron activity via other neurons in the posterior slope. Taken together, it becomes increasingly clear that HS cells receive a variety of motor-related input from currently unknown sources that are presumably located both in the VNC and the cerebral ganglia. It has been shown that other visual output neurons in the lobula plate and optic glomeruli similarly receive input that encodes motor context [84, 85]. Speculatively, modulation of visual neurons is a general principle of the *Drosophila* brain to integrate multimodal information adapted to specific needs.

Every action causes reafferent input and EC (used interchangeably with corollary discharge here) can act on all levels of sensory integration. In the classification of EC signaling proposed in [32], the mechanism explored here falls under the category of sensory filtration. In arthropods, identified instances of ECs are often acting on early stages of sensory processing or the receptor cells themselves, like in cockroach hair cell-triggered escape circuits [36] or auditory processing during crickets' stridulation [118]. Cricket auditory filtering operates on a timescale of ≈50 ms, in phase with single stridulation movements (syllables), and acts on an auditory direction-selective interneuron [104]. In these respects it is analogous to our EC in HSN neurons, with the duration of the signal in the range ≈200 ms, or faster for the constituents of biphasic ECs. In the case of the cricket, however, the source of the EC has been located to be a single neuron receiving input from the central pattern generator that controls singing. For HS cells, an EC originating in the wing motor centers would require an ascending signal that a saccade is actively being performed. Alternatively, the EC signal derives from a motor command specific for saccadic turns that is generated in the cerebral ganglia. In that case, it needs to be ensured that EC and saccade coincide, which touches upon the question of motor control by descending neurons. Such a mode of action is conceptually simpler to realize if DNs act as labeled lines instead of a population code. Some evidence for labeled lines has been found in flying *Drosophila* [122, 131], but this question is under active investigation [16, 50, 112]. Other instances of identified EC sources in arthropods similarly inhibit reafferents via a single interneuron [32].

To the best of our knowledge, no comparable case has so far been described in which an EC acts differentially upon closely related subtypes of neurons. The subtype specificity indicates that the complexity of EC mechanisms is related to the complexity of motor control. It exemplifies how small brains can accomplish surprisingly complex tasks by tailoring information processing to behavioral needs and depicts a coevolution of perception and motor control. As locomotor-related signals appear to pervade the brain, including mechanosensory and

olfactory neuropils in other insect groups as well as *Drosophila* [23, 27], it becomes more and more apparent that behavioral context is integrated at relatively early stages of sensory systems, before information from different sensory modalities is merged. From an evolutionary perspective, it is interesting to note that organisms with less developed central nervous systems can implement the same strategy, as it does not rely on central ("higher") associative functions.

The EC we observed was specific to HSN, with HSS receiving different input. However, the modeled reafference showed a highly similar reafferent input to HSN and HSS. This supports the notion that HSS is relevant for another behavior than HSN. In this case, although the visual response properties of all three HS subtypes are very similar, the EC signal provides evidence for functional subdivision. Therefore, we investigated a downstream neuron that is well-posed to relay and transform output from HSN specifically to the VNC, and so hypothetically represents the link where the EC affects the motor centers.

This neuron, labeled DNp15 by Namiki *et al.* [111] and previously referred to as DNHS1 [138], integrates binocular visual input, and prefers rotational to translational optic flow by tonic depolarization in the preferred direction. EM reconstructions from the Hemibrain project predict notable input from ipsilateral HS and contralateral H2, which aligns well with our intracellular recordings. These input neurons only account for a fraction of synapses, and hypothetically other modalities are integrated at the level of the dendrite of DNp15. For comparison, an analogous neuron in the blowfly *Calliphora* extends dendrites dorsally up to the ocelli, supporting a role as integrator of sensory information at the larger scale [66].

On the behavioral level, bilateral silencing established that DNp15 is directly relevant for optomotor behavior, but ectopic activation does not apparently cause turning. Additionally, the silencing effect was apparent only at the lower range of stimulus velocities. Taken together, this strongly suggests that other DNs are active together with DNp15 under natural free flight conditions. As silencing upstream HS and H2 cells does not markedly suppress optomotor turns in flight [84, 152], other visual output neurons may be involved and target those additional DNs. Speculatively, the visual output could converge onto an optomotor-turn command DN that in turn relies on DNp15 among other DNs. However, because DNp15 is strongly driven by visual input directly in quiescence, individual aspects of turning behavior could be controlled by parallel pathways with different thresholds or temporal frequency tuning.

How DNp15 (in-)activity coordinates with other DNs ties into the question of how descending motor control is organized. Some DNs have been shown to act as command-like neurons that direct downstream motor circuits (e.g. [122, 131] in flight), but many DNs do not directly elicit a specific behavior and many DNs are coactive in spontaneous behaviors [3, 112]. An

interesting line of evidence recently showed that command-like DNs could act by coactivating populations of downstream DNs, thus unifying the opposing paradigms [16]. In this view, some DNs may essentially constitute gating signals, without which certain steering muscles can not be configured for the flight maneuver, while other DNs set the muscle activity that facilitates the wing motion in question. Indeed, recently a set of DNs has been found to be involved in optomotor turns of the body and head, but unilateral activation increases wing stroke amplitude bilaterally [114]. Speculatively, DNs that act on steering muscles (including DNp15) could asymmetrically distribute the increased flight power that is delivered via DNg02 activity. To test this hypothesis, observation of network activity would be the logical next step to elucidate how brains control flight. Current methods for imaging VNC activity require removing the flight power muscles [25, 76]. While the population activity of DNs was measured by Ca-imaging of their axons in the neck connective in walking flies, the required close contact with the neck hinders wing movements [3]. Adaptation of these techniques to flight behavior is not trivial, but could reveal great insights.

Notwithstanding, important properties of DNp15, namely the absence of action potentials and relaying of hyperpolarization, could only be observed by recording intracellularly. Indeed, an analogous mode of transmission has been reported in other DNs that relay rotational optic from VS cells to the VNC in both *Calliphora* and *Drosophila* [66, 138]. In what way these properties are relevant for behavior remains to be determined. While unilateral activation did not elicit measurable responses, unilateral hyperpolarization might provide insights into the way that optomotor turns are generated in the future. Future scrutiny could also clarify whether the hyperpolarization is caused via diminishing the excitatory drive from HS synapses with an otherwise high baseline of neurotransmitter release, or a possible computational implication of electrical synapses with HS cells [117]. In the same way as ND optic flow, the hyperpolarizing EC that is acting on HS cells is relayed downstream to DNp15. In the present work, the HS EC effect was not strictly shown to act on DNp15 during saccades, but DNp15 in quiescent flies exhibit the same reduced PD response as HS cells after an ipsilateral looming stimulus. Together with the fact that silencing this DN markedly reduces optomotor turns indicates that indeed, the saccade-related potential in HS cells can negate responses to reafferent optic flow.

Until now, our knowledge of descending control of flight is very limited. Some research has elucidated the role of single command-like neurons during flight [1, 122, 131], but to our knowledge neck and flight motor control have not been measured jointly before in silencing and activation experiments on DNs. Head and flight turns are closely correlated at the behavioral level. Indeed, a number of DNs including DNp15 project to both the neck and

haltere, but not the wing tectulum. The effects of DNp15 activity reported here align well with the control-loop hypothesis, which states that wing movements are ultimately controlled via the halteres to integrate fast, wing stroke-synchronous proprioceptive feedback with slower non-synchronized signals from the brain [38]. Because silencing reduces flight turns, the output of DNp15 likely influences wing movements via the halteres. Alternatively, output from DNp15 and similar DNs could serve to suppress haltere afferents that stabilize body orientation by feedback to the wings, while other DNs evoke the flight turns directly. Although this aligns with the lack of activation responses, it is unlikely for several reasons. The DNs that project to the halteres target haltere MNs directly, not just interneurons and there is little indication for postsynaptic sensory neurons. Overall, flight power and steering muscles are innervated mostly by local interneurons and receive little descending control [91]. Finally, neck and flight turns are similarly affected by silencing DNp15, although the wing neuropil was not directly in contact with silenced input in contrast to neck MNs. While haltere afferents have been found to project to the neck [136], they are not sufficiently effective to synchronize the head and wings [119]. Together, this paints a picture where input from the brain is integrated in the haltere tectulum to modulate haltere feedback. Having established the implication of a specific DN in flight turns may help to develop the control-loop hypothesis further by filling in the missing links between sensory perception and steering muscle activity via the halteres. Thus, this work contributes to a full understanding of the chain of neural processing that links perception to behavior in the case of optomotor turns.

5 Materials & Methods

5.1 Methods

5.1.1 Fly husbandry

Strains of *Drosophila melanogaster* were bred on premixed cornmeal-agar medium (JazzMix Drosophila food, Fisherbrand) at 25 °C on a 12h day/12h night cycle.

Flies used for efference copy experiments were of either wild-type Canton S (two flies) or expressing GFP in HS cells using the Gal4/UAS system (GMR81G07-GAL4 or GMR27B03-GAL4). All individuals had at least one wild-type allele for the *white* gene. To avoid side-effects of in-breeding, GMR27B03-GAL4; 2xUAS-EGFP flies were back-crossed to wildtype flies (Canton S and Top Banana), and offspring selected for fluorescence every few generations. We used female flies aged 2 to 5 days after eclosion for all experiments.

For silencing experiments involving DNp15, the split-Gal4 line SS01556 (hemi-drivers GMR11E07 & GMR77F05) was crossed to UAS effector lines for 2xUAS-EGFP, UAS-TeTxLC (tetanus toxin light chain) or UAS-Kir2.1. The same UAS lines were crossed to an empty split-Gal4 line for negative controls. For a list of fly stocks see **??**.

5.1.2 Fly Perspective Modeling

The visual input that a fly experiences during a flight maneuver in free flight was modeled in 3D animation software by moving an camera along a real-world flight trajectory. These flight trajectories were extracted from a dataset of high-speed trackings of *Drosophila hydei* in a free flight arena while being confronted with a looming stimulus, recorded by Muijres *et al.* [109]. Only the trajectories analogous to our electrophysiological recordings were selected, more specifically those where the looming disc approached the fly at an angle in the range $\pm\,[105, 145]$. The traces were downsampled to match the average wing stroke frequency of 189 Hz (above the flicker fusion frequency of 120 Hz [60]) by choosing the closest corresponding frame to decrease the computational expense and obtain sufficiently large motion steps in between frames. Additionally, the reference frame of body orientation was adjusted from an aeronautic-based representation, which is a right-handed coordinate system with the z-axis pointing downwards, to a right-handed system with upward-pointing z-axis. In contrast, the reference frame of fly position is right-handed with an upward-pointing z-axis.

The extracted trajectories were fed into Blender 3D-animation software ([10] version 3.1) as the position and Euler angle (ZYX order, extrinsic rotation) of a fly model or a camera respectively. In a first step, the trajectory was applied to a schematic fly model and rendered at each frame from three orthogonal directions by three orthographic cameras to visually verify the correctness of the conversion between reference frames. A visual scenery was created in Blender by projecting a 360° image to the background and distributing additional objects in the vicinity of the coordinate origin. The same trajectory was applied to render a 360° equirectangular projection of the scene to obtain a first-person view of the panorama during the maneuver. The resulting rendered images served as the basis for optic flow estimation.

The optic flow was calculated using the algorithm developed by Yuan and Christian [161], designed specifically for the case of 360-degree spherical field-of-view images. Importantly, the procedure projects tangent images onto an icosahedron, and estimates the optic flow locally on its faces, thus remedying to the fact that the image wraps around as well as the increasing distortion towards the edges of a rectangular projection. The resulting optic flow field has the same resolution as the rendered images. The individual vectors were mapped to and averaged by ommatidia of a generic fly according to the viewing angles of each ommatidium as measured by E. Buchner [18, 74] (digitized by Andrew Straw [44]), inspired by the approach taken by Floris van Breugel[17].

The receptive field of all three HS cell types were obtained from Schnell *et al.* [129], and upsampled to fit the resolution and size of the rendered images without extrapolating the

receptive field.Finally, the full-resolution vector fields were multiplied with the upsampled receptive field to predict y- and x-components of HS cell responses, and the two components summed up to form the inner product, corresponding to the membrane potential of the given HS cell in arbitrary linear units.

5.1.3 Electrophysiology

In vivo patch-clamp recordings of neurons were performed in whole-cell configuration in current-clamp mode. Flies were anesthetized on a cold-plate, legs amputated, and fixed by the head to custom-made pyramidal holders [97] that allow access to portions of the head while offering free space to the wings using UV-curing glue. The head was bent forward to expose the posterior part in the surgery window of the holder. The head capsule was covered with extracellular saline prepared according to Wilson and Laurent [156], in mM: 103 NaCl, 4 MgCl2, 3 KCl, 1.5 CaCl2, 26 NaHCO3, 1 NaH2PO4, 10 Trehalose, 10 Glucose, 2 Sucrose and 5 TES, adjusted to 275 mOsm) and cut open using a syringe needle. The brain was perfused with extracellular saline bubbled with 95% O2 / 5% CO2 to reach pH 7.3 . The neurolemma and extracellular matrix covering the area of interest was digested by applying Collagenase (0.5 mg mL^{-1} Collagenase IV in extracellular saline, Worthington) through a low-resistance pipette (BF150-110-10, Sutter Instruments). Cell bodies were targeted under visual control with a 40x immersion objective (Nikon NIR Apo 40x/0.80W), phase-contrast filter, IR lighting (850 nm, Thorlabs) and CMOS camera (Thorcam Quantalux, Thorlabs). GFP-expression was visualized by a brief excitation of eGFP in transgenic flies. Patch pipettes were pulled with a P-1000 Flaming/Brown puller (Sutter Instruments) from thick-walled capillaries (BF150-86-10, Sutter Instruments), adjusted to a resistance of 6 MΩ to 8 MΩ. Intracellular solution was prepared according to [156] (140 mM potassium aspartate, 1 mM KCl, 10 mM HEPES, 1 mM EGTA, 4 mM MgATP, 0.5 mM NaGTP, 0.5 % biocytin, adjusted to pH 7.3 and 265 mOsm) plus AlexaFluor-568. Signals were recorded with a BA-01X bridge amplifier (npi electronics) and a BNC-2090A digitizer (National Instruments) with MATLAB (version R2017b, The MathWorks).

The measured membrane potential was adjusted by a liquid junction potential of −13 mV. In recordings from DNp15 cells, the resting membrane potential was typically around -52.4 ± 3.8 mV, in the range −49 mV to −59 mV. If the resting membrane potential was above −40 mV or the cell depolarized to both PD and ND directions, the data was discarded.

5.1.4 Immunostaining

Female flies were dissected to retrieve the CNS including the VNC. These were fixated for 30 min at room temperature in 4 % paraformaldehyde (PFA). Subsequently, brains were washed with phosphate-buffered saline (PBS, pH 7.2, diluted from 10X, Sigma Aldrich, MA, USA) 3 times for 10 min. Before antibody application, brains were permeabilized for 20 min in PBS supplemented with 0.2 % Triton X-100 (PBS-Tx). Primary antibodies were diluted in 5% normal goat serum (NGS, Invitrogen, LOT# 0930521) diluted in PBS-Tx and incubated overnight at 4 °C. Primary antibodies were rinsed off by incubating 3 times in PBS-Tx for 10 min at room temperature. Secondary antibodies were diluted in PBS-Tx supplemented by 5 % NGS to 1:200 and applied overnight at 4 °C. Brains were thereafter washed for 15 min in PBS-Tx, followed by at least 4 repetitions in PBS for 10 min each. The stained brains were mounted in Vectashield (Vector Laboratories, CA, USA) and analyzed using confocal microscopy (Leica SP8 or Leica STELLARIS 8).

The following antibodies were used to visualize HS cells after recording intracellularly: anti-GFP polyclonal (1:1000, rabbit, ThermoFisher Scientific, MA, USA, LOT# 2477546) primary antibody, along with the polyclonal secondary antibody anti-rabbit AlexaFluor488 (1:200, goat, ThermoFisher Scientific, LOT# 1966932). Strepavidin-AlexaFluor633 (1:1000, ThermoFisher Scientific) added to the application of secondary antibodies to stain against biocytin, which was delivered by the patch pipette.

Additionally, after intracellular recordings of DNp15 cells, the staining was simplified to a one-step process by applying only GFPbooster-Atto488 (1:200, ChromoTek) and Streptavidin-AlexaFluor633 (1:1000, ThermoFisher Scientific), omitting the secondary antibody and washing steps between the primary and the secondary antibodies.

For visualizing markers of neurotransmitter usage, GFPbooster-Atto488 (1:200, ChromoTek) was combined with RFPbooster-Atto594 (1:200, ChromoTek) and no secondary antibody was needed.

5.1.5 Behavioral Monitoring and Tethering

Flight behavior was monitored in tethered flies by proxy of measuring the left and right wing stroke amplitudes (WSA). Turning behavior was quantified as the difference between left and right WSA (L-R WSA), and thrust as their sum (ΣWSA). Tethered flies were observed

from below by an IR-sensitive camera (Basler acA645-100gm equipped with a 1.0X 94 mm WD InfiniStix lens, Infinity Photo-Optical). The wings were illuminated from the fly's posterior by light-guides coupled to 850 nm IR LEDs (Thorlabs M850F2). The wing stroke amplitude was detected using a modified version of the Kinefly software ([138]) running on ROS (version Kinetic Kame), which outputs a voltage signal via a DAC (Phidgets analog) that was recorded jointly with the electrophysiological signal. The WSA was detected as the first threshold crossing of the derivative of the luminance signal extracted from the image stream, which made the detection less error-prone in our setup than the original Kinefly algorithm.

Flies were tethered using UV-curing glue in two different ways for experiments. For intracellular recordings and optogenetic activation, flies were tethered to custom-made pyramidal holders ([97]), which allowed tethering by the head and leaves the wings free to move. To permit head movements, flies were tethered at the notum to 55 mm insect pins (0.03 mm tip diameter, Fine Science Tools, Germany) bent at a defined point by 30°. The pin was inserted and fastened to a custom adapter to the microscope (designed using FreeCAD), analogous to the classic rigid pin tether paradigm [73].

5.1.6 LED arena and visual stimulation

The fly was positioned in the center of a half-cylindrical arena of LED panels (IO Rodeo) as described [120]. Our arena is made of green monochromatic LEDs (565 nm) where each pixel subtends an angle of 2.25° on the fly eye, covering a total visual field of about 195° in azimuth and 60° in elevation. In this setup, the frame shift rate was set to 50 Hz, while the arena was tuned to a flicker rate of about 744 Hz.

Looming stimulus

The looming stimulus has been described in detail in Fischer and Schnell [53], (see attached paper in **??**). For ease of reading and because the same stimulus was used during intracellular recordings from DNp15, that description is repeated here.

The visual scene presented to the fly as background consisted of dark squares on a bright background with maximal contrast. Centered at an angle of 54° on either the left or right side, a dark disc expanded, simulating an object approaching at constant speed of 1.5 m//second. Thus, the visual angle covered by the imaginary object is given by $\Theta = 2arctan\left(\frac{-h}{vt}\right)$ with h =

0.1 m, v = 1.5 m/s and t = 0 at the expected moment of impact [58]. The half-size to approach ratio (h/v) is therefore 66.7 ms. The maximal lateral extent of the stimulus was 76.5°. At time t' > 0, the looming disc disappears. The background consisted of randomly distributed dark rectangles on a bright background with 100 % nominal contrast, with each rectangle measuring at least 5° × 5° in the visual field. This background was rotated with a speed of 112.5 ° s^{-1} for 240 ms either clockwise or counter-clockwise, which we call optomotor stimulus in this context. In a given trial, the stimulus consisted of either looming (left/right) only, background rotation (either direction) only, or looming followed by background rotation, making for a total of eight different stimulus combinations. Each trial lasted for 1.35 s, with an inter-trial interval of 3 s. The order of these stimuli was permuted. Each fly completed several experimental runs.

Visual motion frequency tuning

Vertical stripes with a sinusoidal luminance profile using 16 equidistant intensities tiled the entire arena periodically. The spatial period of stripes was either 18° ("thin") 36° ("wide"). Rotational velocities were set to result in specific temporal frequencies of visual features moving at any given point in the visual field. Frequencies of 0.5 Hz, 1 Hz, 2 Hz, 4 Hz and 6 Hz correspond to 9 ° s^{-1}, 18 ° s^{-1}, 36 ° s^{-1}, 72 ° s^{-1} and 108 ° s^{-1} for thin stripes and 18 ° s^{-1}, 36 ° s^{-1}, 72 ° s^{-1}, 144 ° s^{-1} and 216 ° s^{-1} for wide stripes. The order of these stimuli was permuted semi-randomly, such that a given period-velocity combination was presented first clockwise and then counter-clockwise before testing another combination. Each fly completed several experimental runs to obtain enough trials.

Half-field motion

Vertical square-wave stripes tiled the arena with a spatial period of 36°. The visual field in front of the fly contained a 36° wide stationary dark stripe to exclude the area of binocular overlap. The stripes moved at a velocity of 28.125 ° s^{-1}, corresponding to a frequency of about 0.75 Hz, with dithered intermediate steps to render the motion more fluid. Visual motion was presented bilaterally to mimic rotation or translation respectively, or unilaterally (left/right) to dissect contributions from each hemisphere. A given trial consisted in a combination of left and right sides moving in front-to-back (FtB) or back-to-front (BtF) direction or staying stationary. Thus, the protocol consists of 8 combinations which can be labeled as left or right side only in FtB or BtF direction for unilateral motion, full-field clockwise/counter-clockwise and full-field FtB/BtF motion. The order of these stimuli was permuted semi-randomly, such that e.g. left-sided FtB was followed by BtF on the same side before testing a different combination of left/right motion. Each fly completed several experimental runs to obtain enough trials.

5.1.7 Optogenetic activation

Flies intended for optogenetic activation experiments were bred on standard food and subjected to a heat-shock at 37 °C to induce stochastic expression of optogenetic constructs by excision of a STOP cassette mediated by a hsp-FLP recombinase. Heat-shock durations tested were 30 min, 60 min, 70 min and 100 min with 70 min proving to be the most effective for achieving unilateral expression of CsChrimson while still providing a sufficient number without expression. After eclosion, flies were transferred onto food vials supplemented with 50 µL 100 mM all-trans-retinal applied after onto prepared, cool food, and kept in the dark for at least 48 h. The epifluorescence light path of the microscope was used to deliver red light for activation using a mercury lamp (Excelitas X-Cite 200DC) with a 630 ± 10 nm bandpass filter (Thorlabs FBH630-10). Activating light power was measured as total power delivered through the objective in the full range of settings used in these experiments using a photometer (PM120VA, Thorlabs). During experiments, the light was restrained to an area of ≈100 µm radius and the power flux was estimated accordingly as the total power distributed evenly across this circular area. Preliminary intracellular recordings from neurons expressing CsChrimson were shown to reliably elicit depolarization upon illumination.

For consistency, in behavioral recordings flies were prepared in the same way as for electrophysiology (**??**) by tethering to pyramidal holders and opening the cuticle under perfusion with extracellular saline. Before conducting experiments, expression of the fluorescent reporter fused to CsChrimson was verified and documented under epifluorescence, thus asserting sufficiently strong expression. Unless detailed otherwise, light was delivered as a continuous pulse of 1 s duration through a 40x immersion objective (Nikon NIR Apo 40x/0.80W), focused on and laterally restricted to the target neuron.

5.1.8 Data analysis

Analysis procedures for the HS cell data during saccades is described in the Methods section of the publication in **??**. This section describes the analysis for DNp15 data.

Head data preprocessing

The algorithm that detected the head angle from the camera stream automatically determined reference points for tracking, but these points occasionally shifted in between frames which

led to sudden changes in angle that did not represent head motion. Therefore the head angular position data was cleaned before further analysis. The original head data was downsampled by a custom procedure which fits a piece-wise constant function to the data. To neutralize the shifts in reference points, the first derivative was set to 0 when crossing a threshold of $0.2\,\mathrm{rad\,s^{-1}}$ ($\gtrapprox 11.5\,^\circ\,\mathrm{s^{-1}}$) and the angular position then reconstructed through integration over time. Stretches of data where the derivative did not surpass $5 \times 10^{-3}\,\mathrm{rad\,s^{-1}}$ were marked as missing data points because the algorithm presumably failed to detect motion. Finally the signal was upsampled again to the original size by expanding the previously fitted piece-wise constant function. Further analysis was conducted on the preprocessed data.

Head saccade detection

In general, detecting head saccades is simpler than detecting flight saccades (also noted by Cellini *et al.* [22]). First, the preprocessed head data was downsampled by a custom procedure which fits a piece-wise constant function to the data to retrieve the angle values which underlie the recorded trace. In this way, a smoothly differentiable function was obtained. Saccades were defined as fast and short head movements, i.e. large transient in the derivative of the angular position. The head angle was median filtered in a window of 100 ms and the derivative was calculated using the central difference method with a 30 ms half-width. Saccade candidates were determined as velocity peaks with a minimum amplitude of $0.5\,\mathrm{rad\,s^{-1}}$ using the *scipy.find_peaks* routine. Within a time window of 200 ms, smaller peaks were rejected to eliminate artifacts of saccade termination and very fast smooth turns. Additionally, peaks in the angular position were detected with a constant minimum height (0.05 rad) and prominence (0.08 rad). Saccade candidates were eliminated if there was no peak in angular position that could be attributed to a peak in velocity within 100 ms to ensure that only those candidates with a clear end point and without gaps in the trace were retained. The peak in angular position is considered to be the peak of the saccade. This algorithm was applied on the inverted signal for responses to clockwise stimuli, such that only saccades antidirectional to the stimulus were detected.

Head velocity estimation

Initial head velocity at stimulus onset was computed by linear regression on the section 70 ms to 145 ms from stimulus onset of the average response for each individual fly.

Head velocity following saccades was computed by linear regression on the downsampled data (to original 50 Hz) covering the stretch of 140 ms starting at the saccade peak for each individual saccade.

5.2 Material & resources

5.2.1 Fly stocks

Resource	Source	Identifier	notes
Drosophila melanogaster: Wild-type Canton S	Gaia Tavosanis	RRID:BDSC_64349	used in **??**
D. melanogaster: Wild-type Top Banana	Eugenia Chiappe	N/A	
D. melanogaster w[1118]; P{y[+t7.7] w[+mC] = GMR81G07-GAL4}attP2	BDSC	RRID:BDSC_40122	used in **??**
D. melanogaster w[1118]; P{y[+t7.7] w[+mC] = GMR27B03-GAL4}attP2	BDSC	RRID:BDSC_49211	used in **??**
D. melanogaster: w[1118]; P{y[+t7.7] w[+mC]=R11E07-p65.AD}attP40/CyO, P{2xTb[1]-RFP}CyO; P{y[+t7.7] w[+mC]=R77F05-GAL4.DBD}attP2/TM6B, Tb[1]	Janelia Fly Bank	RRID:BDSC_75953	split-Gal4 driver for DNp15
D. melanogaster: w[1118]; P{y[+t7.7] w[+mC]=p65.AD.Uw}attP40; P{y[+t7.7] w[+mC]=GAL4.DBD.Uw}attP2	BDSC	RRID:BDSC_79603	empty split-Gal4 (**??**)
D. melanogaster: TI{2A-lexA::GAD}ChAT[2A-lexA]	BDSC	RRID:BDSC_84379	cholinergic neuron driver in **??**
D. melanogaster y[*] w[*]; P{w[+mC] = UAS-2xEGFP}AH3	BDSC	RRID:BDSC_6658	
D. melanogaster +; P{w[+mC] = UAS-2xEGFP}AH3	this work	N/A	used in **??**
D. melanogaster: w[*]; P{w[+mC]=UAS-Hsap\KCNJ2.EGFP}1	BDSC	RRID:BDSC_6596	DNp15 silencing (**??**)
D. melanogaster: w[*]; P{w[+mC]=UAS-TeTxLC.tnt}E2	BDSC	RRID:BDSC_28837	DNp15 silencing (**??**)
D. melanogaster: UAS-FRT-STOP-FRT-CsChrimson.mVenus in attP18, hsFlp2:PEST in attP3	Alex Mauss, M. H. Dickinson	N/A	stochastic unilateral expression (**??**)
D. melanogaster: w[1118] P{y[+t7.7] w[+mC]=20XUAS-IVS-CsChrimson.mVenus}attP18	BDSC	RRID: BDSC_55134	used in **??**
D. melanogaster: y[1] w[*] P{y[+t7.7] w[+mC]=10XUAS-IVS-mCD8::RFP}attP18 P{y[+t7.7] w[+mC]=13XLexAop2-mCD8::GFP}su(Hw)attP8	BDSC	RRID:BDSC_32229	reporter for **??**

5.2.2 Software

Name, version	Publisher	Location
Python $\geqslant$ 3.7	Python Software Foundation	https://www.python.org
SciPy Library $\geqslant$1.9	SciPy	https://scipy.org
Kinefly	Steve Safarik [138]	https://github.com/ssafarik/Kinefly
ROS Kinetic Kame	Open Robotics	https://www.ros.org
ROS phidgets support	Steve Safarik	https://github.com/ssafarik/phidgets
MATLAB	MathWorks	https://www.mathworks.com/
WinWCP	University of Strathclyde, Glasgow	https://spider.science.strath.ac.uk/sipbs/software_ses.htm
FreeCAD	FreeCAD	https://www.freecad.org/

A Multiple mechanisms mediate suppression of motion vision

iScience

CellPress
OPEN ACCESS

Article

Multiple mechanisms mediate the suppression of motion vision during escape maneuvers in flying *Drosophila*

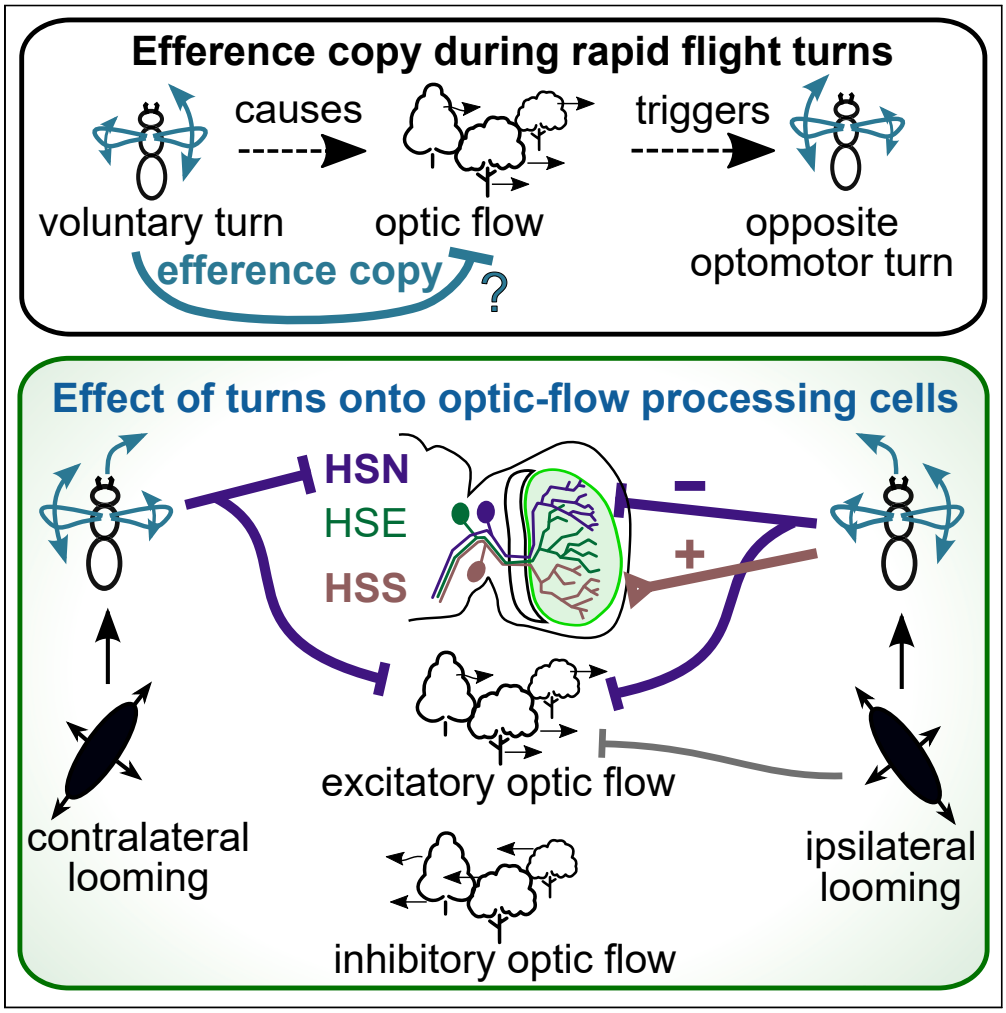

Philippe Jules Fischer, Bettina Schnell

bettina.schnell@mpinb.mpg.de

Highlights

HS cells are directionally tuned to horizontal motion and drive optomotor responses

Only the dorsal HS cells receive an inhibitory efference copy during voluntary turns

This efference copy can suppress responses to preferred direction motion

Aversive looming stimuli themselves can inhibit motion responses of all HS cells

Fischer & Schnell, iScience *25*, 105143
October 21, 2022
https://doi.org/10.1016/j.isci.2022.105143

iScience

CellPress
OPEN ACCESS

Article

Multiple mechanisms mediate the suppression of motion vision during escape maneuvers in flying *Drosophila*

Philippe Jules Fischer[1] and Bettina Schnell[1,2,*]

SUMMARY

During voluntary behaviors, animals need to disable any reflexes that could interfere with the intended movements. With the optomotor response, flies stabilize a straight flight path by correcting for unintended deviations sensed as the panoramic motion of the surround. HS cells of the fly are thought to mediate optomotor responses to horizontal motion. During spontaneous flight turns, an efference copy acts on HS cells with the right sign to counteract the visual input elicited by the fly's own behavior. Here, we investigated, whether looming-elicited turns in flying *Drosophila* have a similar effect on HS cells. We show that looming stimuli themselves can influence the processing of panoramic motion stimuli in HS cells and that an inhibitory efference copy suppresses excitatory motion responses during turns in both directions, but only in a subset of HS cells. Our findings support the notion that the processing of sensory information is finely tuned to behavioral context.

INTRODUCTION

Animals must be able to discriminate self-generated (reafferent) from external (exafferent) sensory input. Although seminal work by von Holst and Mittelstaedt suggested that this can be achieved via an efference copy of the intended behavior that counteracts reafferent sensory input (Cullen, 2004; Von Holst and Mittelstaedt, 1950), its neuronal underpinnings have largely remained elusive.

In the optomotor response, for example, flies compensate for unintended deviations from a straight flight path, which they sense as the motion of the surround or optic flow (Götz, 1968; Leonte et al., 2021; Mronz and Lehmann, 2008). However, this reflex-like compensation needs to be suppressed, when a fly performs a voluntary turn, which is also called a saccade. Saccades are rapid whole-body maneuvers that flies perform to change direction during flight (Muijres et al., 2015, 2014; Schilstra and van Hateren, 1999; Schilstra and van Hateren, 1998). Saccades do not only occur spontaneously but can be triggered by looming stimuli, indicative of an impending collision or approaching predator (Bender and Dickinson, 2006; Heisenberg and Wolf, 1979; Tammero and Dickinson, 2002a, 2002b). In head-fixed flight, intended saccades can be measured as fast changes in the difference between the left and right-wing stroke amplitude (L-R WSA), which allows for studying their influence on visual processing in the fly brain (Heisenberg and Wolf, 1979; Maimon et al., 2010; Schnell et al., 2017). Saccades have been shown to follow a different motor program when executed spontaneously compared to when they are evoked by a looming stimulus (Dickinson and Muijres, 2016), but are indistinguishable in tethered flight quantified by changes in L-R WSA.

HS (horizontal system) cells are a class of large-field lobula plate tangential cells that respond to horizontal motion in a directionally selective fashion (Hausen, 1982a, 1982b; Schnell et al., 2010). They receive ipsilateral input from columnar motion-detecting cells on their dendritic trees, but also contralateral input from heterolateral lobula plate tangential cells (Haag and Borst, 2001). There are three HS cells per hemisphere, HSN, HSE, and HSS, which differ in the position of their dendritic trees in the lobula plate and thus their receptive fields within the fly's visual field (Hausen, 1982b; Schnell et al., 2010; Scott et al., 2002). Based on their response properties as well as activation and silencing experiments, they are thought to control stabilizing optomotor turns of the head and body during walking and flight (Busch et al., 2018; Fujiwara et al., 2017; Haikala et al., 2013; Kim et al., 2017), but have also been implicated in the processing of translational optic flow (Boeddeker et al., 2005). It has been shown that during spontaneous saccades an

[1]Emmy Noether Group Neurobiology of Flight Control, Max Planck Institute for Neurobiology of Behavior – caesar, 53175 Bonn, Germany

[2]Lead contact

*Correspondence: bettina.schnell@mpinb.mpg.de

https://doi.org/10.1016/j.isci.2022.105143

efference copy acts on HS cells, which has the appropriate sign to counteract responses to the visual stimulus that would be caused by the flies' self-motion (Kim et al., 2015, 2017). However, it remained largely unclear how this effect influences the processing of large-field motion in HS cells, which are thought to underlie stabilizing optomotor responses to horizontal motion.

We investigated, whether spontaneous and looming-elicited saccades have a similar effect on HS cells and how they affect the cells' processing of horizontal motion using whole-cell patch-clamp recordings during head-fixed flight (Joesch et al., 2008; Maimon et al., 2010; Schnell et al., 2014). In contrast to previous studies, we found a large variability between different HS cells regarding the impact of an efference copy on their activity during both spontaneous and looming-elicited saccades (Fenk et al., 2021; Kim et al., 2015, 2017). If present, the efference copy is able to inhibit responses to preferred direction horizontal motion in HS cells consistent with the idea that it counteracts reafferent sensory input. However, we also found that the looming stimulus itself, when presented on the ipsilateral side, has a similar effect independent of whether the fly performed a saccade or not. Therefore, the processing of optomotor stimuli is not only affected by an efference copy, but also by stimulus history.

RESULTS

To study the effect of an efference copy on the optomotor pathway, we recorded the membrane potential of HS cells from head-fixed flies during tethered flight, while monitoring turning behavior by measuring the difference between the left and right-wing stroke amplitudes (L-R WSA) (Figure 1) (Maimon et al., 2010; Suver et al., 2016). HS cells in the right optic lobe respond to clockwise motion with depolarization and to counterclockwise motion with hyperpolarization. We recorded from randomly selected HS cells from the right side of the brain only, whose dendritic receptive field, therefore, covers the right visual hemisphere.

HS cell activity during saccades elicited by ipsilateral looming

To elicit turns, we presented a looming stimulus from either the left (contralateral) or the right (ipsilateral) side using an LED display (Figure 1D). This stimulus mimicked an object approaching at a velocity of 1.5 m/s and was sufficient to elicit changes in L-R WSA. This change in L-R WSA likely corresponds to a free-flight saccade away from the stimulated side. In the following, we refer to these changes in L-R WSA as saccades, although the flies cannot actually perform a turn under our experimental conditions. Execution of saccades was variable, meaning that flies did not always respond to the looming stimulus with a change in L-R WSA (Figure 1E). We made use of this variability to test, whether an efference copy of the flies' behavior influences the membrane potential of HS cells similar to what has been reported for spontaneous saccades (Kim et al., 2015, 2017). We used a saccade detection algorithm on the L-R WSA data from all flies to separate trials with saccades from those without saccades (see STAR Methods and Figure S1) and averaged the HS cell membrane potential and L-R WSA across the two groups.

For looming stimuli presented on the right, which elicits a turn to the left (measured as a decrease in L-R WSA) (Figure 2A), we did not find a qualitative difference in the average HS cell membrane potential between trials with and without a saccade (Figure 2B). We did notice, however, that after the end of the stimulus presentation, when the looming stimulus disappeared, the membrane potential of the HS cells dropped rapidly and became slightly hyperpolarized (arrow in Figure 2B) independent of whether the flies performed a saccade or not.

HS cell activity during spontaneous saccades

It has been reported previously that spontaneous saccades to the left lead to a transient hyperpolarization of HS cells in the right lobula plate (Kim et al., 2015). We detected spontaneous saccades in our recordings using a similar algorithm as for the looming-elicited saccades, but limited to periods, during which visual stimuli were stationary (Figure 2C). We confirmed that on average HS cells in the right hemisphere hyperpolarize during leftward saccades, although there was a lot of variability across cells with two HS cells even exhibiting a slight depolarization during the peak of the saccade (Figure 2D). Plotting the amplitude of the voltage change against the amplitude of the concomitant change in L-R WSA for the most hyper- and depolarizing as well as a non-polarizing cell shows that responses are consistent within individual HS cells and that differences between cells are not owing to differences in the magnitude of the behavior (Figure S2A). Considering all recorded cells, there is no correlation between the magnitude of the mean saccade-related-potentials and the amplitude of the behavior (Figure S2B).

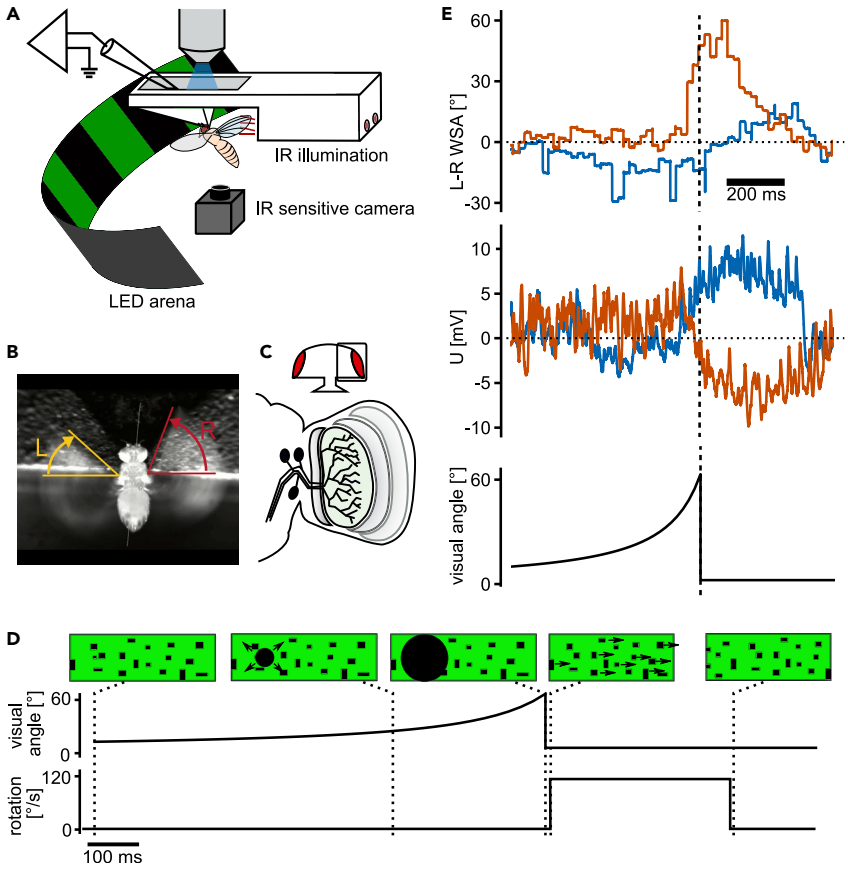

Figure 1. Whole-cell recording of HS cells in tethered flying *Drosophila* reacting to looming stimuli

(A) Schematic of the setup combining analysis of flight behavior under visual stimulation with whole-cell patch-clamp recordings in head-fixed *Drosophila*.

(B) Example image of the video stream demonstrating the analysis of wing stroke amplitude.

(C) Schematic representation of the three HS cells located in the lobula plate within the optic lobe of the fly brain.

(D) Visual stimulation protocol: a dark spot expands to a disc covering a large part of the visual field to simulate an object approaching at a constant speed (looming stimulus) within either the left or right visual hemisphere. In some trials, this stimulus is immediately followed by a rotation of the whole field (called optomotor stimulus).

(E) Example traces of behavioral response to looming from the left visual field from one fly. In many trials, the fly executed a rapid turn (saccade) away from the stimulated side (red trace, L-R $\gg$ 0 corresponds to a rightward turn). The same individual does not perform a saccade in other trials (blue). The membrane potential from the simultaneously recorded HS cells exhibits hyperpolarization only during trials where the fly initiates a saccade. Saccades typically occur shortly before the looming disc reaches its maximal size.

To test whether spontaneous saccades had a different effect on HS cells than looming-elicited saccades, we sorted our recorded cells into two groups based on whether they exhibited a hyperpolarization during spontaneous saccades (HP_{spont} group, N = 6) or no change in polarization (NP_{spont} group, N = 5, omitting the depolarizing cells). Cells in the HP_{spont} group also showed a hyperpolarization during looming-elicited saccades (Figure 2E, see also Figure S2C), which is comparable to spontaneous saccades (Figure 2G). This is the case despite changes in L-R WSA being larger during looming-elicited saccades. In the NP_{spont} groupm there was no difference between trials with and without a saccade during the looming stimulus (Figure 2F, see also Figure S2C). For a quantitative analysis, the mean membrane potential was calculated for each trial in a window of 50 ms starting 30 ms after the end of the looming stimulus, which coincides approximately with the peak L-R WSA. The change in membrane potential is significantly different from zero only during saccades in the HP_{spont} group ($p = 0.001$, two-sided Wilcoxon signed-rank test) (Figure S2D), which is also significantly lower than in trials without saccades ($p = 0.037$, one-sided Mann-Whitney-U test). In the NP_{spont} group, responses cluster around zero regardless of the behavior ($p = 0.77$ and $p = 0.30$ in trials with or without saccades, respectively). These results indicate that a

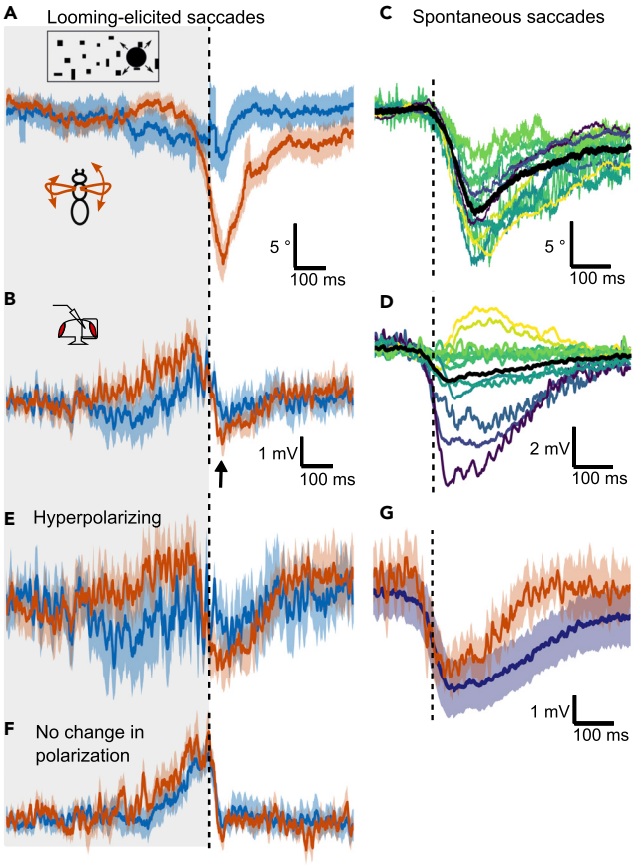

Figure 2. HS cell responses during looming-induced saccades to the left

(A) Mean ± SEM of L-R WSA of all flies in trials with a looming stimulus presented on the right (ipsilateral) side separated into trials, during which flies reacted with a saccade to the left (red, n = 62) or not (blue, n = 65), using a wavelet-based algorithm (see STAR Methods and Figure S1). The dotted line marks the end of the looming stimulus. N = 13 flies.

(B) Simultaneously recorded membrane potential of HS cells averaged across cells as in (A). One cell was recorded per fly. Shown are means ± SEM.

(C) L-R WSA during spontaneous saccades to the left for the same flies as in (A). Each color represents the mean of one fly. The population average is shown in black.

(D) Mean changes in HS cell membrane potential during spontaneous saccades corresponding to (C).

(E) Membrane potential of a subset of cells selected based on their hyperpolarizing response during spontaneous saccades (HP_{spont}) (see D) from looming trials with an escape saccade (red, n = 25) or without a saccade (blue, n = 21) averaged across flies ± SEM (N = 6 cells).

(F) Average membrane potential ± SEM of the remaining cells (NP_{spont}, N = 5 cells) as in (E) (n = 18/27 trials).

(G) Means ± SEM of the cells that hyperpolarized during spontaneous saccades (peak voltage lower than 0, purple, N = 6 cells). For comparison, the responses of the same cells during looming-elicited saccades from (C) are replotted in red. See also Figure S2.

hyperpolarizing efference copy acts on only a subset of HS cells during both spontaneous and looming-elicited saccades.

As the HP_{spont} and NP_{spont} subsets also respond significantly differently to the looming stimulus itself (compare Figures 2E and 2F, quantified in Figure S2D), we hypothesized that they may correspond to different HS subtypes. There are three HS cells per hemisphere, which cover different parts of the visual field, and are called HSN (north → dorsal part), HSE (equatorial), and HSS (south → ventral part) (Figure 3A) (Fischbach and Dittrich, 1989; Schnell et al., 2010). However, for the majority of cells shown here, we did not obtain good intracellular dye fills and thus do not know the precise subtype. To test, whether the effect of an efference copy depends on subtype, we drew on data recorded in another context and extracted spontaneous saccades to the left from them (Figure 3B) (Schnell et al., 2014). Applying the same algorithm to this data with additional selection criteria (see

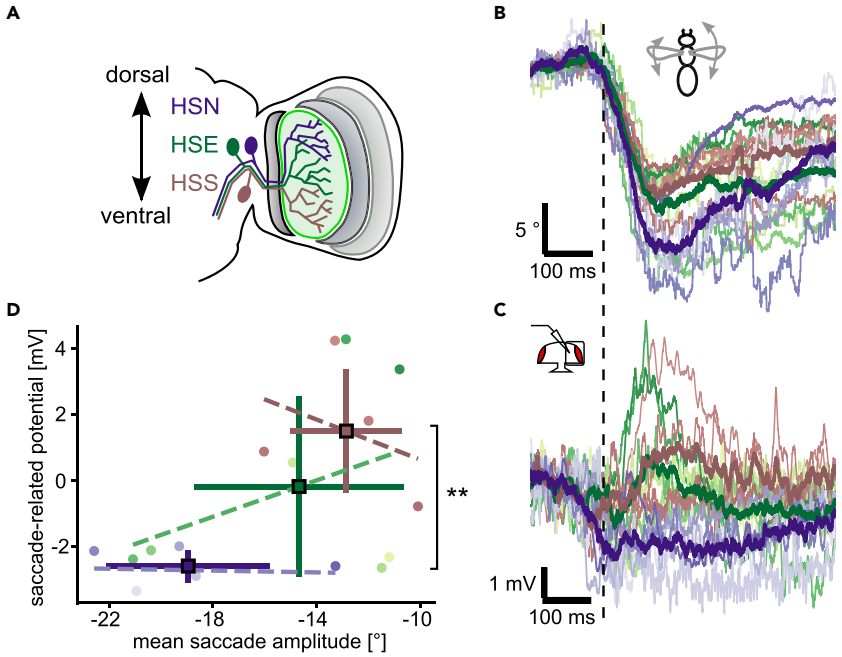

Figure 3. The influence of spontaneous saccades on different HS cell subtypes

(A) Schematic of the three HS subtypes, HSN (purple), HSE (green) and HSS (brown). Dendritic receptive fields cover different areas along the dorsoventral axis with considerable overlap.

(B) L-R WSA changes classified as spontaneous saccades to the left of previously recorded data. Each line represents the mean for one fly, color-coded according to HS cell subtype as in A. Thick lines represent the mean of the different subtypes. N = 16 (5 HSN, 7 HSE, and 4 HSS cells).

(C) Mean membrane potential changes in HS cells during spontaneous saccades corresponding to L-R WSA data shown in B.

(D) Scatterplot of average saccade amplitude and peak voltage change for each cell, color-coded according to subtype. Mean and SD are marked by squares. Membrane potential changes in HSN and HSS are significantly different from each other ($p = 0.0095$, Mann-Whitney-U 2-sided test), while those of HSN and HSE are not ($p = 0.079$). Linear regressions are represented by dashed lines for each subtype separately (HSN: $y = -0.014\,x - 3.0$, $r^2 = 0.0055$; HSE: $y = 0.28\,x + 3.9$, $r^2 = 0.17$; HSS: $y = -0.30\,x - 2.4$, $r^2 = 0.12$).

STAR Methods), we obtained saccade-related-potentials in the absence of visual stimulation for 16 HS cells with known subtypes. Similar to the case above, saccade-related potentials vary from hyper-to depolarizing despite exhibiting strong saccades in a narrow range of amplitudes (Figures 3C and 3D). However, results vary between subtypes. Prominently, all HSN cells exhibited a hyperpolarization. In contrast, three out of four HSS cells exhibited a biphasic response with a weak hyperpolarization at saccade onset, followed by a depolarization that reached its peak just after the peak L-R WSA. HSE cell responses fall in between with some exhibiting a hyperpolarization and some a depolarization. Accordingly, we find the difference in saccade-related-potentials between HSN and HSS to be statistically significant ($p < 0.01$, two-sided Mann-Whitney-U test), which is not the case for HSN and HSE ($p \approx 0.08$). Average changes in L-R WSA are smaller for HSS cells compared to HSN cells, which could confound the data. However, linear regressions indicate that the voltage changes are not proportional to the behavioral amplitude (L-R WSA) within each subtype (Figure 3C, dashed lines), suggesting that differences in behavior cannot explain the differences between HS cell subtypes. To further exclude this possibility, Spearman correlation coefficients were computed with either L-R WSA or the HS subtype as the independent variable and omitting the other, which corroborates the link between membrane potential change and subtype ($\rho = 0.68$, $p = 0.002$) rather than L-R WSA ($\rho = 0.4$, $p = 0.10$). Altogether, these data confirm the cell-to-cell variability, which can be explained by assuming that an efference copy during saccades has different effects on the different HS cell subtypes

HS cell activity during saccades elicited by contralateral looming

To test for the effect of saccades in the opposite direction, we presented looming stimuli on the left (contralateral) side, which elicits an increase in L-R WSA corresponding to a rightward saccade in most trials

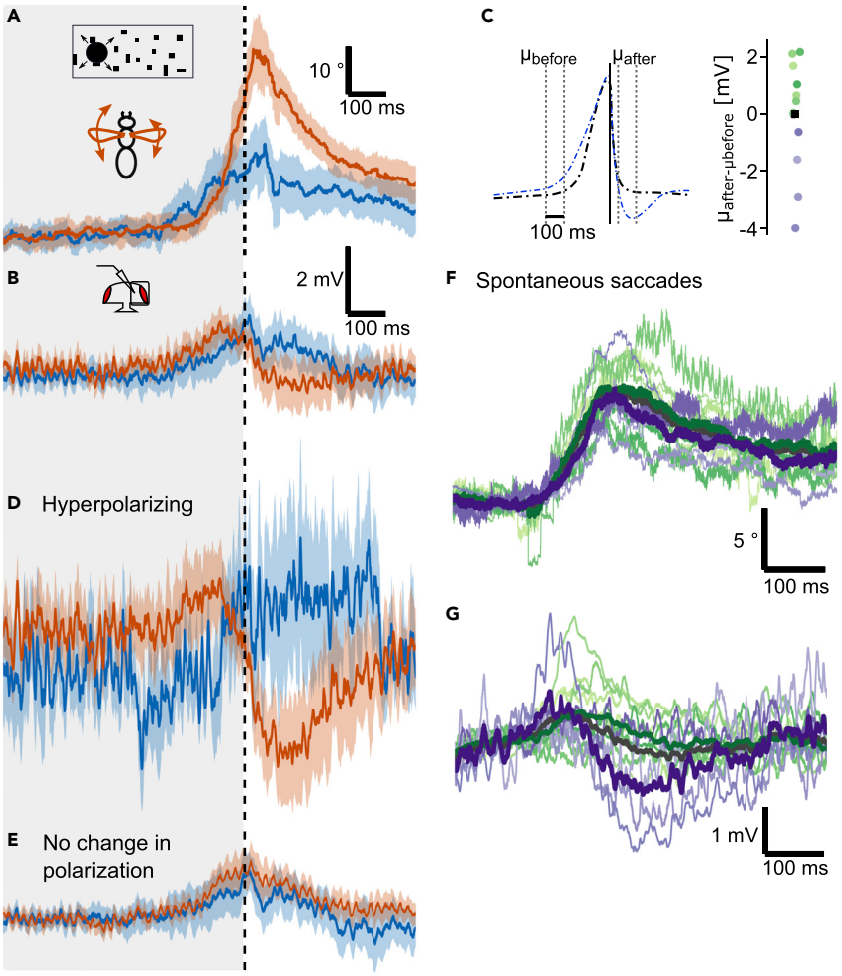

Figure 4. HS cell responses during looming-induced saccades to the right

(A) Mean L-R WSA ±SD in response to looming on the contralateral side (with respect to recorded cell) averaged across trials with a detected saccade (red, n = 74 trials) and those without (blue, n = 53 trials). N = 13 flies.

(B) HS cell membrane potential changes corresponding to the L-R WSA data shown in A. One cell was recorded from each fly.

(C) Criterion to split HS cells into groups according to their response to the looming stimulus during tethered flight. The mean membrane potential after the stimulus is subtracted from a baseline in the middle of the expansion (300 ms before maximal size). Flies are grouped by whether this difference is below (purple dots, HP_{contra}) or above average (green dots, NP_{contra}).

(D) Membrane potential of the HP_{contra} subset of HS cells (purple cells from C, N = 4) for trials with (red, n = 23) and without saccades (blue, n = 8). Shown here is the mean ± SD across all trials from all flies because of too few non-saccade trials per fly.

(E) Same as (D), but for NP_{contra} cells (green dots from C, N = 9 flies, n = 51/45 trials).

(F) L-R WSA during spontaneous saccades to the right for the same flies as in (A). Each color represents the mean of one fly. Thick lines represent averages across the different subsets according to (C) and across all flies (gray).

(G) Membrane potential of HS cells during spontaneous saccades corresponding to (F).

See also Figure S3.

(Figure 4A), and repeated the same analysis as described for ipsilateral looming. The membrane potential of the recorded HS cells became on average slightly hyperpolarized during trials with a saccade compared to trials without (Figure 4B). This hyperpolarization occurred after the presentation of the stimulus when the L-R WSA reached its peak. We also see the effect, when comparing trials from just one fly, suggesting that this is not simply owing to variability between different flies (Figure 1E). Thus, there is evidence that an efference copy influences the contralateral HS cell membrane potential during visually elicited saccades.

Table 1. Summary of classification of recorded cells according to their change in membrane potential during spontaneous saccades away from the ipsilateral side (HP_{spont}/NP_{spont}, see Figure 2) and according to their response to a contralateral looming stimulus (HP_{contra}/NP_{contra}, see Figure 4)

	Contralateral looming	
Ipsilateral looming	HP_{contra} (N = 4)	NP_{contra} (N = 9)
HP_{spont} (N = 6)	4	2
NP_{spont} (N = 5)	0	5
Depolarizing (N = 2)	0	2

Groups are highly overlapping, with HP_{contra} being a subset of HP_{spont} and NP_{spont} a subset of NP_{contra}. HP = hyperpolarized, NP = no change in polarization.

When looking at individual flies, we did not find a hyperpolarization during rightward saccades in all of the cells we recorded from. Rather, we were able to separate our recordings into two groups based on whether we were able to observe the effect (HP_{contra}) or not (NP_{contra}) (Figure 4C). In four HS cells from four different flies, we observed a clear hyperpolarization (Figure 4D). In the remaining nine cells, we saw no clear difference in HS cell membrane potential between trials with and without a saccade (Figure 4E). A quantitative analysis confirms the qualitative intuition provided by the time series (Figure S3). Hyperpolarizations occur in the HP_{contra} group during saccades with very high significance ($p = 5*10^{-6}$, 2-sided Wilcoxon rank test). Responses in the NP_{contra} group vary significantly from zero in all trials as well, but with a small positive amplitude, which is, therefore, likely an after-effect of the looming stimulus. Unlike the ipsilateral stimulus, the contralateral looming stimulus evokes only a small, albeit significant excitation, which is not limited to a specific subset of HS cells.

The hyperpolarization we observed is different from the effect reported during spontaneous saccades. For spontaneous saccades, a depolarization has been reported during rightward turns (Kim et al., 2015). We also observed a slightly stronger depolarization during the presentation of the looming stimulus in trials with a saccade compared to those without (Figure 4D), which occurred before L-R WSA started to rise. Because the depolarization could also be caused by the visual stimulus via input from contralateral lobula plate tangential cells for example, and is similar to the NP_{contra} cells as well, we cannot conclusively say, whether it is influenced by an efference copy or not.

When we averaged the HS cell membrane potential during spontaneous saccades to the right of only the HP_{contra} group, we observed a similar hyperpolarization (Figures 4F and 4G). This hyperpolarization is again preceded by a small depolarization, suggesting that both are, indeed, the consequence of an efference copy. Note that the cells contained in the HP_{contra} group also hyperpolarize during saccades elicited by ipsilateral looming (HP_{spont}, see Table 1) and therefore likely represent HSN and/or HSE cells as well. Altogether, there is no qualitative difference between the effect of spontaneous and looming-elicited saccades onto HS cells, although there is substantial cell-to-cell variability. In conclusion, for looming stimuli presented on the contralateral side, we did find evidence for a hyperpolarizing efference copy acting on a subset of HS cells.

Impact of looming-elicited saccades on processing of horizontal motion stimuli

A major advantage of our approach, compared to studying spontaneous saccades, is that we can elicit the behavior and thus study its effect on a subsequent optomotor stimulus. To study, whether motion responses are altered in HS cells after a saccade, we presented a large-field horizontal motion stimulus directly after the looming stimulus, when the peak of the saccade occurred (Figure 1D). Note that we chose stimulus parameters that are slower than what flies would perceive during a free flight saccade to drive strong HS cell responses. This stimulus pattern consisted of random dots moving either clockwise or counterclockwise. As a comparison, we measured responses to just the moving dots without the preceding looming stimulus. A looming stimulus presented on the right triggers a saccade to the left, which during free flight would lead to clockwise motion, which depolarizes the HS cells in the right optic lobe. We observed that the response to clockwise motion after the looming stimulus was rising much slower when compared to the response to the motion stimulus presented alone (Figures 5A and 5B). However, this was the case during flight saccades (red) as well as during non-flight trials (green). Furthermore, the cells in the NP_{spont} group, which did not show any hyperpolarization to the looming stimulus (Figure 2E), have a similarly suppressed motion response (Figure 5B).

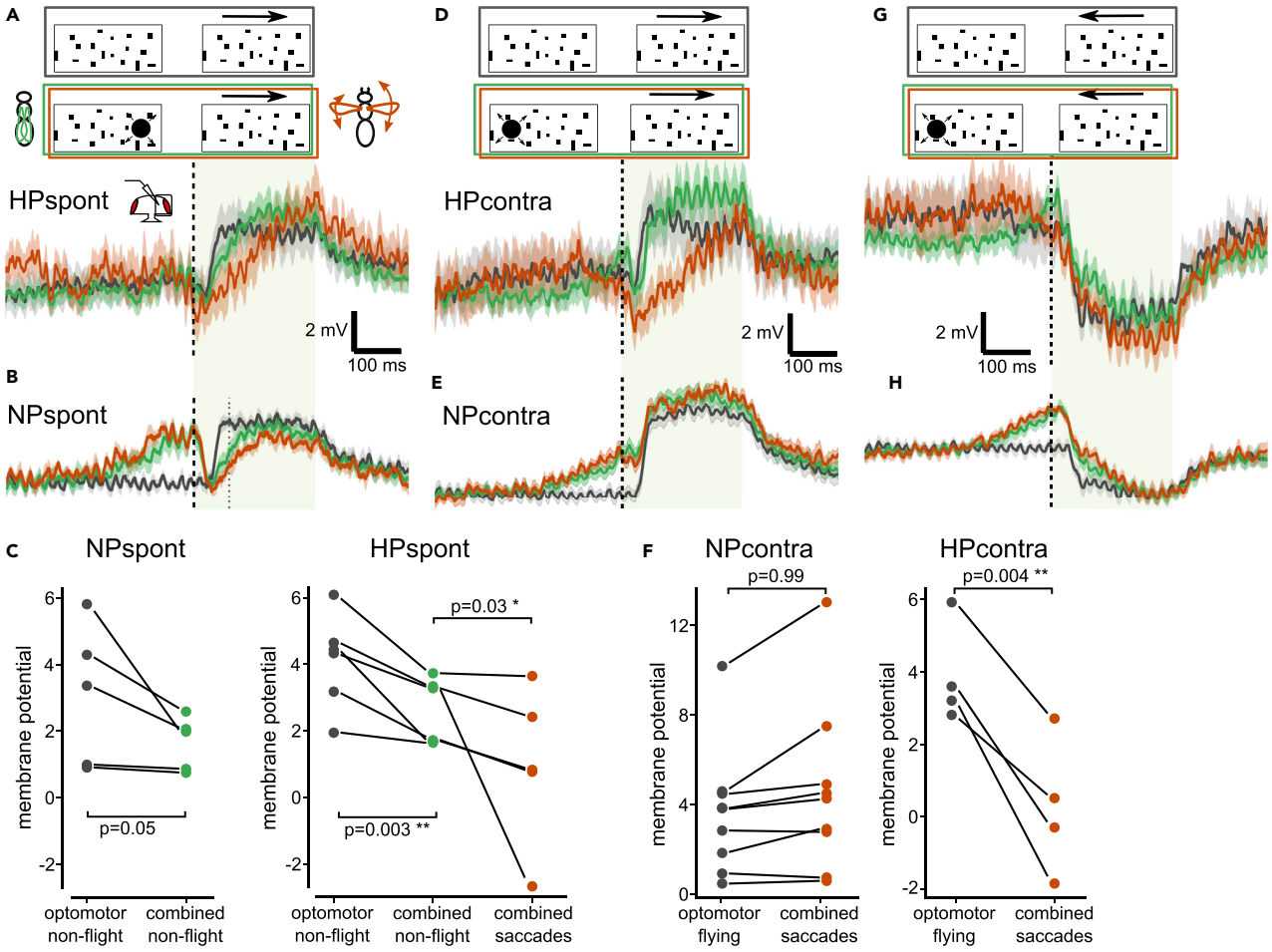

Figure 5. Processing of horizontal motion after a looming stimulus in HS cells

(A) Response to an excitatory (clockwise) motion stimulus after a looming stimulus on the ipsilateral side of cells that hyperpolarize during saccades (HP_{spont}, same subset as in Figure 2E, N = 6). Trials with saccades are shown in red (n = 19), non-flight trials in green (n = 70), and responses to the optomotor stimulus without preceding looming in gray (n = 50).

(B) Same as (A), but for NP_{spont} (subset of HS cells that do not hyperpolarize, see Figure 2D, N = 5, n = 24/62/48).

(C) Average change in membrane potentials during the early phase of the optomotor stimulus (80 ms after looming, gray dotted line in B) for each cell in the NP_{spont} and HP_{spont} group, respectively. Color code as in A. A paired t-test was used for comparing responses to the combined stimulus during non-flight with the optomotor stimulus, a Wilcoxon paired sign test for comparing trials with saccades during the combined stimulus with the opotmotor stimulus only.

(D) Response to an excitatory (clockwise) motion stimulus after a looming stimulus presented in the contralateral (left) visual hemisphere of cells that hyperpolarize during saccades HP_{contra} (same subset as in Figure 4D, N = 4, n = 24/45/28). Color code as in (A).

(E) Same as (D), but for NP_{contra} (subset of HS cells that do not show hyperpolarization, see Figure 4E, N = 9, n = 41/115/101).

(F) Average membrane potential for each cell as in (C). A Wilcoxon paired sign test was used for the NP_{contra} cells and a paired t-test for the HP_{contra} cells (Shapiro-Wilk normality test, p = 0.99).

(G) Response to an inhibitory (counterclockwise) motion stimulus after a looming stimulus on the contralateral side of HP_{contra} (same subset as in panel D, n = 25/43/29). Color code as in (A).

(H) Same as (G), but for NP_{contra} subset (same subset as in panel E, n = 48/109/105).

All traces represent mean ± SEM membrane potential.

We quantified this response by averaging the membrane potential during the early phase of the optomotor stimulus (Figure 5C). Considering all cells together, the response during the combined looming and optomotor stimulus during non-flight was reduced very significantly compared to the presentation of the optomotor stimulus alone ($p = 1.6*10^{-3}$, two-sided t-test; p values of individual groups marked in Figure 5C). We, therefore, conclude that this suppression of the response to horizontal motion is induced by the looming stimulus itself presented within the dendritic receptive field of the recorded HS cells and not by the flies' behavior. Therefore, in the case of an ipsilateral looming stimulus, an efference copy might not be

necessary to suppress reafferent responses to panoramic motion that could interfere with the execution of the saccade. However when the behavior is executed, in HP_{spont} cells (hyperpolarizing during saccades toward the left) the response to the clockwise (rightward) motion is even further suppressed compared to non-flight trials, showing that the presumed efference copy has an additional effect on motion processing (Figures 5A and 5C) ($p = 0.031$, one-sided Wilcoxon paired sign test).

For the looming stimulus presented on the left or contralateral side, we again plotted averaged responses separately for HP_{contra} cells (which showed the hyperpolarization) and NP_{contra} cells (which did not) (Figures 5D and 5E). Here we found that responses to the clockwise motion were again rising significantly slower after a saccade compared to the response to just the wide-field motion stimulus, but only in the HP_{contra} cells, where we found evidence for the hyperpolarizing efference copy, and only during saccades ($p = 0.0042$, one-sided paired t-test) (Figure 5F). Responses to counterclockwise motion, which hyperpolarizes the recorded HS cells, were not strongly affected during saccades (Figures 5G and 5H). This finding suggests that the efference copy acting on HS cells during a contralateral looming stimulus serves to suppress responses to motion that would normally depolarize the cell.

DISCUSSION

In the optomotor pathway of *Drosophila*, an efference copy has been shown to act on HS cells during spontaneous saccades (Kim et al., 2015, 2017). HS cells compute information about large-field horizontal motion elicited by self-rotation of the fly and are thought to mediate compensatory optomotor responses. Therefore, their activity could interfere with the self-elicited turn.

Here, we show that looming stimuli eliciting evasive saccades have a similar effect on HS cells as spontaneous saccades (Figures 2 and 4). In contrast to the previous studies, however, we found a large cell-to-cell variability within the recorded HS cells with respect to the action of an efference copy. In addition, we observed that excitatory responses to preferred-direction horizontal motion in HS cells are suppressed after looming stimuli on the ipsilateral side of the recorded cell even in non-flying flies and thus independent of the execution of a saccade (Figure 5). This suppression is, therefore, likely a consequence of the looming stimulus itself and not of an efference copy of the motor command controlling the saccade, although the latter appears to play an additional role in a subset of HS cells. This inhibition could be either a specific effect of the looming stimulus through a feedback mechanism or a consequence of light or motion adaptation in response to the dark disc or the brightness increase after its disappearance. Further experiments will be needed to test, whether other stimuli have a similar inhibitory effect.

After a looming stimulus on the contralateral side, we also observed a hyperpolarizing response only in a subset of HS cells, which was dependent on the execution of a saccade and thus likely mediated through an efference copy (Figure 4). This efference copy was able to suppress responses to a subsequent excitatory motion stimulus, but did not affect an inhibitory motion stimulus (Figure 5). This finding is surprising given that a saccade toward the contralateral side is expected to elicit null-direction horizontal motion and therefore hyperpolarize HS cells. Although hyperpolarization of HS cells has been shown to be able to elicit behavioral responses during walking (Busch et al., 2018), our findings suggest that predominantly excitatory responses of HS cells are suppressed during flight saccades. However, we did not study motion responses during the early phase of the saccade, when the looming stimulus was still present, so we cannot exclude that inhibitory responses are affected during that time.

We also found that the cell-to-cell variability with respect to the action of an efference copy can partially be explained by taking the different subtypes of HS cells into account (Figure 3). The hyperpolarization during spontaneous saccades toward the contralateral side was predominantly observed in HSN cells and some HSE cells, while HSS cells even showed a depolarization. A recent study found evidence for an efference copy acting on HS cells during saccades elicited by looming stimuli presented on the ipsilateral side of the recorded cells (Fenk et al., 2021). Fenk et al. did not report a similar variability between cells as our study, which is likely owing to the fact that they only recorded from HSN cells. Although our data on looming-elicited saccades did not discriminate between HS subtypes, the correlation between responses to spontaneous and looming-elicited saccades suggests that predominantly HSN and some HSE cells receive hyperpolarizing input during escape saccades. Although we generally confirm the results of their study, we find that the effect of both the stimulus as well as saccades on HS cells is surprisingly complex, which has implications for the search of the neurons that mediate the efference copy.

What might explain the large cell-to-cell variability we observed regarding the effect of saccades on HS cells? Because of the complexity of these flight maneuvers, we do not know how the different types of HS cells would respond to the visual motion stimulus that would be caused by the fly's self-motion during a saccade in free flight. It is possible that the different types of HS cells because of their different receptive fields (Krapp et al., 2001; Schnell et al., 2010) could be differently affected by the motion stimulus during a saccade. Therefore, an efference copy might only act on some cells and not others. Alternatively, different HS cell subtypes might have different functions in controlling flight behavior and therefore could be differently affected by an efference copy during saccades. In contrast to HSN and HSE cells, which receive input from heterolateral LPTCs, for example, HSS is not responding as much to back-to-front motion on the contralateral side (Hausen, 1982a; Schnell et al., 2010) and might therefore play a role in regulating forward motion rather than turning. Our data are consistent with a circuit, in which HSN receives inhibitory and HSS excitatory input during saccades toward the contralateral side. Because of the electrical coupling between HS cells (Haag and Borst, 2002, 2005; Schnell et al., 2010), HSE could receive indirect input via HSN and HSS with one or the other dominating in some cells, which might explain the response variability we observe in our recordings. Alternatively, there may be subtle differences in the behavior that we are not aware of, as we only measure L-R WSA. These differences in behavior could lead to different effects on HS cells. Further research is needed to discriminate between these different possibilities.

A saccade during free flight is a complex maneuver consisting of a roll, a counter-roll, and a yaw turn to realign the body with the new heading (Muijres et al., 2014, 2015; Schilstra and van Hateren, 1999). It is, therefore, difficult to judge, what the changes in L-R WSA correspond to. During free flight saccades, changes in L-R WSA were shown to be small and seem to have more impact on roll than on yaw torque, suggesting that the changes in L-R WSA we measure during tethered flight could correspond to the roll maneuver (Dickinson and Muijres, 2016). It has been shown that during looming-elicited escape saccades in free flight the fly sacrifices stability for speed (Muijres et al., 2014, 2015). Spontaneous saccades on the other hand are more stereotyped and the yaw maneuver happens with smaller delay, such that times of motion blur are minimized (Land, 1999). The quantitative difference we find between spontaneous and looming-elicited saccades might, therefore, be owing to the difference in the motor programs underlying these two behaviors. Although a descending neuron has been described that is active during changes in L-R WSA associated with spontaneous as well as looming-elicited saccades (Schnell et al., 2017), it is still unclear, which neural substrate could mediate the efference copy to the HS cells.

Especially for flying insects, vision is an essential modality, to which a sizable portion of their brain is dedicated. The processing of visual information, however, needs to depend on the context, such as the behavioral and motivational state of an animal or the presence of other stimuli, to lead to the appropriate behavioral response. Looming stimuli for example can signal an approaching predator or an impending collision. Illustrating the dependence on behavioral context, they can elicit escape jumps in stationary flies, whereas in a flying fly they can trigger either a landing response or an evasive turn (Ache et al., 2019; Bender and Dickinson, 2006; Tammero and Dickinson, 2002a, 2002b; von Reyn et al., 2014).

Efference copies and corollary discharge signals have been shown to influence sensory processing in a variety of different systems and at different levels culminating in the predictive coding hypothesis (Combes et al., 2008; Crapse and Sommer, 2008; França de Barros et al., 2022; Fukutomi and Carlson, 2020; Poulet and Hedwig, 2006; Sommer and Wurtz, 2008; Wurtz, 2008). Despite decades of research, the mechanisms underlying the action of efference copies remain largely speculative. In *Drosophila*, the genetic tools, as well as the recording techniques, will give us the chance to dissect the circuitry underlying efference copies, which could provide fundamental insights into the way nervous systems work.

Here, we show that in *Drosophila* an efference copy is able to suppress responses to panoramic visual motion in the optomotor system during self-elicited turns, however, with a large cell-to-cell variability. Our study supports the notion that information processing already at early stages, i.e. at the level of sensory systems, is strongly influenced by stimulus history as well as the behavioral state. The more important it is to consider the behavioral context when studying nervous system function.

Limitations of the study

A limitation of the study is that in our preparation the fly is stationary and cannot actually perform a saccade. Rather, we measure intended turns as changes in the L-R WSA. In tethered flight, these changes are much larger than in free flight, though, and follow a longer time course. It is, therefore, difficult to assess, to what

part of the free flight maneuver they correspond. In addition, the visual feedback received during free flight is likely much faster than the stimulus we used in this study. It, therefore, still remains unclear, what role the efference copy that is received by the HS cells plays during a free flight saccade.

STAR★METHODS

Detailed methods are provided in the online version of this paper and include the following:

- KEY RESOURCES TABLE
- RESOURCE AVAILABILITY
  - Lead contact
  - Materials availability
  - Data and code availability
- EXPERIMENTAL MODEL AND SUBJECT DETAILS
- METHOD DETAILS
  - Electrophysiology
  - Behavioral monitoring
  - LED arena and visual stimulation
  - Quality criteria
  - Saccade detection
- QUANTIFICATION AND STATISTICAL ANALYSIS

SUPPLEMENTAL INFORMATION

Supplemental information can be found online at https://doi.org/10.1016/j.isci.2022.105143.

ACKNOWLEDGMENTS

We want to thank Tim Krause for maintaining fly stocks, Gaia Tavosanis, Eugenia Chiappe, and Michael Dickinson for sharing fly stocks and Elhanan Ben-Yishay and Kevin Briggman for comments on the article. This work was funded by the German Research Foundation (DFG) through the Emmy-Noether program.

AUTHOR CONTRIBUTIONS

Conceptualization: B.S.; Methodology: P.F., B.S.; Software: P.F.; Formal Analysis: P.F.; Investigation: P.F., B.S.; Writing (Original Draft): P.F., B.S.; Writing (Review & Editing): P.F., B.S.; Visualization: P.F.; Funding Acquisition: B.S.; Supervision: B.S.; Project Administration: B.S.

DECLARATION OF INTERESTS

The authors declare no competing interests.

Received: July 11, 2022
Revised: August 15, 2022
Accepted: September 12, 2022
Published: October 21, 2022

REFERENCES

Ache, J.M., Namiki, S., Lee, A., Branson, K., and Card, G.M. (2019). State-dependent decoupling of sensory and motor circuits underlies behavioral flexibility in Drosophila. Nat. Neurosci. *22*, 1132–1139.

Bender, J.A., and Dickinson, M.H. (2006). Visual stimulation of saccades in magnetically tethered Drosophila. J. Exp. Biol. *209*, 3170–3182.

Boeddeker, N., Lindemann, J.P., Egelhaaf, M., and Zeil, J. (2005). Responses of blowfly motion-sensitive neurons to reconstructed optic flow along outdoor flight paths. J. Comp. Physiol. A Neuroethol. Sens. Neural Behav. Physiol. *191*, 1143–1155.

Busch, C., Borst, A., and Mauss, A.S. (2018). Bi-directional control of walking behavior by horizontal optic flow sensors. Curr. Biol. *28*, 4037–4045.e5.

Combes, D., Le Ray, D., Lambert, F.M., Simmers, J., and Straka, H. (2008). An intrinsic feed-forward mechanism for vertebrate gaze stabilization. Curr. Biol. *18*, R241–R243.

Crapse, T.B., and Sommer, M.A. (2008). Corollary discharge across the animal kingdom. Nat. Rev. Neurosci. *9*, 587–600.

Cullen, K.E. (2004). Sensory signals during active versus passive movement. Curr. Opin. Neurobiol. *14*, 698–706.

Dickinson, M.H., and Muijres, F.T. (2016). The aerodynamics and control of free flight manoeuvres in Drosophila. Philos. Trans. R. Soc. Lond. B Biol. Sci. *371*, 20150388.

Du, P., Kibbe, W.A., and Lin, S.M. (2006). Improved peak detection in mass spectrum by incorporating continuous wavelet transform-based pattern matching. Bioinformatics *22*, 2059–2065.

Fenk, L.M., Kim, A.J., and Maimon, G. (2021). Suppression of motion vision during course-changing, but not course-stabilizing, navigational turns. Curr. Biol. *31*, 4608–4619.e3.

Fischbach, K.F., and Dittrich, A.P.M. (1989). The optic lobe of drosophila-melanogaster. 1. A golgi analysis of wild-type structure. Cell Tissue Res. *258*, 441–475.

França de Barros, F., Bacqué-Cazenave, J., Taillebuis, C., Courtand, G., Manuel, M., Bras, H., Tagliabue, M., Combes, D., Lambert, F.M., and Beraneck, M. (2022). Conservation of locomotion-induced oculomotor activity through evolution in mammals. Curr. Biol. *32*, 453–461.e4.

Fujiwara, T., Cruz, T.L., Bohnslav, J.P., and Chiappe, M.E. (2017). A faithful internal representation of walking movements in the Drosophila visual system. Nat. Neurosci. *20*, 72–81.

Fukutomi, M., and Carlson, B.A. (2020). A history of corollary discharge: contributions of mormyrid weakly electric fish. Front. Integr. Neurosci. *14*, 42. https://doi.org/10.3389/fnint.2020.00042.

Gabbiani, F., Krapp, H.G., and Laurent, G. (1999). Computation of object approach by a wide-field, motion-sensitive neuron. J. Neurosci. *19*, 1122–1141.

Götz, K.G. (1968). Flight control in Drosophila by visual perception of motion. Kybernetik *4*, 199–208.

Haag, J., and Borst, A. (2005). Dye-coupling visualizes networks of large-field motion-sensitive neurons in the fly. J. Comp. Physiol. A Neuroethol. Sens. Neural Behav. Physiol. *191*, 445–454.

Haag, J., and Borst, A. (2002). Dendro-dendritic interactions between motion-sensitive large-field neurons in the fly. J. Neurosci. *22*, 3227–3233.

Haag, J., and Borst, A. (2001). Recurrent network interactions underlying flow-field selectivity of visual interneurons. J. Neurosci. *21*, 5685–5692.

Haikala, V., Joesch, M., Borst, A., and Mauss, A.S. (2013). Optogenetic control of fly optomotor responses. J. Neurosci. *33*, 13927–13934.

Hausen, K. (1982a). Motion sensitive interneurons in the optomotor system of the fly. 1. The horizontal cells - structure and signals. Biol. Cybern. *45*, 143–156.

Hausen, K. (1982b). Motion sensitive interneurons in the optomotor system of the fly. 2. The horizontal cells - receptive-field organization and response characteristics. Biol. Cybern. *46*, 67–79.

Heisenberg, M., and Wolf, R. (1979). On the fine structure of yaw torque in visual flight orientation of Drosophila melanogaster. J. Comp. Physiol. *130*, 113–130.

Joesch, M., Plett, J., Borst, A., and Reiff, D.F. (2008). Response properties of motion-sensitive visual interneurons in the lobula plate of Drosophila melanogaster. Curr. Biol. *18*, 368–374.

Kim, A.J., Fenk, L.M., Lyu, C., and Maimon, G. (2017). Quantitative predictions orchestrate visual signaling in Drosophila. Cell *168*, 280–294.e12.

Kim, A.J., Fitzgerald, J.K., and Maimon, G. (2015). Cellular evidence for efference copy in Drosophila visuomotor processing. Nat. Neurosci. *18*, 1247–1255.

Krapp, H.G., Hengstenberg, R., and Egelhaaf, M. (2001). Binocular contributions to optic flow processing in the fly visual system. J. Neurophysiol. *85*, 724–734.

Land, M.F. (1999). Motion and vision: why animals move their eyes. J. Comp. Physiol. *185*, 341–352.

Leonte, M.-B., Leonhardt, A., Borst, A., and Mauss, A.S. (2021). Aerial course stabilization is impaired in motion-blind flies. J. Exp. Biol. *224*, jeb242219.

Maimon, G., Straw, A.D., and Dickinson, M.H. (2010). Active flight increases the gain of visual motion processing in Drosophila. Nat. Neurosci. *13*, 393–399.

Mronz, M., and Lehmann, F.-O. (2008). The free-flight response of Drosophila to motion of the visual environment. J. Exp. Biol. *211*, 2026–2045.

Muijres, F.T., Elzinga, M.J., Iwasaki, N.A., and Dickinson, M.H. (2015). Body saccades of Drosophila consist of stereotyped banked turns. J. Exp. Biol. *218*, 864–875.

Muijres, F.T., Elzinga, M.J., Melis, J.M., and Dickinson, M.H. (2014). Flies evade looming targets by executing rapid visually directed banked turns. Science *344*, 172–177.

Poulet, J.F.A., and Hedwig, B. (2006). The cellular basis of a corollary discharge. Science *311*, 518–522.

Reiser, M.B., and Dickinson, M.H. (2008). A modular display system for insect behavioral neuroscience. J. Neurosci. Methods *167*, 127–139.

Schilstra, C., and van Hateren, J.H. (1998). Stabilizing gaze in flying blowflies. Nature *395*, 654.

Schilstra, C., and van Hateren, J.H. (1999). Blowfly flight and optic flow. I. Thorax kinematics and flight dynamics. J. Exp. Biol. *202*, 1481–1490.

Schnell, B., Joesch, M., Forstner, F., Raghu, S.V., Otsuna, H., Ito, K., Borst, A., and Reiff, D.F. (2010). Processing of horizontal optic flow in three visual interneurons of the Drosophila brain. J. Neurophysiol. *103*, 1646–1657.

Schnell, B., Ros, I.G., and Dickinson, M.H. (2017). A descending neuron correlated with the rapid steering maneuvers of flying Drosophila. Curr. Biol. *27*, 1200–1205.

Schnell, B., Weir, P.T., Roth, E., Fairhall, A.L., and Dickinson, M.H. (2014). Cellular mechanisms for integral feedback in visually guided behavior. Proc. Natl. Acad. Sci. USA *111*, 5700–5705.

Scott, E.K., Raabe, T., and Luo, L. (2002). Structure of the vertical and horizontal system neurons of the lobula plate in Drosophila. J. Comp. Neurol. *454*, 470–481.

Sommer, M.A., and Wurtz, R.H. (2008). Brain circuits for the internal monitoring of movements. Annu. Rev. Neurosci. *31*, 317–338.

Suver, M.P., Huda, A., Iwasaki, N., Safarik, S., and Dickinson, M.H. (2016). An array of descending visual interneurons encoding self-motion in Drosophila. J. Neurosci. *36*, 11768–11780.

Tammero, L.F., and Dickinson, M.H. (2002a). The influence of visual landscape on the free flight behavior of the fruit fly Drosophila melanogaster. J. Exp. Biol. *205*, 327–343.

Tammero, L.F., and Dickinson, M.H. (2002b). Collision-avoidance and landing responses are mediated by separate pathways in the fruit fly, Drosophila melanogaster. J. Exp. Biol. *205*, 2785–2798.

Von Holst, E., and Mittelstaedt, H. (1950). The principle of reafference. Naturwissenschaften *37*, 464–476.

von Reyn, C.R., Breads, P., Peek, M.Y., Zheng, G.Z., Williamson, W.R., Yee, A.L., Leonardo, A., and Card, G.M. (2014). A spike-timing mechanism for action selection. Nat. Neurosci. *17*, 962–970.

Wilson, R.I., and Laurent, G. (2005). Role of GABAergic inhibition in shaping odor-evoked spatiotemporal patterns in the Drosophila antennal lobe. J. Neurosci. *25*, 9069–9079.

Wurtz, R.H. (2008). Neuronal mechanisms of visual stability. Vis. Res. *48*, 2070–2089.

STAR★METHODS

KEY RESOURCES TABLE

REAGENT or RESOURCE	SOURCE	IDENTIFIER
Deposited data		
Electrophysiological and behavioral data	This paper	EDMOND: https://doi.org/10.17617/3.92
Experimental models: Organisms/strains		
Drosophila melanogaster: Wild-type Canton S	Gaia Tavosanis	N/A
D. melanogaster: Wild-type Top Banana	Eugenia Chiappe	N/A
D. melanogaster: w[1118]; P{y[+t7.7] w[+mC] = GMR27B03-GAL4}attP2	BDSC	RRID:BDSC_49211
D. melanogaster: w[1118]; P{y[+t7.7] w[+mC] = GMR81G07-GAL4}attP2	BDSC	RRID:BDSC_40122
D. melanogaster: y[*] w[*]; P{w[+mC] = UAS-2xEGFP}AH3	BDSC	RRID:BDSC_6658
D. melanogaster: w[+]; P{w[+mC] = UAS-2xEGFP}AH3	This paper	N/A
Software and algorithms		
Python 3.7	Python Sotware Foundation	https://www.python.org/
SciPy Package	SciPy	https://scipy.org/
Kinefly	Steve Safarik (Suver et al., 2016)	https://github.com/ssafarik/Kinefly
ROS phidgets support	Steve Safarik	https://github.com/ssafarik/phidgets
ROS Kinetic Kame	Open Robotics	https://www.ros.org
MATLAB	MathWorks	https://www.mathworks.com/
WinWCP	University of Strathclyde, Glasgow	https://spider.science.strath.ac.uk/sipbs/software_ses.htm
Saccade detection and data processing	This paper	Zenodo: https://github.com/phifisch/flyEscapeSaccades/ https://doi.org/10.5281/zenodo.6988868

RESOURCE AVAILABILITY

Lead contact

Further information and requests for resources and reagents should be directed to and will be fulfilled by the lead contact, Bettina Schnell (bettina.schnell@mpinb.mpg.de).

Materials availability

This study did not generate new unique reagents.

Data and code availability

- Raw and processed data have been deposited at the EDMOND repository of the Max-Planck Digital Library and are publicly available at Edmond: https://doi.org/10.17617/3.92https://doi.org/10.17617/3.92.
- All original code has been deposited via Github at Zenodo: https://doi.org/10.5281/zenodo.6988868 and is publicly available.
- Any additional information required to reanalyze the data reported in this paper is available from the lead contact upon request.

EXPERIMENTAL MODEL AND SUBJECT DETAILS

Strains of *Drosophila melanogaster* were bred on premixed cornmeal-agar medium (JazzMix Drosophila food, Fisherbrand) at 25°C on a 12 h day/12 h night cycle. Flies used for experiments were of either

wild-type CantonS (two flies) or expressing GFP in HS cells using the Gal4/UAS system using driver lines GMR81G07-GAL4 (RRID:BDSC_40122) or GMR27B03-GAL4 (RRID:BDSC_49211) and effector line RRID:BDSC_6658. All individuals had at least one wild-type allele for the *white* gene. To avoid side-effects of in-breeding, GMR27B03-GAL4; 2xUAS-EGFP flies were backcrossed to wildtype flies (Canton S and Top Banana), and offspring selected for fluorescence every few generations. We used female flies aged 2 to 5 days after eclosion for all experiments.

METHOD DETAILS

Electrophysiology

In vivo patch-clamp recordings of HS cells were performed in whole-cell configuration in current-clamp mode. Flies were anaesthetized on a cold-plate, legs amputated, and fixed by the head to custom-made pyramidal holders (Maimon et al., 2010) that allow access to portions of the head while offering free space to the wings using UV-curing glue. The head was bent forward to expose the posterior part in the surgery window of the holder. The head capsule was covered with extracellular saline (prepared according to Wilson and Laurent (2005), in mM: 103 NaCl, 4 $MgCl_2$, 3 KCl, 1.5 $CaCl_2$, 26 $NaHCO_3$, 1 NaH_2PO_4, 10 Trehalose, 10 Glucose, 2 Sucrose and 5 TES, adjusted to 275 mOsm) and cut open using a syringe needle. The brain was perfused with extracellular saline bubbled with 95% O_2/5% CO_2 to reach pH 7.3. The neurolemma and extracellular matrix covering the lobula plate was digested by applying Collagenase (0.5 mg/mL Collagenase IV in extracellular saline, Worthington) through a low-resistance pipette (BF150-110-10, Sutter Instruments). HS cells were targeted under visual control with a 40x immersion objective (Nikon NIR Apo 40x/0.80W), phase-contrast filter, IR lighting (850 nm, Thorlabs) and CMOS camera (Thorcam Quantalux, Thorlabs). GFP-expression was visualized by a brief excitation of eGFP in transgenic flies. Patch pipettes were pulled with a P-1000 Flaming/Brown puller (Sutter Instruments) from thick-walled capillaries (BF150-86-10, Sutter Instruments), adjusted to a resistance of 6–8 MΩ. Intracellular solution was prepared according to (Wilson and Laurent, 2005) (in mM: 140 mM potassium aspartate, 1 mM KCl, 10 mM HEPES, 1 mM EGTA, 4 mM MgATP, 0.5 mM NaGTP, 0.5% biocytin, adjusted to pH 7.3 and 265 mOsm) plus AlexaFluor-568. Signals were recorded with a BA-01X bridge amplifier (npi electronics) and a BNC-2090A digitizer (National Instruments) with MATLAB (version R2017b, The MathWorks). Recordings from HS cells presented in Figure 3 were performed using the flies and setup described previously (Schnell et al., 2014).

Behavioral monitoring

The flight behavior was observed by an IR-sensitive camera (Basler acA645-100gm equipped with a 1.0X 94 mm WD InfiniStix lens, Infinity Photo-Optical) placed below the fly and illuminating the wings from the fly's posterior with the IR LEDs mentioned above. The front edge of the wing was detected from the image stream using the Kinefly software (Suver et al., 2016) running on ROS (version Kinetic Kame, https://www.ros.org), which outputs a signal that was fed into the same digitizer as the electrophysiological signal. An important change has been made to the Kinefly wing detection algorithm. The front edge of the wing was determined as the first threshold crossing of a derivative luminance signal extracted from the image, which made the detection less error-prone.

LED arena and visual stimulation

The fly was at the center of a cylindrical arena of LED panels (IO Rodeo) as described (Reiser and Dickinson, 2008). Our arena is made of monochromatic LEDs (565 nm) where each pixel subtends an angle of 2.25° on the fly eye, covering a total visual field of about 195° in azimuth and 60° in elevation. Here, we used a frame shift rate of 50 Hz, while the arena was tuned to a flicker rate of about 744 Hz. The visual scene presented to the fly consisted of dark squares on a bright background with maximal contrast. Centered at an angle of 54° on either the left or right side, a dark disc expanded, simulating an object approaching at constant speed of 1.5 m/s. Thus the visual angle covered by the imaginary object is given by $\Theta(t) = 2arctan\left(\frac{-h}{vt}\right)$ with h = 0.1 m, v = 1.5 m/s and t = 0 at the expected moment of impact (Gabbiani et al., 1999). The half-size to approach ratio (h/v) is therefore 66.7 ms. The maximal lateral extent of the stimulus was 76.5°. At time t' > 0, the looming disc disappears. The background consisted of randomly distributed dark rectangles on a bright background with 100% nominal contrast, with each rectangle measuring at least 5° × 5° in the visual field. This background was rotated with a speed of 112.5°/s for 240 ms either clockwise or counter-clockwise, which we call optomotor stimulus. In a given trial, the stimulus consisted of either looming (left/right) only, background rotation (either direction) only, or looming followed by background rotation, making for a total of

eight different stimulus combinations. Each trial lasted for 1.35 s, with an inter-trial interval of 3 s. The order of these stimuli was permuted. Each fly completed several experimental runs.

Quality criteria

All data analysis was performed in Python (version 3.7). To make sure that we would be able to detect a hyperpolarizing effect of an efference copy, we excluded HS cell recordings, if they did not respond to a square-wave pattern rotating counter-clockwise by a tonic hyperpolarization < -2 mV. All experimental runs for one fly were gathered and divided into trials, including 100 ms before and 250 ms after the actual trial. An angular threshold was applied to the wing stroke amplitude data of both wings to avoid contamination of the data by misdetections due to reflection artifacts. This angle depended on preparation and light conditions, but in most instances was $< 8°$, which does not occur in normal flight. If both wings were consistently below threshold, the trial was classified as non-flying. If there was a discrepancy between left and right wing (above/below threshold) for more than 30 ms in a trial, corresponding to less than two detection frames, the trial was discarded. Spontaneous saccades were extracted from data during the inter-trial intervals, where the visual input consisted of the static background only. In the older datasets (recorded as described in (Schnell et al., 2014)), the experimental data were truncated where resting membrane potential started to drift more than $\approx$ 0.01 mV/s.

Saccade detection

Saccades were detected using an algorithm based on continuous wavelet transform (CWT) applied to a differentiated signal without relying on low- or high-pass filtering to avoid boundary artifacts in shorter flight bouts. Briefly, any signal can be decomposed into a linear sum of many smaller wavelet functions, which have a limited width in the time and frequency domains. An abrupt event of significant amplitude shows in CWT as a time-localized peak over a broad range of wavelet scales. Thus, it is detectable by tracking the uninterrupted peaks in the CW-transformed signal over scales. We use the algorithm developed by Du et al. (2006), as implemented in the scipy.signal (scipy version 1.6.2) package. First, to simplify saccade detection, we downsampled the noise-corrupted piece-wise-constant data obtained by recording the wing stroke amplitude together with electrophysiological data through a fitting procedure to obtain a single value per analysis frame (see Figure S1). The downsampled signal was median-filtered with filter width 3 to remove single outliers, and then differentiated using the central difference formula with a half-width of 50 ms, to build the detection signal. These data were fed into the peak-detection function with scales $\{2^{2+j/16}\}$, $j = \{0,2,\ldots,15\}$, window size of 10 frames, gap threshold of 1, and noise percentage of 5, which constitute numerical values. To detect saccades to the left, the negative of the signal was used. Spontaneous saccades, where the direction of the saccade is not determined by the stimulus, were detected in the same way on both the positive and negative signal with a window size of 20 frames and noise percentage of 10 to be more restrictive. For each putative saccade we calculated the peak and onset time and peak amplitude. The peak time was determined by moving forward from the putative peak and finding the first occurrence of crossing zero (indicating a local extremum) in the signal used for detection and adding the half-width of the differentiation. The onset time was defined as the first minimum before the putative peak in the simple differential (not central difference) of the downsampled original signal. Peak amplitude was calculated by taking the average L-R WSA in the interval of peak time +/− 30 ms. To eliminate cases, where the falling slope of a previous saccade was detected as a saccade in the opposite direction, we removed candidate saccades if another deviation from baseline was detected within 160 ms preceding the onset, which exceeded the following percentage of the peak amplitude. For spontaneous saccades, that percentage was 60%, while we chose 75% for saccades during looming trials. Trials were then classified according to whether they contained a saccade that was synchronized to the time when the looming stimulus reached its maximum expansion within a tolerance window of [-200 ms; 60 ms]. As a consequence of these steps, trials classified as non-saccades mostly consist of slow deviations to either side, consecutive turns to unclear direction, and very rarely contained very early saccades (long before the looming stimulus ends).

Additional criteria for the selection of saccades were applied to the data for different HS cell subtypes, shown in Figure 3, to further reduce the rate of false positives. First, a threshold was applied to the saccade amplitudes, tuned to 4.7, 7.4, 8.8 or 11.8°, where the two highest values were by far the most common. Further, putative saccades were eliminated if there were less than 500 ms between the onset of saccades in opposite directions or if a deviation from baseline before putative saccade onset exceeded 65% of saccade amplitude. Finally a candidate saccade was accepted only if the onset preceded the peak in

the derivative signal by at most 100 ms and the peak of the saccade followed by at most 300 ms. This procedure removed a majority of candidates, and the resulting putative saccades were visually verified.

QUANTIFICATION AND STATISTICAL ANALYSIS

No statistical tests were used to predetermine sample sizes, which were, however, in the range of other publications in the field. Detailed numbers including 'N' of individual animals and 'n' of trials are given in every figure legend. Electrophysiology data of each trial were baseline-corrected to the mean potential in the window of 400 ms from the beginning of the trial. This window contains no responses to the looming stimulus. The data from trials were in most cases averaged per fly, before calculating an average of averages +/− s.e.m. In cases of low number of trials per fly in certain subsets, all trials were instead treated as drawn from the same distribution, and therefore the mean ± s.d. was given. Which of these methods was applied, is stated in the figure captions.

To divide the cells into different subgroups, the difference in membrane potential before and after the looming stimulus was calculated on the mean membrane potential U for each fly for trials with looming stimulus only (no background rotation).

$$\mu_{before} - \mu_{after} = \mu[U(t|t \in [-140, -40]ms)] - \mu[U(t|t \in [+40, +110]ms)]$$

Flies were then grouped in the hyperpolarizing category if that difference was lower (more negative) than the average difference.

To quantify the voltage changes depending on escape saccades (see Figures S2 and S3), the membrane potential deviations from baseline were calculated as the mean in a window of 50 ms width starting 30 ms after the looming stimulus reaches its maximum, which corresponds approximately to the time when the behavioral response reached its peak. For each resulting distribution of measurements, Wilcoxon signed rank tests were applied individually to establish if the resulting value distributions were significantly different from zero, given that many distributions were not gaussian (as determined by Shapiro-Wilk-test). Accordingly, the statistical significance of differences between the saccade and non-saccade trials was established via Mann-Whitney-U tests.

Responses to the looming stimulus itself were obtained by averaging the baseline-corrected membrane potential in the 200 ms window preceding the maximal looming expanse for all trials. To assess the significance between responses in the different subgroups, two-sided Mann-Whitney-U tests were performed.

We quantified the response to the panoramic motion stimulus under the different conditions (see Figure 5) by averaging the baseline-corrected membrane potential for each fly in a window of 80 ms +/− 8 ms after the looming stimulus reached its maximal extension. A Shapiro-Wilk-test was performed to ascertain normality of the distribution with significance threshold $p = 0.10$, followed by a dependent t-test for paired samples. If the distribution was non-normal, a Wilcoxon's paired sign test was applied. Clarifications on which test was used is given in figure captions. Statistical significance of the results on subtype-specificity of responses during spontaneous saccades (see Figure 3D) was determined by two-sided Mann-Whitney-U tests.

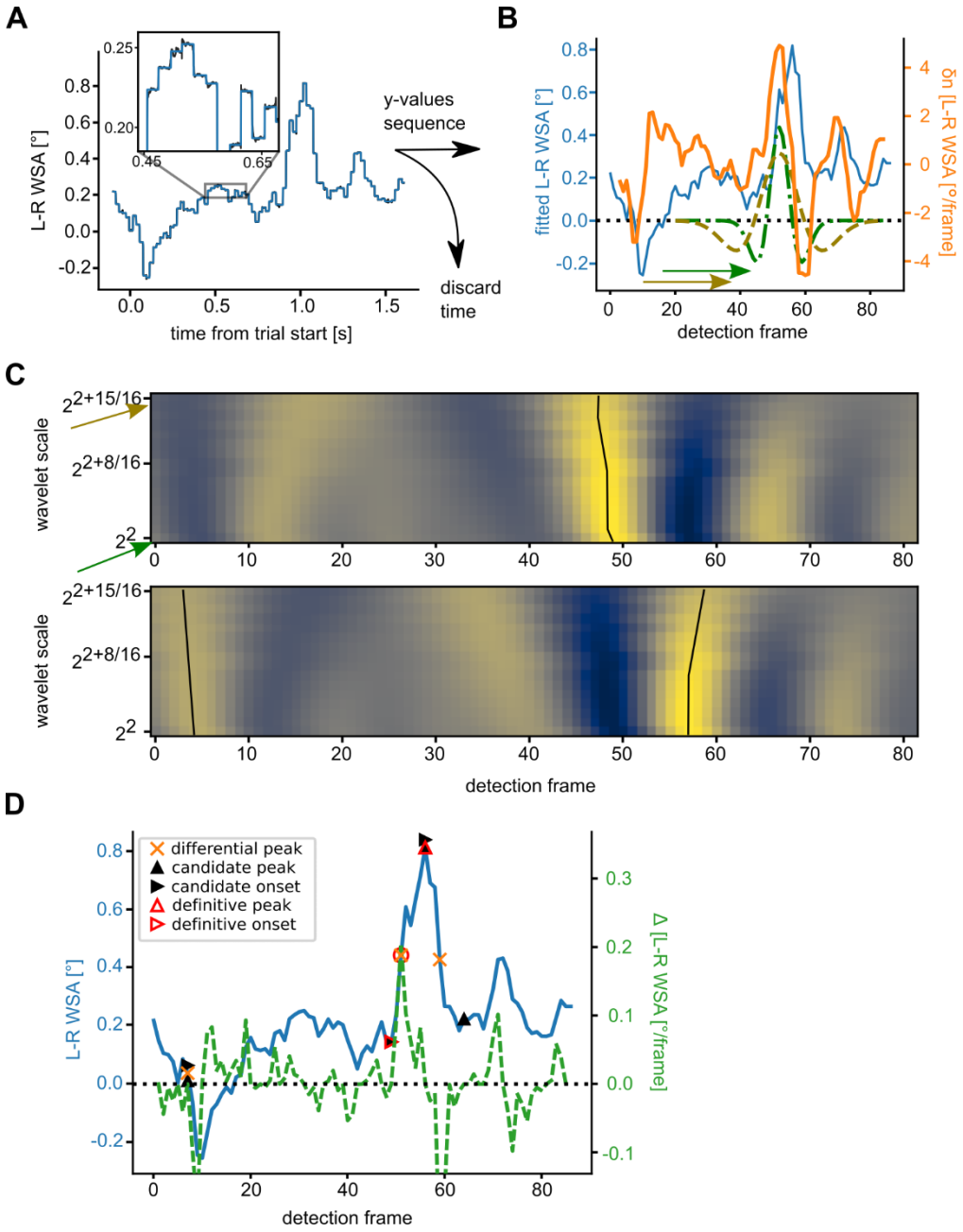

Figure S1

Illustration of the saccade detection algorithm, related to STAR Methods. (**A**) The wingbeat amplitude signal is corrupted by additive noise, which persists in the L-R WSA (black). Using the prior knowledge of approximate camera frame rate, a piece-wise-constant function is fitted to it (blue), to retrieve a distortion-free downsampled signal as a sequence of y-values. (**B**) Y-values form a continuous-value time-series (blue), which is differentiated using the central difference theorem (orange). Wavelet functions of the Ricker (derivative of a gaussian) family are applied as filters for peaks in the derived signal with scales between 4 (green) and 8 (brown) similar to a convolution. (**C**) Exemplary result of continuous wavelet transform (CWT) in the given range. Top shows CWT of positive signal, bottom is CWT of negative, arrows point at scales of wavelets in (B). Ridges across wavelet scales correspond to sharp transients, which are candidates for saccades. Rightward saccades correspond to peaks in the positive signal, and leftward saccades to peaks in the negative. (**D**) Ridge locations in CWT in positive and negative signals are treated as candidate peaks and additional post-selection criteria used to identify sufficiently prominent, stand-alone peaks in L-R WSA as saccades. Saccade onset and peak times are identified as time points closest to zero in the simple (backward difference) derivative.

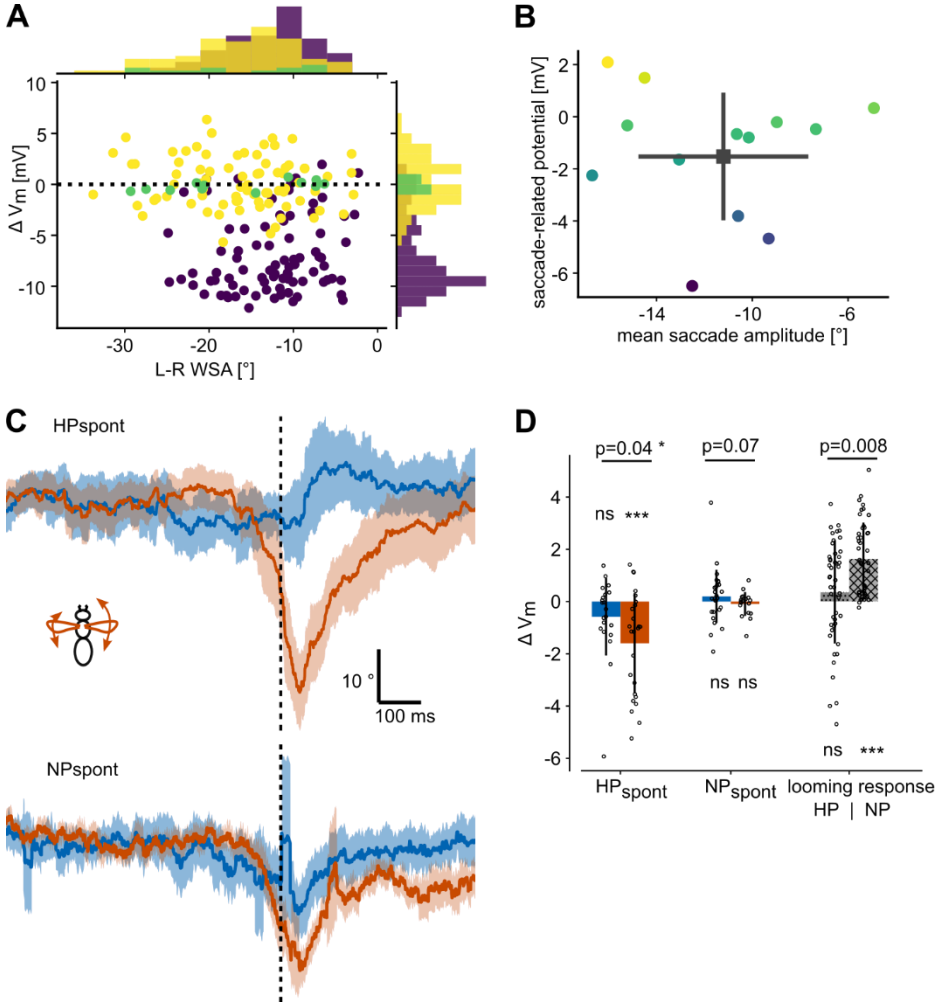

Figure S2

Quantitative analysis of HS cell responses during saccades to the left, related to Figure 2. (**A**) Voltage deviation from baseline (ΔV_m) against L-R WSA for all spontaneous saccades of three exemplary HS cells from Fig. 2D color-code accordingly (violet: hyperpolarizing cell, yellow: depolarizing cell, green: no change in polarization). (**B**) Mean ΔV_m plotted against mean L-R WSA for each recorded cell during spontaneous saccades to the left (color-coded as in Fig. 2C, D). (**C**) Mean ± s.e.m. of L-R WSA of the HP_{spont} subgroup (top, N = 6 flies) and the NP_{spont} subgroup (N = 5 flies) corresponding to Fig. 2E and F (saccade trials shown in blue, non-saccade trials in red). (**D**) Mean ΔV_m during trials with (red) or without (blue) looming-elicited saccades (individual trials are indicated by circles) for the HP_{spont} and NP_{spont} subgroups corresponding to Fig. 2E and F. A two-sided Wilcoxon test was performed to test whether the distributions are significantly different from zero, a one-sided Mann-Whitney-U to test for saccade-dependent differences. Responses to the ipsilateral looming stimulus itself (indicated by grey bars and circles) are significantly different between HP_{spont} (gray dotted) and NP_{spont} (gray hatched) groups ($p = 0.0081$) with the latter being significantly different from zero ($p = 1.0*10^{-8}$).

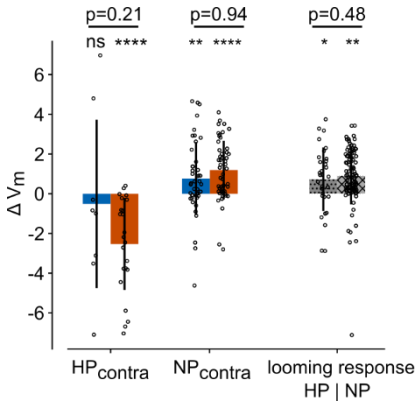

Figure S3

Quantitative analysis of response to contralateral looming, related to Figure 4. Mean ΔV_m during trials with (red) or without (blue) looming-elicited saccades (individual trials are indicated by circles) for the HP_{contra} and NP_{contra} subgroups corresponding to Fig. 4D and E. A two-sided Wilcoxon test was performed to test whether the distributions are significantly different from zero, a one-sided Mann-Whitney-U to test for saccade-dependent differences. The looming stimulus significantly depolarizes all cells without significant difference between HP_{contra} (gray dotted, $p = 0.015$) and NP_{contra} (gray hatched, $p = 1.6*10^{-10}$) subsets.

B Supplementary figures

B.1 Fly perspective

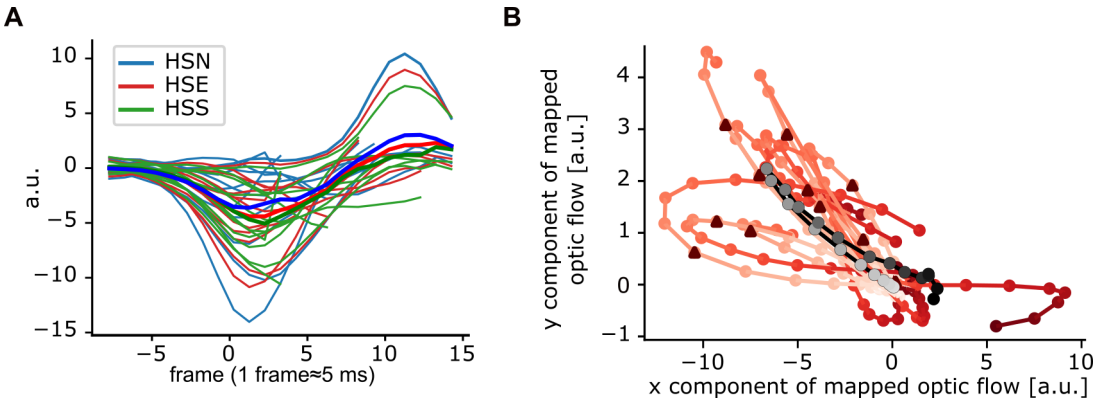

Figure 17: Zero-roll visual experience reconstruction
(A) Reconstructed voltage response of HS cells to reafferent visual motion during saccades to the right in arbitrary linear units, color-coded by subtype with individual trajectories (thin lines) and average (thick lines) of HSN (blue), HSE (red) and HSS (green), under the premise of zero roll rotation. **(B)** Corresponding reafferent visual motion in rightward saccades without roll rotation subdivided in horizontal and vertical components weighted by HS subtype sensitivity, individual trajectories shown as colored lines progressing from early (light color) to late phases (dark color) and body yaw onset marked by triangle, average in grey, shown for HSE.

Figure 18: Fly visual experience during exemplary saccade
Animation modeling the visual experience of a fly throughout a saccade in a forested environment, mapped to the ommatidial layout of the eyes in a Mollweide projection. Ovals mark approximate receptive fields of HSN (blue), HSE (red) and HSS (green)

Figure 19: Reafferent optic flow in the entire visual field during exemplary saccade
Animation showing reafferent optic flow vectors evolve throughout a saccade, mapped to the ommatidial layout of the complex eyes in a Mollweide projection. The Mollweide projection distorts directions with respect to azimuth ("longitude"), but projects equal elevation ("latitude") as horizontal lines. Ovals mark approximate receptive fields of HSN (blue), HSE (red) and HSS (green)

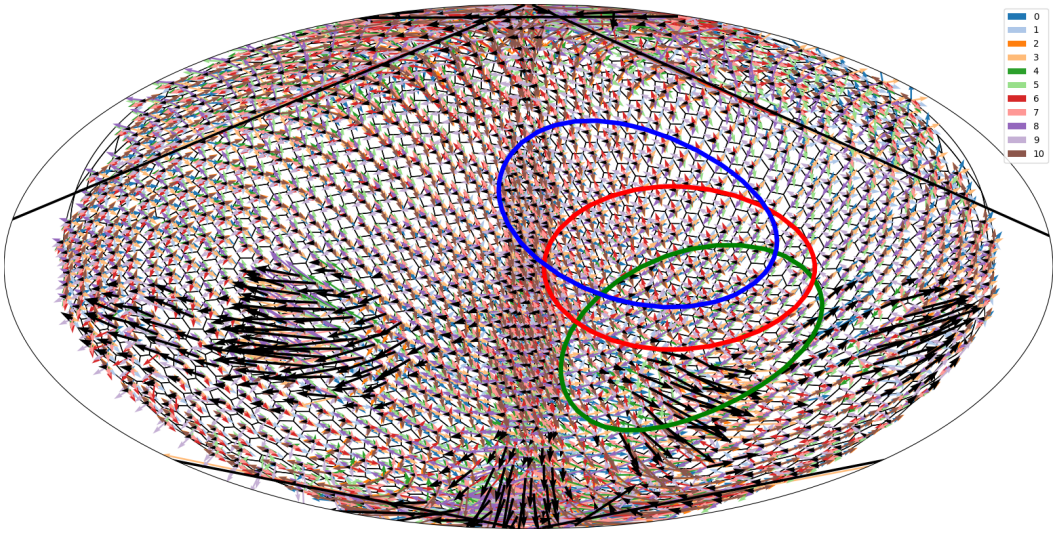

(20A) frame $t_0 - 6$,

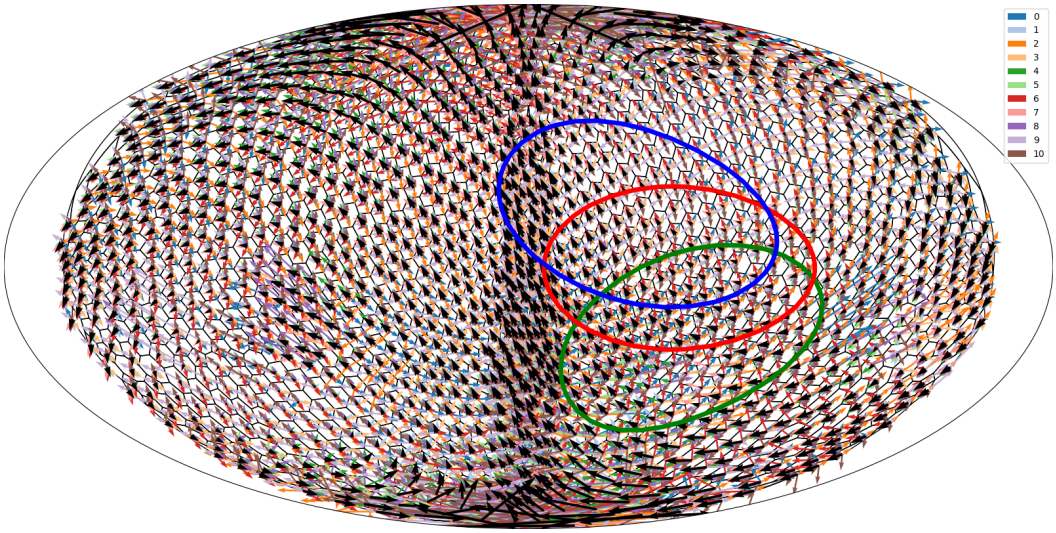

(20B) frame $t_0 - 4$,

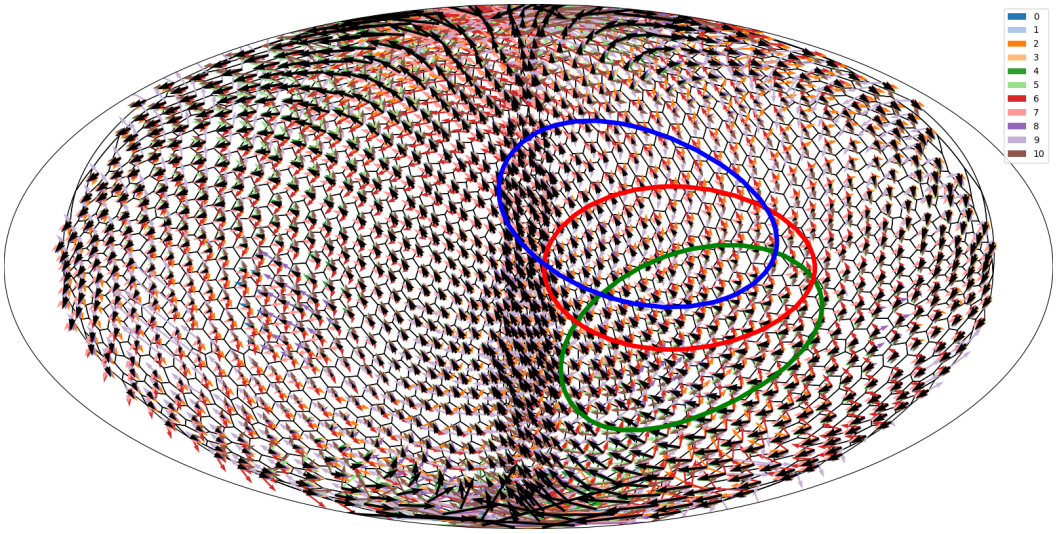

(20C) frame $t_0 - 2$,

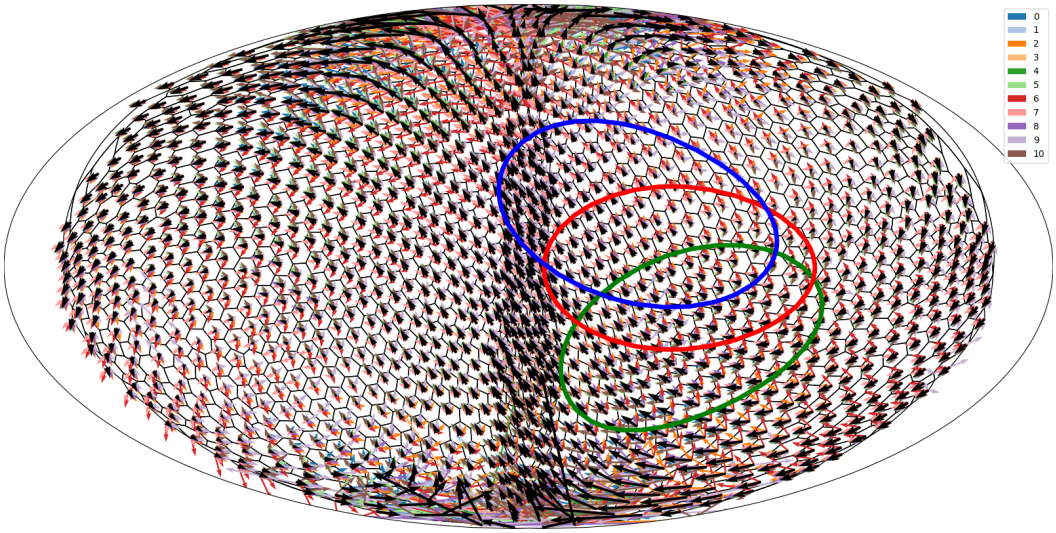

(20D) frame t_0,

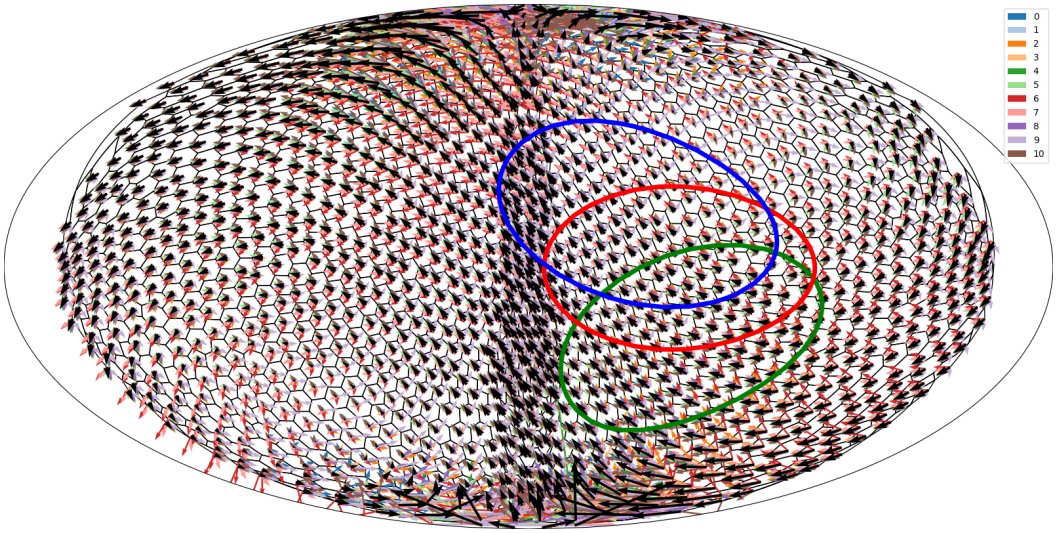

(20E) frame $t_0 + 2$,

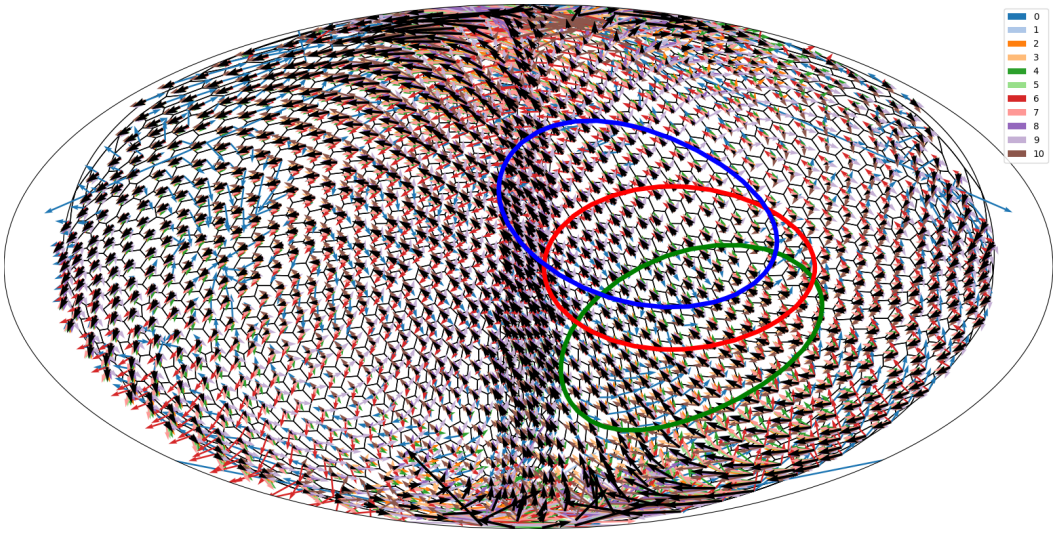

(20F) frame $t_0 + 4$,

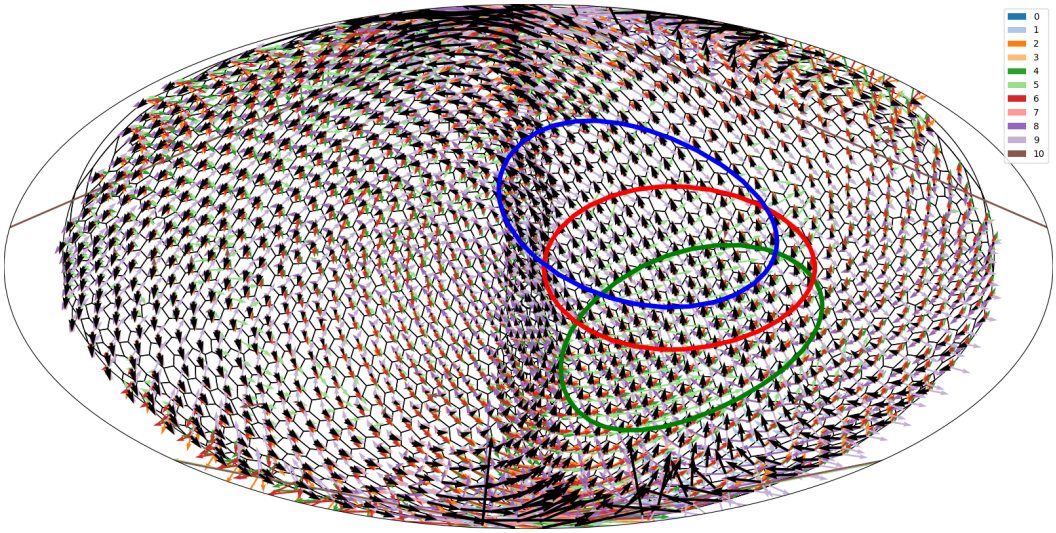

(20G) frame $t_0 + 6$,

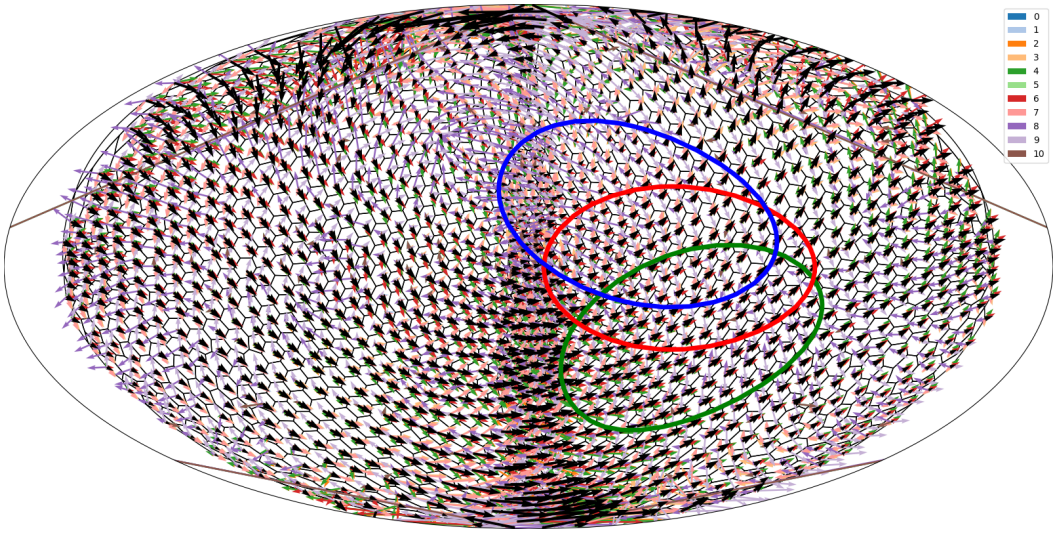

(20H) frame $t_0 + 8$,

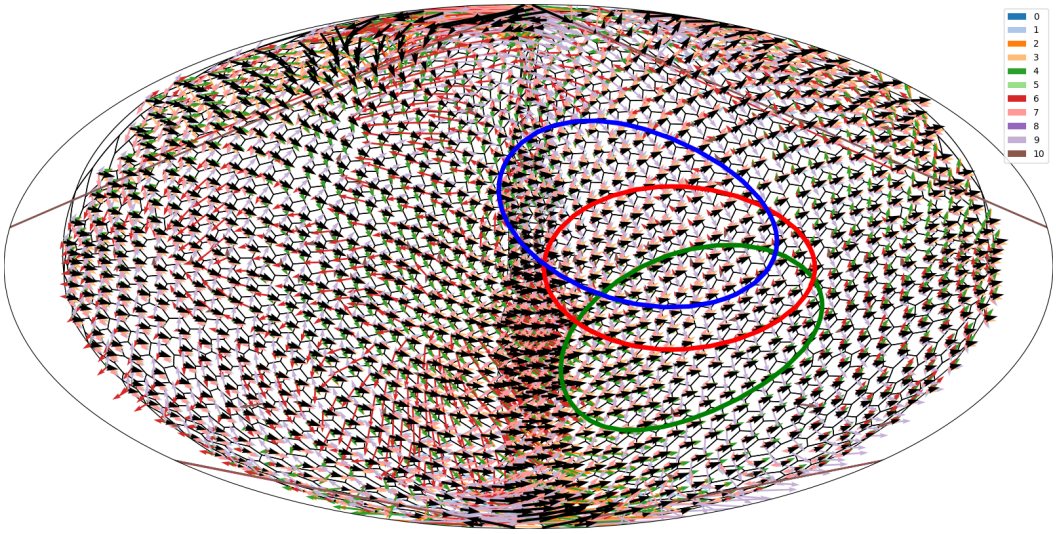

(20I) frame $t_0 + 10$,

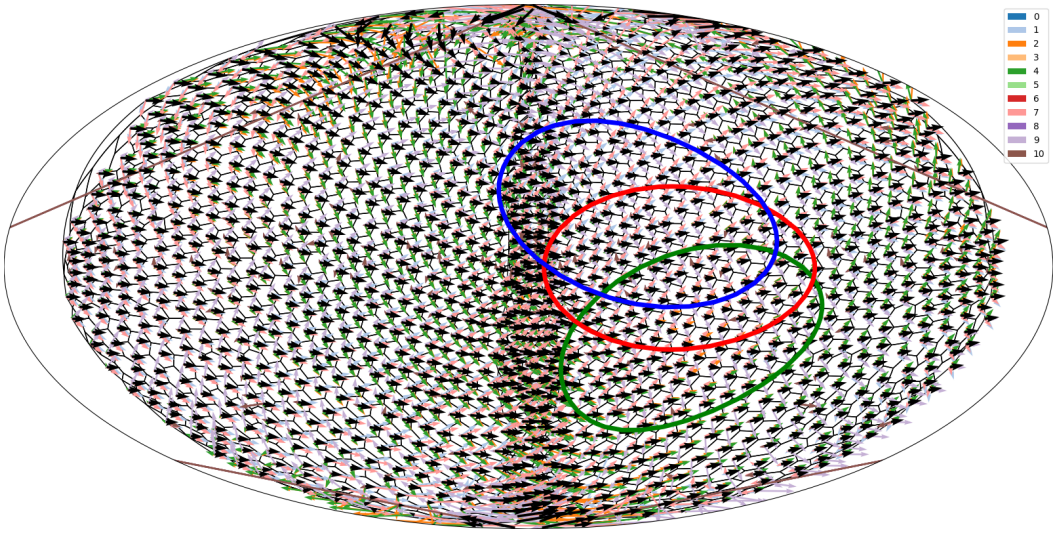

(20J) frame $t_0 + 12$,

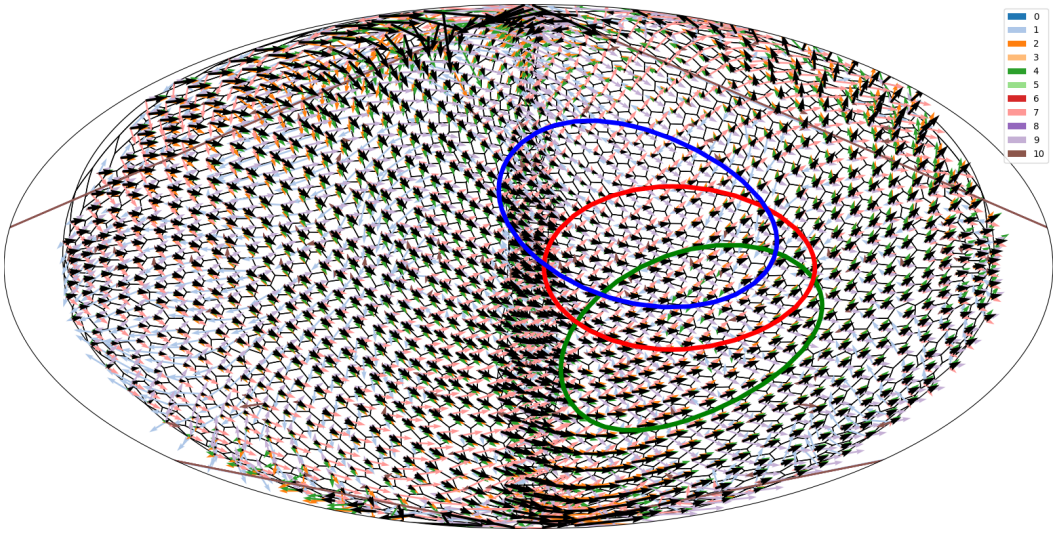

(20K) frame $t_0 + 14$,

Figure 20: Reafferent optic flow vectors throughout a saccade frame by frame, mapped to the ommatidial layout of the complex eyes in a Mollweide projection. Colors of vector field mark individual trials throughout the frames. The Mollweide projection distorts directions with respect to azimuth ("longitude"), but projects equal elevation ("latitude") as horizontal lines. Ovals mark approximate receptive fields of HSN (blue), HSE (red) and HSS (green).

B.2 DNp15 optogenetic activation

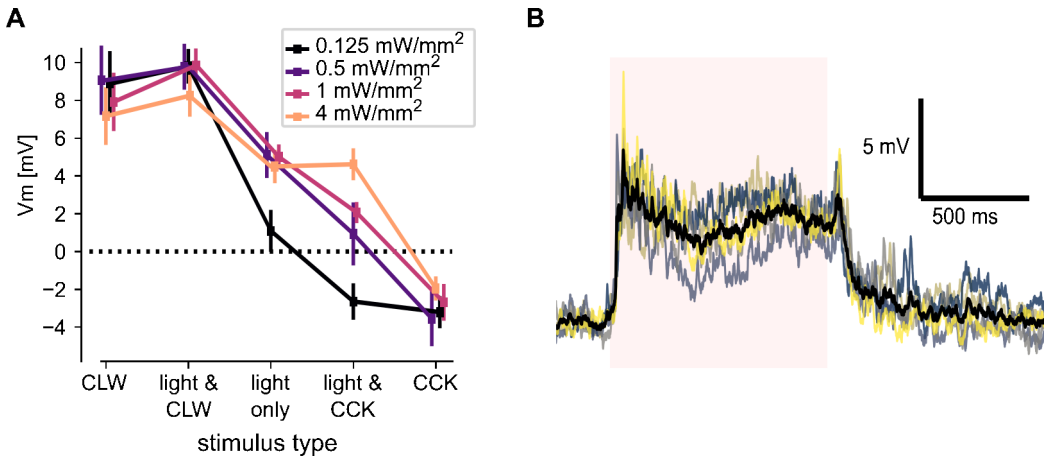

Figure 21: Intracellular recordings in optogentically activated DNp15
(A) Dose-response curve of intracellular recordings of a DNp15 cell expressing the optogenetic construct without Stop-cassette, averages and s.d. marked per light condition (n=5 trials each, N=1 fly). **(B)** All trials for a given intensity, color-coded by timing from earliest (dark blue) to latest (yellow) trial shows no adaptation to light stimulus (n=5 trials).

Bibliography

[1] J. M. Ache, S. Namiki, A. Lee, K. Branson, and G. M. Card, "State-dependent decoupling of sensory and motor circuits underlies behavioral flexibility in Drosophila," *Nature Neuroscience*, vol. 22, no. 7, pp. 1132–1139, (2019).

[2] G. Ammer, R. M. Vieira, S. Fendl, and A. Borst, "Anatomical distribution and functional roles of electrical synapses in Drosophila," *Current Biology*, vol. 32, no. 9, (2022).

[3] F. Aymanns, C.-L. Chen, and P. Ramdya, "Descending neuron population dynamics during odor-evoked and spontaneous limb-dependent behaviors," *eLife*, vol. 11, e81527, (2022).

[4] R. A. Baines, J. P. Uhler, A. Thompson, S. T. Sweeney, and M. Bate, "Altered electrical properties in Drosophila neurons developing without synaptic transmission," *Journal of Neuroscience*, vol. 21, no. 5, pp. 1523–1531, (2001).

[5] M. Barth and M. Heisenberg, "Vision affects mushroom bodies and central complex in Drosophila melanogaster," *Learning & Memory*, vol. 4, no. 2, pp. 219–229, (1997).

[6] J. Bartussek and F.-O. Lehmann, "Proprioceptive feedback determines visuomotor gain in Drosophila," *Royal Society Open Science*, vol. 3, no. 1, p. 150 562, (2016).

[7] J. A. Bender and M. H. Dickinson, "A comparison of visual and haltere-mediated feedback in the control of body saccades in Drosophila melanogaster," *Journal of Experimental Biology*, vol. 209, no. 23, pp. 4597–4606, (2006).

[8] J. A. Bender and M. H. Dickinson, "Visual stimulation of saccades in magnetically tethered Drosophila," *Journal of Experimental Biology*, vol. 209, no. 16, pp. 3170–3182, (2006).

[9] S. S. Bidaye, C. Machacek, Y. Wu, and B. J. Dickson, "Neuronal control of Drosophila walking direction," *Science*, vol. 344, no. 6179, pp. 97–101, (2014).

[10] Blender Online Community, *Blender - a 3d modelling and rendering package*, Blender Foundation, Blender Institute, Amsterdam, (2022).

[11] J. Blondeau and M. Heisenberg, "The three-dimensional optomotor torque system of Drosophila melanogaster," *Journal of comparative physiology*, vol. 145, no. 3, pp. 321–329, (1982).

[12] N. Boeddeker, L. Dittmar, W. Stürzl, and M. Egelhaaf, "The fine structure of honeybee head and body yaw movements in a homing task," *Proceedings of the Royal Society B: Biological Sciences*, vol. 277, no. 1689, pp. 1899–1906, (2010).

[13] N. Boeddeker and M. Egelhaaf, "A single control system for smooth and saccade-like pursuit in blowflies," *Journal of Experimental Biology*, vol. 208, no. 8, pp. 1563–1572, (2005).

[14] A. Borst, "Drosophila's view on insect vision," *Current Biology*, vol. 19, no. 1, R36–R47, (2009).

[15] A. H. Brand and N. Perrimon, "Targeted gene expression as a means of altering cell fates and generating dominant phenotypes," *Development*, vol. 118, no. 2, pp. 401–415, (1993).

[16] J. Braun, F. Hurtak, S. Wang-Chen, and P. Ramdya, "Networks of descending neurons transform command-like signals into population-based behavioral control," *bioRxiv*, (2023).

[17] F. v. Breugel, *FlyView*, (2014). [Online]. Available: https://github.com/florisvb/FlyView (visited on 08/28/2023).

[18] E. Buchner, "Dunkelanregung des stationären Flugs der Fruchtfliege Drosophila," diploma thesis, Julius-Maximilians-Universität Würzburg, Germany, (1971).

[19] S. A. Budick, M. B. Reiser, and M. H. Dickinson, "The role of visual and mechanosensory cues in structuring forward flight in Drosophila melanogaster," *Journal of Experimental Biology*, vol. 210, no. 23, pp. 4092–4103, (2007).

[20] C. Busch, A. Borst, and A. S. Mauss, "Bi-directional control of walking behavior by horizontal optic flow sensors," *Current Biology*, vol. 28, no. 24, 4037–4045.e5, (2018).

[21] J. Cande, S. Namiki, J. Qiu, W. Korff, G. M. Card, J. W. Shaevitz, D. L. Stern, and G. J. Berman, "Optogenetic dissection of descending behavioral control in Drosophila," *eLife*, vol. 7, e34275, (2018).

[22] B. Cellini, W. Salem, and J.-M. Mongeau, "Mechanisms of punctuated vision in fly flight," *Current Biology*, vol. 31, no. 18, 4009–4024.e3, (2021).

[23] P. D. Chapman, R. Burkland, S. P. Bradley, B. Houot, V. Bullman, A. M. Dacks, and K. C. Daly, "Flight motor networks modulate primary olfactory processing in the moth manduca sexta," *Proceedings of the National Academy of Sciences*, vol. 115, no. 21, pp. 5588–5593, (2018).

[24] Y.-C. D. Chen, Y.-C. Chen, R. Rajesh, N. Shoji, M. Jacy, H. Lacin, T. Erclik, and C. Desplan, "Using single-cell RNA sequencing to generate predictive cell-type-specific split-GAL4 reagents throughout development," *Proceedings of the National Academy of Sciences*, vol. 120, no. 32, e2307451120, (2023).

[25] C.-L. Chen, L. Hermans, M. C. Viswanathan, D. Fortun, F. Aymanns, M. Unser, A. Cammarato, M. H. Dickinson, and P. Ramdya, "Imaging neural activity in the ventral nerve cord of behaving adult Drosophila," *Nature Communications*, vol. 9, no. 1, p. 4390, (2018).

[26] H. S. J. Cheong *et al.*, "Transforming descending input into behavior: The organization of premotor circuits in the Drosophila male adult nerve cord connectome," *bioRxiv*, p. 2023.06.07.543976, (2023), Preprint. DOI: 10.1101/2023.06.07.543976.

[27] H. S. J. Cheong *et al.*, "Organization of an ascending circuit that conveys flight motor state," *bioRxiv*, p. 2023.06.07.544074, (2023), Preprint. DOI: 10.1101/2023.06.07.544074.

[28] M. E. Chiappe, J. D. Seelig, M. B. Reiser, and V. Jayaraman, "Walking modulates speed sensitivity in Drosophila motion vision," *Current Biology*, vol. 20, no. 16, pp. 1470–1475, (2010).

[29] D. Combes, D. Le Ray, F. M. Lambert, J. Simmers, and H. Straka, "An intrinsic feed-forward mechanism for vertebrate gaze stabilization," *Current Biology*, vol. 18, no. 6, R241–R243, (2008).

[30] R. Court *et al.*, "A systematic nomenclature for the Drosophila ventral nerve cord," *Neuron*, vol. 107, no. 6, 1071–1079.e2, (2020).

[31] J. A. Coyne, I. A. Boussy, T. Prout, S. H. Bryant, J. S. Jones, and J. A. Moore, "Long-distance migration of Drosophila," *The American Naturalist*, vol. 119, no. 4, pp. 589–595, (1982).

[32] T. B. Crapse and M. A. Sommer, "Corollary discharge across the animal kingdom," *Nature Reviews Neuroscience*, vol. 9, no. 8, pp. 587–600, (2008).

[33] K. E. Cullen, "Sensory signals during active versus passive movement," *Current Opinion in Neurobiology*, vol. 14, no. 6, pp. 698–706, (2004).

[34] T. A. Currier, A. M. Matheson, and K. I. Nagel, "Encoding and control of orientation to airflow by a set of Drosophila fan-shaped body neurons," *eLife*, vol. 9, e61510, (2020).

[35] K. Deisseroth and P. Hegemann, "The form and function of channelrhodopsin," *Science*, vol. 357, no. 6356, eaan5544, (2017).

[36] F. Delcomyn, "Corollary discharge to cockroach giant interneurones," *Nature*, vol. 269, no. 5624, pp. 160–162, (1977).

[37] T. Deora, A. K. Singh, and S. P. Sane, "Biomechanical basis of wing and haltere coordination in flies," *Proceedings of the National Academy of Sciences*, vol. 112, no. 5, pp. 1481–1486, (2015).

[38] B. H. Dickerson, "Timing precision in fly flight control: Integrating mechanosensory input with muscle physiology," *Proceedings of the Royal Society B: Biological Sciences*, vol. 287, no. 1941, p. 20 201 774, (2020).

[39] B. H. Dickerson, A. M. de Souza, A. Huda, and M. H. Dickinson, "Flies regulate wing motion via active control of a dual-function gyroscope," *Current Biology*, vol. 29, no. 20, 3517–3524.e3, (2019).

[40] M. H. Dickinson and M. S. Tu, "The function of dipteran flight muscle," *Comparative Biochemistry and Physiology Part A: Physiology*, vol. 116, no. 3, pp. 223–238, (1997).

[41] M. H. Dickinson, "Death valley, Drosophila, and the Devonian toolkit," *Annual Review of Entomology*, vol. 59, no. 1, pp. 51–72, (2014).

[42] M. H. Dickinson and F. T. Muijres, "The aerodynamics and control of free flight manoeuvres in Drosophila," *Philosophical Transactions of the Royal Society B: Biological Sciences*, vol. 371, no. 1704, (2016).

[43] S. Dorkenwald *et al.*, "Neuronal wiring diagram of an adult brain," *bioRxiv*, p. 2023.06.27.546656, (2023), Preprint. DOI: 10.1101/2023.06.27.546656.

[44] *Drosophila eye map*, (2023). [Online]. Available: https://github.com/strawlab/drosophila_eye_map (visited on 10/02/2023).

[45] B. J. Duistermars, D. M. Chow, M. Condro, and M. A. Frye, "The spatial, temporal and contrast properties of expansion and rotation flight optomotor responses in Drosophila," *Journal of Experimental Biology*, vol. 210, no. 18, pp. 3218–3227, (2007).

[46] E. Ehrhardt *et al.*, "Single-cell type analysis of wing premotor circuits in the ventral nerve cord of Drosophila melanogaster," *bioRxiv*, p. 2023.05.31.542897, (2023), Preprint. DOI: 10.1101/2023.05.31.542897.

[47] M. Erginkaya, "Movement-dependent central processing of visual feedback for self-motion estimation in Drosophila melanogaster," Ph.D. dissertation, Universidade Nova de Lisboa, Portugal, Lisbon, Portugal, (2022).

[48] M. Erginkaya, T. Cruz, M. Brotas, K. Steck, A. Nern, F. Torrão, N. Varela, D. Bock, M. Reiser, and M. E. Chiappe, "A competitive disinhibitory network for robust optic flow processing in Drosophila," *bioRxiv*, (2023), Preprint. DOI: 10.1101/2023.08.06.552150.

[49] A. W. Ewing, "The neuromuscular basis of courtship song in Drosophila: The role of the indirect flight muscles," *Journal of comparative physiology*, vol. 119, no. 3, pp. 249–265, (1977).

[50] K. Feng, R. Sen, R. Minegishi, M. Dübbert, T. Bockemühl, A. Büschges, and B. J. Dickson, "Distributed control of motor circuits for backward walking in Drosophila," *Nature Communications*, vol. 11, no. 1, p. 6166, (2020).

[51] L. M. Fenk, S. C. Avritzer, J. L. Weisman, A. Nair, L. D. Randt, T. L. Mohren, I. Siwanowicz, and G. Maimon, "Muscles that move the retina augment compound eye vision in Drosophila," *Nature*, vol. 612, no. 7938, pp. 116–122, (2022).

[52] L. M. Fenk, A. J. Kim, and G. Maimon, "Suppression of motion vision during course-changing, but not course-stabilizing, navigational turns," *Current Biology*, vol. 31, no. 20, (2021).

[53] P. J. Fischer and B. Schnell, "Multiple mechanisms mediate the suppression of motion vision during escape maneuvers in flying Drosophila," *iScience*, vol. 25, no. 10, p. 105 143, (2022).

[54] G. Fraenkel and J. W. S. Pringle, "Biological sciences: Halteres of flies as gyroscopic organs of equilibrium," *Nature*, vol. 141, no. 3577, pp. 919–920, (1938).

[55] F. França de Barros, J. Bacqué-Cazenave, C. Taillebuis, G. Courtand, M. Manuel, H. Bras, M. Tagliabue, D. Combes, F. M. Lambert, and M. Beraneck, "Conservation of locomotion-induced oculomotor activity through evolution in mammals," *Current Biology*, vol. 32, no. 2, 453–461.e4, (2022).

[56] T. Fujiwara, M. Brotas, and M. E. Chiappe, "Walking strides direct rapid and flexible recruitment of visual circuits for course control in Drosophila," *Neuron*, vol. 110, no. 13, 2124–2138.e8, (2022).

[57] T. Fujiwara, T. L. Cruz, J. P. Bohnslav, and M. E. Chiappe, "A faithful internal representation of walking movements in the Drosophila visual system," *Nature Neuroscience*, vol. 20, no. 1, pp. 72–81, (2017).

[58] F. Gabbiani, H. G. Krapp, and G. Laurent, "Computation of object approach by a wide-field, motion-sensitive neuron," *Journal of Neuroscience*, vol. 19, no. 3, pp. 1122–1141, (1999).

[59] C. Gilbert and E. Bauer, "Resistance reflex that maintains upright head posture in the flesh fly neobellieria bullata (sarcophagidae)," *Journal of Experimental Biology*, vol. 201, no. 19, pp. 2735–2744, (1998).

[60] P. T. Gonzalez-Bellido, T. J. Wardill, and M. Juusola, "Compound eyes and retinal information processing in miniature dipteran species match their specific ecological demands," *Proceedings of the National Academy of Sciences*, vol. 108, no. 10, pp. 4224–4229, (2011).

[61] P. T. Gonzalez-Bellido, T. J. Wardill, R. Kostyleva, I. A. Meinertzhagen, and M. Juusola, "Overexpressing temperature-sensitive dynamin decelerates phototransduction and bundles microtubules in Drosophila photoreceptors," *Journal of Neuroscience*, vol. 29, no. 45, pp. 14 199–14 210, (2009).

[62] K. G. Götz, "Optomotorische Untersuchung des visuellen Systems einiger Augenmutanten der Fruchtfliege Drosophila," *Kybernetik*, vol. 2, no. 2, pp. 77–92, (1964).

[63] K. G. Götz, "Flight control in Drosophila by visual perception of motion," *Kybernetik*, vol. 4, no. 6, pp. 199–208, (1968).

[64] K. G. Götz and H. Wenking, "Visual control of locomotion in the walking fruitfly Drosophila," *Journal of comparative physiology*, vol. 85, no. 3, pp. 235–266, (1973).

[65] N. W. Gouwens and R. I. Wilson, "Signal propagation in Drosophila central neurons," *Journal of Neuroscience*, vol. 29, no. 19, pp. 6239–6249, (2009).

[66] J. Haag, A. Wertz, and A. Borst, "Integration of lobula plate output signals by DNOVS1, an identified premotor descending neuron," *Journal of Neuroscience*, vol. 27, no. 8, pp. 1992–2000, (2007).

[67] J. Haag, A. Wertz, and A. Borst, "Central gating of fly optomotor response," *Proceedings of the National Academy of Sciences*, vol. 107, no. 46, pp. 20 104–20 109, (2010).

[68] V. Haikala, "The role of horizontal system cells in optomotor responses in Drosophila melanogaster," Ph.D. dissertation, Ludwig-Maximilian-Universität München, Germany, (2013).

[69] V. Haikala, M. Joesch, A. Borst, and A. S. Mauss, "Optogenetic control of fly optomotor responses," *Journal of Neuroscience*, vol. 33, no. 34, pp. 13 927–13 934, (2013).

[70] R. C. Hardie, "Phototransduction mechanisms in Drosophila microvillar photoreceptors," *Wiley Interdisciplinary Reviews: Membrane Transport and Signaling*, vol. 1, no. 2, pp. 162–187, (2012).

[71] G. Heide, "Proprioceptive feedback dominates the central oscillator in the patterning of the flight motoneuron output in Tipula (Diptera)," *Journal of comparative physiology*, vol. 134, no. 2, pp. 177–189, (1979).

[72] G. Heide and K. G. Götz, "Optomotor control of course and altitude in Drosophila melanogaster is correlated with distinct activities of at least three pairs of flight steering muscles," *Journal of Experimental Biology*, vol. 199, no. 8, pp. 1711–1726, (1996).

[73] M. Heisenberg and R. Wolf, "On the fine structure of yaw torque in visual flight orientation of Drosophila melanogaster," *Journal of comparative physiology*, vol. 130, no. 2, pp. 113–130, (1979).

[74] M. Heisenberg and R. Wolf, *Vision in Drosophila: genetics of microbehavior*. Springer-Verlag, (1984), vol. 12, ISBN: 978-3-642-699357-5.

[75] R. Hengstenberg, D. C. Sandeman, B. Hengstenberg, and G. A. Horridge, "Compensatory head roll in the blowfly Calliphora during flight," *Proceedings of the Royal Society of London. Series B. Biological Sciences*, vol. 227, no. 1249, pp. 455–482, (1986).

[76] L. Hermans, M. Kaynak, J. Braun, V. L. Ríos, C.-L. Chen, A. Friedberg, S. Günel, F. Aymanns, M. S. Sakar, and P. Ramdya, "Microengineered devices enable long-term imaging of the ventral nerve cord in behaving adult Drosophila," *Nature Communications*, vol. 13, no. 1, p. 5006, (2022).

[77] J. Hodge, "Ion channels to inactivate neurons in Drosophila," *Frontiers in Molecular Neuroscience*, vol. 2, (2009).

[78] E. von Holst and H. Mittelstaedt, "Das Reafferenzprinzip," *Naturwissenschaften*, vol. 37, no. 20, pp. 464–476, (1950).

[79] M. Isaacson, L. Ferguson, F. Loesche, I. Ganguly, J. Chen, A. Chiu, J. Liu, W. Dickson, and M. B. Reiser, "A high-speed, modular display system for diverse neuroscience applications," *bioRxiv*, (2022), Preprint. DOI: 10.1101/2022.08.02.502550.

[80] M. Joesch, J. Plett, A. Borst, and D. F. Reiff, "Response properties of motion-sensitive visual interneurons in the lobula plate of Drosophila melanogaster," *Current Biology*, vol. 18, no. 5, pp. 368–374, (2008).

[81] S. N. Jung, A. Borst, and J. Haag, "Flight activity alters velocity tuning of fly motion-sensitive neurons," *Journal of Neuroscience*, vol. 31, no. 25, pp. 9231–9237, (2011).

[82] I. Kauer, A. Borst, and J. Haag, "Complementary motion tuning in frontal nerve motor neurons of the blowfly," *Journal of Comparative Physiology A*, vol. 201, no. 4, pp. 411–426, (2015).

[83] A. Keller, "Drosophila melanogaster's history as a human commensal," *Current Biology*, vol. 17, no. 3, R77–R81, (2007).

[84] A. J. Kim, L. M. Fenk, C. Lyu, and G. Maimon, "Quantitative predictions orchestrate visual signaling in Drosophila," *Cell*, vol. 168, no. 1, pp.
bibrangessep 280–294.e12, (2017).

[85] A. J. Kim, J. K. Fitzgerald, and G. Maimon, "Cellular evidence for efference copy in Drosophila visuomotor processing," *Nature Neuroscience*, vol. 18, no. 9, pp. 1247–1255, (2015).

[86] T. Kitamoto, "Conditional modification of behavior in Drosophila by targeted expression of a temperature-sensitive shibire allele in defined neurons," *Journal of Neurobiology*, vol. 47, no. 2, pp. 81–92, (2001).

[87] N. C. Klapoetke *et al.*, "Independent optical excitation of distinct neural populations," *Nature Methods*, vol. 11, no. 3, pp. 338–346, (2014).

[88] P. Kunze, "Untersuchung des Bewegungssehens fixiert fliegender Bienen," *Zeitschrift für Vergleichende Physiologie*, vol. 44, no. 6, pp. 656–684, (1961).

[89] M. F. Land and T. S. Collett, "Chasing behaviour of houseflies (Fannia canicularis)," *Journal of comparative physiology*, vol. 89, no. 4, pp. 331–357, (1974).

[90] M.-B. Leonte, A. Leonhardt, A. Borst, and A. S. Mauss, "Aerial course stabilization is impaired in motion-blind flies," *Journal of Experimental Biology*, vol. 224, no. 14, jeb242219, (2021).

[91] E. Lesser *et al.*, "Synaptic architecture of leg and wing motor control networks in Drosophila," *bioRxiv*, (2023), Preprint. DOI: 10.1101/2023.05.30.542725.

[92] S. Q. Lima and G. Miesenböck, "Remote control of behavior through genetically targeted photostimulation of neurons," *Cell*, vol. 121, no. 1, pp. 141–152, (2005).

[93] Q. Liu, X. Yang, J. Tian, Z. Gao, M. Wang, Y. Li, and A. Guo, "Gap junction networks in mushroom bodies participate in visual learning and memory in Drosophila," *eLife*, vol. 5, e13238, (2016).

[94] K. Longden and H. Krapp, "Octopaminergic modulation of temporal frequency coding in an identified optic flow-processing interneuron," *Frontiers in Systems Neuroscience*, vol. 4, (2010).

[95] K. D. Longden and H. G. Krapp, "State-dependent performance of optic-flow processing interneurons," *Journal of Neurophysiology*, vol. 102, no. 6, pp. 3606–3618, (2009).

[96] H. Luan, N. C. Peabody, C. R. Vinson, and B. H. White, "Refined spatial manipulation of neuronal function by combinatorial restriction of transgene expression," *Neuron*, vol. 52, no. 3, pp. 425–436, (2006).

[97] G. Maimon, A. D. Straw, and M. H. Dickinson, "Active flight increases the gain of visual motion processing in Drosophila," *Nature Neuroscience*, vol. 13, no. 3, pp. 393–399, (2010).

[98] M. S. Maisak *et al.*, "A directional tuning map of Drosophila elementary motion detectors," *Nature*, vol. 500, no. 7461, pp. 212–216, (2013).

[99] E. C. Marin *et al.*, "Systematic annotation of a complete adult male Drosophila nerve cord connectome reveals principles of functional organisation," *bioRxiv*, (2023), Preprint. DOI: 10.1101/2023.06.05.543407.

[100] A. S. Mauss, K. Pankova, A. Arenz, A. Nern, G. M. Rubin, and A. Borst, "Neural circuit to integrate opposing motions in the visual field," *Cell*, vol. 162, no. 2, pp. 351–362, (2015).

[101] R. S. McIsaac, C. N. Bedbrook, and F. H. Arnold, "Recent advances in engineering microbial rhodopsins for optogenetics," *Current Opinion in Structural Biology*, vol. 33, pp. 8–15, (2015).

[102] G. W. Meissner *et al.*, "A searchable image resource of Drosophila GAL4 driver expression patterns with single neuron resolution," *eLife*, vol. 12, e80660, (2023).

[103] F. Mohammad, J. C. Stewart, S. Ott, K. Chlebikova, J. Y. Chua, T.-W. Koh, J. Ho, and A. Claridge-Chang, "Optogenetic inhibition of behavior with anion channelrhodopsins," *Nature Methods*, vol. 14, no. 3, pp. 271–274, (2017).

[104] J. Molina and A. Stumpner, "Effects of pharmacological treatment and photoinactivation on the directional responses of an insect neuron," *Journal of Experimental Zoology Part A: Comparative Experimental Biology*, vol. 303A, no. 12, pp. 1085–1103, (2005).

[105] M. Mronz and F.-O. Lehmann, "The free-flight response of Drosophila to motion of the visual environment," *Journal of Experimental Biology*, vol. 211, no. 13, pp. 2026–2045, (2008).

[106] L. Mu, J. P. Bacon, K. Ito, and N. J. Strausfeld, "Responses of Drosophila giant descending neurons to visual and mechanical stimuli," *Journal of Experimental Biology*, vol. 217, no. 12, pp. 2121–2129, (2014).

[107] F. T. Muijres, M. J. Elzinga, N. A. Iwasaki, and M. H. Dickinson, "Body saccades of Drosophila consist of stereotyped banked turns," *Journal of Experimental Biology*, vol. 218, no. 6, pp. 864–875, (2015).

[108] F. T. Muijres, M. J. Elzinga, J. M. Melis, and M. H. Dickinson, "Flies evade looming targets by executing rapid visually directed banked turns," *Science*, vol. 344, no. 6180, pp. 172–177, (2014).

[109] F. T. Muijres, M. J. Elzinga, J. M. Melis, and M. H. Dickinson, "Flies evade looming targets by executing rapid visually directed banked turns," *Science*, vol. 344, no. 6180, pp. 172–177, (2014).

[110] S. Mureli and J. L. Fox, "Haltere mechanosensory influence on tethered flight behavior in Drosophila," *Journal of Experimental Biology*, vol. 218, no. 16, pp. 2528–2537, (2015).

[111] S. Namiki, M. H. Dickinson, A. M. Wong, W. Korff, and G. M. Card, "The functional organization of descending sensory-motor pathways in Drosophila," *eLife*, vol. 7, e34272, (2018).

[112] S. Namiki, I. G. Ros, C. Morrow, W. J. Rowell, G. M. Card, W. Korff, and M. H. Dickinson, "A population of descending neurons that regulates the flight motor of Drosophila," *Current Biology*, vol. 32, no. 5, 1189–1196.e6, (2022).

[113] T. A. Ofstad, C. S. Zuker, and M. B. Reiser, "Visual place learning in Drosophila melanogaster," *Nature*, vol. 474, no. 7350, pp. 204–207, (2011).

[114] E. H. Palmer, J. J. Omoto, and M. H. Dickinson, "The role of a population of descending neurons in the optomotor response in flying Drosophila," *bioRxiv*, (2022), Preprint. DOI: 10.1101/2022.12.05.519224.

[115] B. D. Pfeiffer, T.-T. B. Ngo, K. L. Hibbard, C. Murphy, A. Jenett, J. W. Truman, and G. M. Rubin, "Refinement of tools for targeted gene expression in Drosophila," *Genetics*, vol. 186, no. 2, pp. 735–755, (2010).

[116] B. D. Pfeiffer *et al.*, "Tools for neuroanatomy and neurogenetics in Drosophila," *Proceedings of the National Academy of Sciences*, vol. 105, no. 28, pp. 9715–9720, (2008).

[117] V. O. Pokusaeva, R. Satapathy, O. Symonova, and M. Jösch, "Gap junctions arbitrate binocular course control in flies," *bioRxiv*, (2023), Preprint. DOI: 10.1101/2023.05.31.543181.

[118] J. F. A. Poulet and B. Hedwig, "The cellular basis of a corollary discharge," *Science*, vol. 311, no. 5760, pp. 518–522, (2006).

[119] M. J. Rauscher and J. L. Fox, "Asynchronous haltere input drives specific wing and head movements in Drosophila," *bioRxiv*, (2023).

[120] M. B. Reiser and M. H. Dickinson, "A modular display system for insect behavioral neuroscience," *Journal of Neuroscience Methods*, vol. 167, no. 2, pp. 127–139, (2008).

[121] T. Retzke, M. Thoma, B. S. Hansson, and M. Knaden, "Potencies of effector genes in silencing odor-guided behavior in Drosophila melanogaster," *Journal of Experimental Biology*, vol. 220, no. 10, pp. 1812–1819, (2017).

[122] C. R. von Reyn, P. Breads, M. Y. Peek, G. Z. Zheng, W. R. Williamson, A. L. Yee, A. Leonardo, and G. M. Card, "A spike-timing mechanism for action selection," *Nature Neuroscience*, vol. 17, no. 7, pp. 962–970, (2014).

[123] M. Rimniceanu, J. P. Currea, and M. A. Frye, "Proprioception gates visual object fixation in flying flies," *Current Biology*, vol. 33, no. 8, pp.
bibrangessep 1459–1471.e3, (2023).

[124] G. M. Rubin and Y. Aso, "New genetic tools for mushroom body output neurons in Drosophila," *bioRxiv*, (2023), Preprint. DOI: 10.1101/2023.06.23.546330.

[125] S. Sadaf, O. V. Reddy, S. P. Sane, and G. Hasan, "Neural control of wing coordination in flies," *Current Biology*, vol. 25, no. 1, pp. 80–86, (2015).

[126] L. K. Scheffer *et al.*, "A connectome and analysis of the adult Drosophila central brain," *eLife*, vol. 9, e57443, (2020).

[127] C. Schilstra and J. H. Van Hateren, "Blowfly flight and optic flow : I. thorax kinematics and flight dynamics," *Journal of Experimental Biology*, vol. 202, no. 11, pp. 1481–1490, (1999).

[128] C. Schilstra and J. Van Hateren, "Stabilizing gaze in flying blowflies [8]," *Nature*, vol. 395, no. 6703, p. 654, (1998).

[129] B. Schnell, M. Joesch, F. Forstner, S. V. Raghu, H. Otsuna, K. Ito, A. Borst, and D. F. Reiff, "Processing of horizontal optic flow in three visual interneurons of the Drosophila brain," *Journal of Neurophysiology*, vol. 103, no. 3, pp. 1646–1657, (2010).

[130] B. Schnell, S. V. Raghu, A. Nern, and A. Borst, "Columnar cells necessary for motion responses of wide-field visual interneurons in Drosophila," *Journal of Comparative Physiology A*, vol. 198, no. 5, pp. 389–395, (2012).

[131] B. Schnell, I. G. Ros, and M. H. Dickinson, "A descending neuron correlated with the rapid steering maneuvers of flying Drosophila," *Current Biology*, vol. 27, no. 8, pp. 1200–1205, (2017).

[132] B. Schnell, P. T. Weir, E. Roth, A. L. Fairhall, and M. H. Dickinson, "Cellular mechanisms for integral feedback in visually guided behavior," *Proceedings of the National Academy of Sciences*, vol. 111, no. 15, pp. 5700–5705, (2014).

[133] J. D. Seelig and V. Jayaraman, "Feature detection and orientation tuning in the Drosophila central complex," *Nature*, vol. 503, no. 7475, pp. 262–266, (2013).

[134] K. Shinomiya, A. Nern, I. A. Meinertzhagen, S. M. Plaza, and M. B. Reiser, "Neuronal circuits integrating visual motion information in Drosophila melanogaster," *Current Biology*, vol. 32, no. 16, 3529–3544.e2, (2022).

[135] R. W. Sperry, "Neural basis of the spontaneous optokinetic response produced by visual inversion.," *Journal of Comparative and Physiological Psychology*, vol. 43, no. 6, pp. 482–489, (1950).

[136] N. J. Strausfeld and H. S. Seyan, "Convergence of visual, haltere, and prosternal inputs at neck motor neurons of calliphora erythrocephala," *Cell and Tissue Research*, vol. 240, no. 3, pp. 601–615, (1985).

[137] G. S. B. Suh, S. B.-T. d. Leon, H. Tanimoto, A. Fiala, S. Benzer, and D. J. Anderson, "Light activation of an innate olfactory avoidance response in Drosophila," *Current Biology*, vol. 17, no. 10, pp. 905–908, (2007).

[138] M. P. Suver, A. Huda, N. Iwasaki, S. Safarik, and M. H. Dickinson, "An array of descending visual interneurons encoding self-motion in Drosophila," *The Journal of Neuroscience*, vol. 36, no. 46, pp. 11 768–11 780, (2016).

[139] M. P. Suver, A. Mamiya, and M. H. Dickinson, "Octopamine neurons mediate flight-induced modulation of visual processing in Drosophila," *Current Biology*, vol. 22, no. 24, pp. 2294–2302, (2012).

[140] S. T. Sweeney, K. Broadie, J. Keane, H. Niemann, and C. J. O'Kane, "Targeted expression of tetanus toxin light chain in Drosophila specifically eliminates synaptic transmission and causes behavioral defects," *Neuron*, vol. 14, no. 2, pp. 341–351, (1995).

[141] S.-y. Takemura *et al.*, "A connectome of the male Drosophila ventral nerve cord," *bioRxiv*, (2023), Preprint. DOI: 10.1101/2023.06.05.543757.

[142] L. F. Tammero and M. H. Dickinson, "Collision-avoidance and landing responses are mediated by separate pathways in the fruit fly, Drosophila melanogaster," *Journal of Experimental Biology*, vol. 205, no. 18, pp. 2785–2798, (2002).

[143] J. B. Thomas and R. J. Wyman, "Mutations altering synaptic connectivity between identified neurons in Drosophila," *Journal of Neuroscience*, vol. 4, no. 2, pp. 530–538, (1984).

[144] A. S. Thum, S. Knapek, J. Rister, E. Dierichs-Schmitt, M. Heisenberg, and H. Tanimoto, "Differential potencies of effector genes in adult Drosophila," *Journal of Comparative Neurology*, vol. 498, no. 2, pp. 194–203, (2006).

[145] L. Tirian and B. J. Dickson, "The VT GAL4, LexA, and split-GAL4 driver line collections for targeted expression in the Drosophila nervous system," *bioRxiv*, (2017), Preprint. DOI: 10.1101/198648.

[146] K. Tschida and V. Bhandawat, "Activity in descending dopaminergic neurons represents but is not required for leg movements in the fruit fly Drosophila," *Physiological Reports*, vol. 3, no. 3, e12322, (2015).

[147] M. S. Tu and M. H. Dickinson, "Modulation of negative work output from a steering muscle of the blowfly Calliphora vicina," *Journal of Experimental Biology*, vol. 192, no. 1, pp. 207–224, (1994).

[148] G. Von Fermi and W. Reichardt, "Optomotorische Reaktionen der Fliege Musca domestica," *Kybernetik*, vol. 2, no. 1, pp. 15–28, (1963).

[149] S. M. Walker, D. A. Schwyn, R. Mokso, M. Wicklein, T. Müller, M. Doube, M. Stampanoni, H. G. Krapp, and G. K. Taylor, "In vivo time-resolved microtomography reveals the mechanics of the blowfly flight motor," *PLOS Biology*, vol. 12, no. 3, e1001823, (2014).

[150] T. Wang, Y. Jiao, and C. Montell, "Dissection of the pathway required for generation of vitamin A and for Drosophila phototransduction," *Journal of Cell Biology*, vol. 177, no. 2, pp. 305–316, (2007).

[151] T. L. Warren, Y. M. Giraldo, and M. H. Dickinson, "Celestial navigation in Drosophila," *Journal of Experimental Biology*, vol. 222, jeb186148, Suppl_1 (2019).

[152] H. Wei, "The diversity of lobula plate tangential cells (LPTCS) in Drosophila," Ph.D. dissertation, New York University, New York, USA, (2020).

[153] P. T. Weir, B. Schnell, and M. H. Dickinson, "Central complex neurons exhibit behaviorally gated responses to visual motion in Drosophila," *Journal of Neurophysiology*, vol. 111, no. 1, pp. 62–71, (2014).

[154] J. Wietek, S. Rodriguez-Rozada, J. Tutas, F. Tenedini, C. Grimm, T. G. Oertner, P. Soba, P. Hegemann, and J. S. Wiegert, "Anion-conducting channelrhodopsins with tuned spectra and modified kinetics engineered for optogenetic manipulation of behavior," *Scientific Reports*, vol. 7, no. 1, p. 14 957, (2017).

[155] J. Wietek, J. S. Wiegert, N. Adeishvili, F. Schneider, H. Watanabe, S. P. Tsunoda, A. Vogt, M. Elstner, T. G. Oertner, and P. Hegemann, "Conversion of channelrhodopsin into a light-gated chloride channel," *Science*, vol. 344, no. 6182, pp. 409–412, (2014).

[156] R. I. Wilson and G. Laurent, "Role of GABAergic inhibition in shaping odor-evoked spatiotemporal patterns in the Drosophila antennal lobe," *Journal of Neuroscience*, vol. 25, no. 40, pp. 9069–9079, (2005).

[157] J. P. Wing, L. Zhou, L. M. Schwartz, and J. R. Nambu, "Distinct cell killing properties of the Drosophila reaper, head involution defective, and grim genes," *Cell Death and Differentiation*, vol. 5, no. 11, pp. 930–939, (1998).

[158] R. Wolf and M. Heisenberg, "Visual control of straight flight in Drosophila melanogaster," *Journal of Comparative Physiology A*, vol. 167, no. 2, (1990).

[159] R. H. Wurtz, "Neuronal mechanisms of visual stability," *Vision Research*, Vision Research Reviews, vol. 48, no. 20, pp. 2070–2089, (2008).

[160] A. M. Yarger and J. L. Fox, "Dipteran halteres: Perspectives on function and integration for a unique sensory organ," *Integrative and Comparative Biology*, vol. 56, no. 5, pp. 865–876, (2016).

[161] M. Yuan and R. Christian, "360° optical flow using tangent images," in *Proceedings of the 32nd British Machine Vision Conference (BMVC)*, (2021). DOI: 10.48550/arXiv.2112.14331.